Analyzing the role of a truncated Adenylyl Cyclase 3 isoform in brown adipose tissue

Doctoral thesis

to obtain a doctorate

from the Faculty of Medicine

of the University of Bonn

Lara-Marie Vagliano

from Offenbach am Main

2025

Written with authorization of

the Faculty of Medicine of the University of Bonn

First reviewer: Prof. Dr. Dagmar Wachten

Second reviewer: Prof. Dr. Kerstin Wilhelm-Jüngling

Day of oral examination: 15.01.2025

From the Institute of Innate Immunity

Directors: Prof. Dr. Dagmar Wachten, Prof. Dr. Felix Meissner

To my brothers, Federico and Gianluca

Table of contents

List of abbreviations

AC	Adenylyl cyclase
Adcy	Adenylyl cyclase
ADP	Adenosine diphosphate
AMP	Adenosine monophosphate
APS	Ammonium persulfate
AR	Adreno receptor
ATGL	Adipocyte triglyceride lipase
AT	Alternate transcript
ATP	Adenosine triphosphate
AU	Arbitrary units
β-AR	β-adrenoceptor
BAT	Brown adipose tissue
BCA	Bicinchoninic assay
BMI	Body-mass index
BSA	Bovine serum albumin
°C	Degree Celsius
C	Catalytic domain
$C_5H_8KNO_4$	Glutamic acid monopotassium salt monohydrate
cAMP	Cyclic adenosine monophosphate
$CaCl_2$	Calcium chloride
CH_3CO_2K	Potassium acetate
ChIP	Chromatin immunoprecipitation
CHO	Chinese hamster ovary cell line
CMV	Cytomegalovirus

CNGA2	Cyclic nucleotide-gated olfactory channel
CO_2	Carbon dioxide
CoA	Coenzyme A
CRE	cAMP responsive element
CREB	cAMP responsive element binding protein
CV	Column volume
Da	Dalton
DAG	Diacylglycerol
DAPI	4',6-diamidin-2-phenylindol
ddH_2O	Double-distilled water
dk	Donkey
DMEM	Dulbecco's modified eagle medium
DMSO	Dimethyl sulfoxide
DNA	Desoxyribonucleic acid
DTT	Dithiothreitol
ECACC	European Collection of Authenticated Cell Cultures
EDTA	Ethylene diamine tetra acetic acid
E	Exon
EBI	European Bioinformatics Institute
E. coli	Escherichia coli
EE	Energy expenditure
EGTA	Triethylene glycol diamine tetra acetic acid
e.g.	Exempli gratia, for example
ELISA	Enzyme-linked immunosorbent assay
EMBL	European Molecular Biology Laboratory
ER	Endoplasmic reticulum

ES	Extracellular solution
et al.	Et alii
eWAT	Epididymal white adipose tissue
F12	Ham's F-12 Nutrient Mixture
$FADH_2$	Flavin adenine dinucleotide
FCS	Fetal calf serum
FFA	Free fatty acid
FL	Full-length
FRET	Foerster resonance energy transfer
FSK	Forskolin
FTO	Fat mass and obesity associated gene
g	gram
x g	x times gravitational force (9.81 m/sec^2)
G418	Geneticin
$G_{\alpha s}$	G_s alpha subunit
GDP	Guanosine 5'-diphosphate
GPCR	G-protein coupled receptor
GRK	G-protein coupled receptor kinase
GTP	Guanosine 5'-triphosphate
gt	Goat
GWAS	Genome-wide association study
h	Hour(s)
H_2O	Dihydrogen monoxide
H3	H3 family of histones
HA	Hemagglutinin
HCl	Hydrochloric acid

HEK	Human embryonic kidney cell line
HEPES	4-(2-hydroxyethyl)-1-piperazineethanesulfonic acid
HRP	Horseradish peroxidase
HSL	Hormone sensitive lipase
IBMX	3-Isobutyl-1-methylxanthin
ICC	Immunocytochemistry
IL-1β	Interleukin-1β
IR	Infrared
Iso	Isoproterenol
iWAT	Inguinal white adipose tissue
K	Lysine
k	Kilo
KCl	Potassium chloride
kDa	Kilodalton
KH_2PO_4	Potassium dihydrogen phosphate
LAPD	Light-activated phosphodiesterase
LB	Lysogeny broth
μ	Micro
M	Molar
m	Milli
m	Mouse
mA	Milliampere
mAb	Monoclonal antibody
MC4R	Melanocortin 4 receptor
me	Methyl group
MEM	Minimum Essential Medium

MeOH	Methanol
$MgCl_2$	Magnesium chloride
min	Minute(s)
mol	Mole
mPic	Mammalian protease inhibitor cocktail
mRNA	Messenger ribonucleic acid
ms	mouse *(Mus musculus)*
MW	Molecular weight
n	Nano
NB	Non-bound
NaCl	Sodium chloride
NADH	Nicotinamide adenine dinucleotide
NADPH	Nicotinamide adenine dinucleotide phosphate (reduced)
Na_2HPO_4	Disodium hydrogen phosphate
NaH_2PO_4	Monosodium phosphate
NaOH	Sodium hydroxide
NE	Norepinephrine
NEAA	Non-Essential Amino Acids
neoR	Neomycin resistance
NP40	Nonidet P-40, Octylphenoxypolyethoxyethanol
NST	Non-shivering thermogenesis
NT	Non-transfected
OAB	Overactive bladder
OD	Optical density
OptiMem	Reduced serum medium
p	Pico

pAb	Polyclonal antibody
PAGE	Polyacrylamide gel electrophoresis
PBS	Phosphate-buffered saline
PBS-T	Phosphate-buffered saline with Tween 20
PDE	Phosphodiesterase
PEI	Polyethylenimine
PFA	Paraformaldehyde
PGE_2	Prostaglandin E_2
pH	p[H+]
PKA	Protein kinase A
PLL	Poly-L-lysine
PM	Plasma membrane
PNGaseF	Peptide-N-glycosidase F
PPARG	Peroxisome proliferator-activated receptor gamma
PVDF	Polyvinylidene difluoride
rb	Rabbit
rER	Rough endoplasmic reticulum
RNA	Ribonucleic acid
ROI	Region of interest
rpm	Rounds per minute
rt	Rat *(Rattus norvegicus)*
RT	Room temperature
SD	Standard deviation
SDS	Sodium dodecyl sulfate
sec	Second(s)
seq	Sequencing

S_n	Transmembrane segment
SNP	Small nucleotide polymorphism
SNS	Sympathetic nervous system
t	Time
TBS	Tris-buffered saline
TCF7L2	Transcription factor 7-like 2
TEMED	Tetramethylethylendiamine
TM	Transmembrane domain
Tris	Tris(hydroxymethyl)aminomethane
TSS	Transcription start site
T2D	Type 2 diabetes
UCP1	Uncoupling protein 1
v	Volume
V	Volt
VSMC	Vascular smooth muscle cell
w	Weight
WB	Western blot
WAT	White adipose tissue
WT	Wild-type

1. Introduction

1.1 Global obesity epidemic

Due to its rapidly increasing prevalence in industrialized as well as developing countries, obesity has become one of the main public health issues in the 21st century (N.C.D. Risk Factor Collaboration, 2016). Obesity is caused by a chronic imbalance between caloric intake and energy expenditure, either due to overnutrition or reduced physical activity. The increase in body fat drives inflammatory processes, which are key mechanisms in the pathogenesis of glucose intolerance and insulin resistance (Hotamisligil, 2017). Thereby, obesity constitutes a significant risk factor in the pathogenesis of a condition known as metabolic syndrome, which comprises abdominal obesity, hyperglycemia, dyslipidemia, and arterial hypertension, ultimately leading to type 2 diabetes (T2D) and cardiovascular diseases (Global B.M.I. Mortality Collaboration, 2016; Prospective Studies Collaboration, 2009; Tune et al., 2017). Restoring a healthy body weight is the major aim in the treatment of obesity. Other than promoting the increase of physical activity and the reduction of caloric intake, there is a great necessity to develop novel therapeutic approaches, specifically targeting the adipose tissue, which is most fundamentally affected by increasing body fat and deeply involved in energy metabolism and homeostasis (Kusminski et al., 2016; Scherer, 2019).

1.1.1 Different types of adipose tissue

1.1.2 White adipose tissue

White adipose tissue (WAT) primarily serves to store surplus caloric energy in the form of lipids, specifically triglycerides. Morphologically, white adipocytes contain a single lipid droplet, in which lipids are deposited and that consumes up to 90 % of the cell's volume (Cannon and Nedergaard, 2004). WAT is mostly found in subcutaneous, visceral, omental, and mesenteric depots. Obesity leads to an increase in adipocyte number (hyperplasia) and adipocyte size (hypertrophy) (White, 2023), which, especially in visceral WAT depots, is strongly associated with cardiometabolic disease in humans (Gruzdeva et al., 2018).

1.1.3 Brown adipose tissue

Brown adipose tissue (BAT) is activated during cold exposure to counteract hypothermia by producing heat through the combustion of carbohydrates and lipids (Christensen et al., 2006; Cypess et al., 2009; Nedergaard et al., 2010). This process is called non-shivering thermogenesis (NST). Morphologically, brown adipocytes contain multiple, small lipid droplets and large numbers of mitochondria, which is a crucial feature for their thermogenic potential (Cannon and Nedergaard, 2004). The locational distribution of BAT in humans varies among individuals but can be categorized into cervical, supraclavicular, axillary, paraspinal, mediastinal, and abdominal depots (Leitner et al., 2017).

1.1.4 Brite adipose tissue

A second type of thermogenic adipose tissue consists of brite (brown-like in white) adipocytes, also referred to as beige adipocytes, which derive from white adipocytes (Jung et al., 2019). Despite originating from white adipocytes, beige adipocytes possess phenotypical characteristics between those of the white adipocyte and the brown adipocyte. Morphologically, beige adipocytes have higher mitochondrial density than white adipocytes and multilocular lipid droplets (Ikeda et al., 2018). The formation of beige fat is triggered by various external factors such as chronic cold exposure and prolonged treatment with peroxisome proliferator-activated receptor gamma (PPARG) agonists (Frontini and Cinti, 2010; Hatori et al., 2012; Kajimura et al., 2015; Klepac et al., 2019; Ohno et al., 2012; Vegiopoulos et al., 2017).

1.2 Anti-obesogenic potential of BAT

Contrary to the long-perceived notion that BAT is the main thermoregulatory organ in newborns due to their incapacity for shivering and maintenance of core temperature, (Dawkins and Scopes, 1965; Ito and Kuroshima, 1967; Silverman et al., 1964), more recent studies prove the persistence of metabolically active BAT beyond infancy. Using ^{18}F-fluorodeoxyglucose positron emission tomography scanning, significant cold-induced BAT activity has been detected in cervical and supraclavicular depots in adults (Cypess

et al., 2009; Nedergaard et al., 2007; van Marken Lichtenbelt et al., 2009; Virtanen et al., 2009).

There is an inverse correlation between obesity and the mass and activity of BAT in humans (Matsushita et al., 2014). Also, cold-induced activation of BAT has been demonstrated to result in weight reduction even in humans devoid of detectable BAT depots under ambient temperatures (Altshuler-Keylin et al., 2016; Hanssen et al., 2015; Nedergaard and Cannon, 2014; van der Lans et al., 2013; Yoneshiro et al., 2013). To date, attempts to therapeutically stimulate BAT have been unsuccessful due to the occurrence of side effects stemming from unintended sympathetic activation. These side effects include hypertension, tachycardia, and elevated levels of circulating metabolic agents such as glucose, insulin, and thyroid hormones (Cypess et al., 2012; Lynes and Tseng, 2015). To design novel therapeutic approaches that activate BAT, it is crucial to understand the molecular pathways promoting thermogenesis.

1.3 Signaling pathways underlying thermogenesis in BAT

1.3.1 Cold-induced BAT activation is mediated by the autonomic nervous system

The sympathetic nervous system (SNS) functions without conscious, voluntary control and plays a crucial role in the maintenance of homeostasis. It innervates different peripheral effector organs and, therefore, enables the organism to adapt to changing environmental conditions. BAT is one of the main effector organs, enabling the body to maintain core temperature under acute thermal stress, such as cold exposure.

Cold is sensed via peripheral neurons which project to central neural circuits and, in turn, activate first-order neurons of the SNS. These synapse on second-order neurons within the sympathetic ganglia, innervating effector sites such as BAT, where SNS-terminals release the neurotransmitter norepinephrine (NE) (Kajimura et al., 2015; Morrison and Madden, 2014).

1.3.2 A central player in BAT activation is cAMP

In BAT, NE activates β-adrenoceptors (β-AR), which are transmembrane G_s-protein-coupled receptors (GPCRs) (Blondin et al., 2020). Activation of these GPCRs results in the dissociation of the attached heterotrimeric G_s-protein into its α-unit and β-γ-complex (Simons et al., 2003). The membrane-anchored $G_{\alpha s}$-unit moves along the membrane and activates adenylyl cyclases (ACs) (Khannpnavar et al., 2020; Reverte-Salisa et al., 2019). ACs and $G_{\alpha s}$ proteins interact via the N-terminus of the AC protein (Dessauer et al., 2017). Binding of $G_{\alpha s}$ induces a conformational change, which aligns the catalytic residues with the substrate adenosine triphosphate (ATP) (Dessauer et al., 2017; Tesmer et al., 1997). In turn, ATP is converted to 3',5' cyclic adenosine monophosphate (cAMP) (Simonds, 1999; Tesmer et al., 1999).

1.3.3 The thermogenic process

The main downstream target for the second messenger molecule cAMP is the protein kinase A (PKA). In brown adipose tissue, the cAMP-PKA signaling cascade mediates the thermogenic process (**Figure 1**) by promoting the phosphorylation of lipolytic enzymes, such as adipocyte triglyceride lipase (ATGL), hormone-sensitive lipase (HSL), and the lipolysis-associated protein perilipin. This facilitates the liberation of free fatty acids (FFAs) from lipid droplets. After being esterified with coenzyme A (CoA) and transported into the mitochondrial matrix, the FFAs undergo mitochondrial β-oxidation, leading to the generation of acetyl-CoA. Subsequently, acetyl-CoA undergoes processing in the citric acid cycle, resulting in the production of reduced electron carriers NADH and $FADH_2$. Within the inner mitochondrial membrane, the reduced electron carriers are oxidized via the respiratory chain, causing the pumping of protons into the intermembrane space, which generates a proton gradient. Uniquely in BAT, the protons can bypass the ATP-synthase by reentering the mitochondrial matrix via the uncoupling protein 1 (UCP1) in the inner mitochondrial membrane. Consequently, UCP1 uncouples the respiratory chain from ATP synthesis, dissipating the energy stored in the proton-motive force as heat (Cannon and Nedergaard, 2004).

The activation of the cAMP-PKA-dependent cascade not only results in the fueling of the thermogenic process but also enhances UCP1 expression via activation of transcription

factors, such as cAMP-responsive element binding-protein (CREB) (Cannon and Nedergaard, 2004). In summary, cold exposure activates BAT through the sympathetic nervous system, stimulating adrenoceptors, and initiating cAMP-dependent signaling pathways, which ultimately lead to heat production.

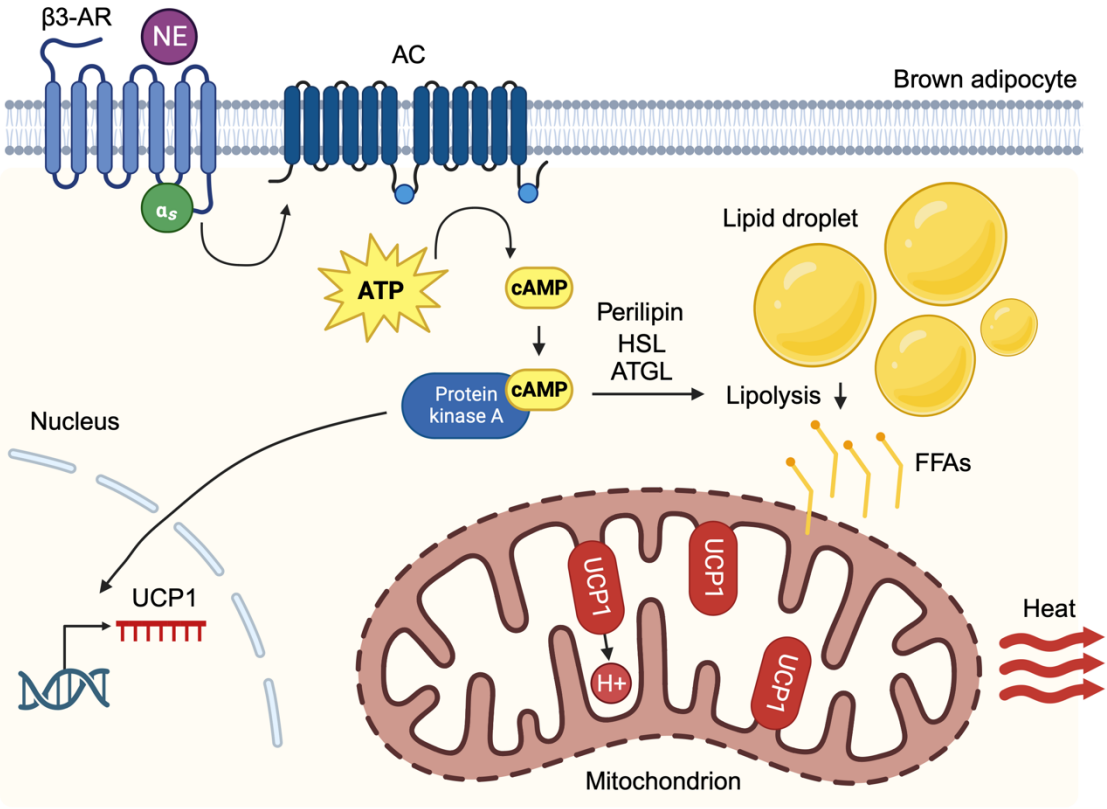

Figure 1: Signaling pathway underlying thermogenesis in brown adipocytes. Modified from Braun et al. (2018). Upon cold exposure, norepinephrine (NE) is released from sympathetic nervous system terminals. NE activates G_s-protein-coupled β-adrenoceptors (β-AR). The G_α unit of the β_3-AR activates adenylyl cyclases (ACs), which produce cAMP. In turn, cAMP activates the protein kinase A (PKA), which promotes the upregulation of the essential thermogenic protein (uncoupling protein 1, UCP 1), as well as the phosphorylation of proteins involved in lipolysis (adipose triglyceride lipase (ATGL), hormone-sensitive lipase (HSL), and perilipin), leading to the liberation of free fatty acids (FFAs) from lipid droplets. The FFAs are transported into the mitochondria, where they act as both fuel for mitochondrial β-oxidation and activators of UCP 1. At the end of the respiratory chain, UCP 1 allows proton (H^+) influx into the mitochondrial matrix, bypassing the synthesis of ATP. Thereby, the chemical energy of nutrients is dissipated as heat.

1.4 Epigenetic regulation of brown adipose tissue

Whereas the main molecular players in BAT activation have been identified, their regulation, e.g., through epigenetic modification, is not well understood. Epigenetic modifications, such as posttranslational modifications of histones, consist of patterns of mono-, di-, and trimethylation or acetylation of lysine residues of histone proteins. These chromatin modifications are known to alter chromatin structure locally and, thereby, regulate the activation or repression of gene transcription (Kouzarides, 2007).

The epigenomic mark H3K4me3 (tri-methylation (me3) at the lysine (K4) residue in the histone protein H3) is a major chromatin modification involved in the regulation of thermogenesis in brown adipose tissue (Musri et al., 2010). H3K4me3 generally marks transcription start sites (TSSs) of active genes and is associated with the local opening of chromatin, activation of promoters, and the initiation of transcription (Barski et al., 2007; Bernstein et al., 2005; Kim et al., 2005; Santos-Rosa et al., 2002).

Using RNA sequencing and ChIP sequencing on BAT in lean and obese mice either kept at ambient (22 °C) or exposed to cold temperatures (4 °C) for 24 h, cold-induced histone modifications, such as H3K4me3, were mapped by the lab of Jan-Wilhelm Kornfeld (University of Southern Denmark) (Engelhard et al., 2022). Amongst other cold-induced changes, a cold-induced H3K4me3-marked promoter in intron 2 of the *adenylyl cyclase 3 (Adcy3)* gene was detected (**Figure 2**). In *Adcy3*, the H3K4me3 domain arising from cold-induction marked a novel TSS (referred to as TSS-2), which is located downstream of the original TSS (referred to as TSS-1) in the 2nd intron of *Adcy3*. By integrating Illumina short-read and Oxford Nanopore Technology, comprehensive, full-length RNA-seq analysis of cold-activated BAT validated that TSS-2 generates a contiguous 5' truncated alternate transcript (AT) spanning from Exon 2b to Exon 22, termed *Adcy3-at* (Khani et al., 2024). While cold exposure promotes the expression of *Adcy3-at*, the level of canonical *Adcy3* mRNA (Exon 1-22) expression remained unaffected by cold exposure. Cold-induced expression of the truncated AC3-AT protein was also verified in primary brown adipocytes by the Kornfeld lab (Khani et al., 2024).

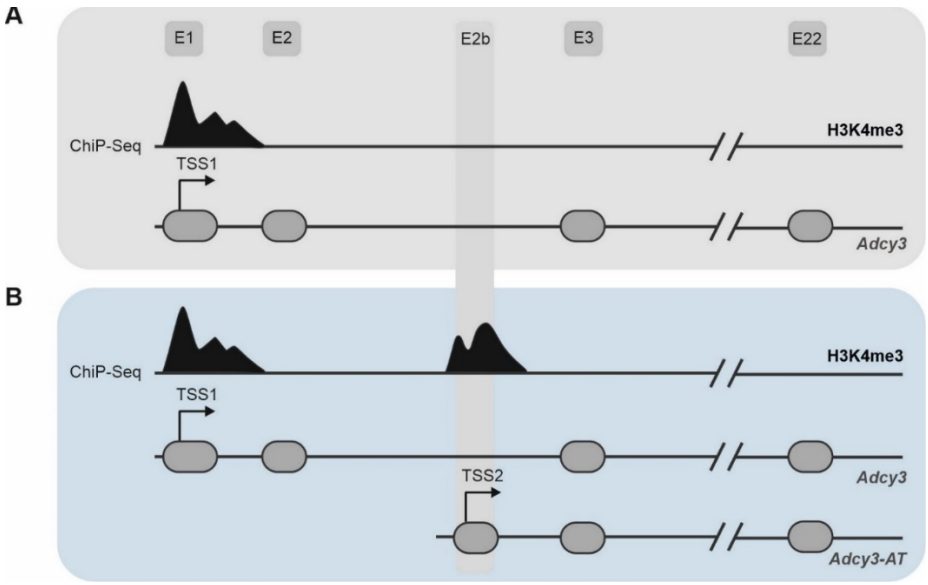

Figure 2: Schematic overview of the H3K4me3 pattern in the *Adcy3* gene. H3K4me3 peaks in ChiP-Seq analysis of the *Adcy3* gene from mice, which were either kept at (A) ambient temperature (22 °C) or (B) exposed to cold temperatures (4 °C). The resulting transcription events are shown below. Transcription start site 1 (TSS1) gives rise to *Adcy3*, which comprises Exons 1-22 (E1-E22). Transcription start site 2 (TSS2) gives rise to *Adcy3-at*, which comprises Exons 2b-22 (E2b-E22).

1.4.1 *Adcy3* dysfunction is a causal contributor in the pathogenesis of obesity and diabetes

Genome-wide association studies (GWAS) have singled out several genomic risk loci linked to adiposity related traits, such as the body-mass index (BMI). Among the most notable genomic risk loci are *fat mass and obesity-associated gene* (FTO), the *transcription factor 7-like 2* (TCF7L2) and the *melanocortin 4 receptor* (MC4R) (Goodarzi, 2018). However, single-nucleotide polymorphisms (SNPs) localized within these genomic risk loci explain only a small fraction of the BMI variation or exhibit unclear physiological significance (Locke et al., 2015; Tian et al., 2018). Using GWAS, Stergiakouli and colleagues investigated the association of SNPs with height-adjusted BMI and identified obesity-associated genomic risk loci in the *Adcy3* gene (Stergiakouli et al., 2014), providing a hint that *Adcy3* dysfunction might be implicated in an increased susceptibility to obesity. Furthermore, it was shown that several *Adcy3* loss-of-function mutations are associated with severe obesity in Greenlandic, Pakistani, and Cypriot populations (Grarup et al., 2018; Saeed et al., 2018; Toumba et al., 2022). Moreover, studies using genetically modified mice identified *Adcy3* dysfunction as a causal contributor in the pathogenesis of

obesity and diabetes (Pitman et al., 2014; Tian et al., 2018; Tong et al., 2016; Wang et al., 2009). This has recently been underlined by studies identifying *Adcy3* mutations in patients with monogenic severe obesity (Tian et al., 2018). Thus, there is a strong link between *Adcy3* dysfunction and the development of obesity. An additional role for *Adcy3* in controlling BAT function might provide a new link between obesity and cellular signaling in adipocytes.

1.4.2 AC3-AT lacks the majority of the first transmembrane domain

AC3 is a member of a family of ten related adenylyl cyclase isoforms. Isoforms AC1 to AC9 are transmembrane proteins (Ostrom et al., 2022), which typically consist of two clusters of six transmembrane domains separated by two intracellular catalytic domains (Bakalyar and Reed, 1990; Cali et al., 1994; Feinstein et al., 1991; Gao and Gilman, 1991; Glatt and Snyder, 1993; Ishikawa et al., 1992; Katsushika et al., 1992; Krupinski et al., 1992; Premont et al., 1992; Qi et al., 2019; Wallach et al., 1994; Yoshimura and Cooper, 1992). Membranous ACs are activated by $G_{\alpha s}$ and forskolin (Dessauer et al., 2017). There are four different families of membranous ACs: calmodulin-stimulated (AC1, AC3, and AC8) (Cooper, 2003; Ferguson and Storm, 2004), $G_{\beta\gamma}$- and Ca^{2+}- inhibitable (AC5, AC6 and AC9) (Cooper, 2003), $G_{\beta\gamma}$-stimulated and Ca^{2+}-insensitive (AC2, AC4 and AC7) (Cooper, 2003), and forskolin-insensitive (AC9) forms (Premont et al., 1996). AC10 is a soluble adenylyl cyclase that localizes in the cytoplasm and is unresponsive to G-protein stimulation (Hanoune and Defer, 2001). It functions as a cytoplasmic bicarbonate sensor (Chen et al., 2000).

The full-length AC3 (AC3-FL) is composed of 1144 amino acids. AC3-FL contains two transmembrane domains (TM1 and TM2), and the N and C termini are localized intracellularly. The two transmembrane domains are linked by a cytoplasmic loop, which encompasses the first catalytic domain (C1) with its subdomains C1a and C1b. TM2 is followed by a second cytoplasmic loop encompassing the second catalytic domain (C2) with its subdomains C2a and C2b (Dessauer et al., 2017).

A

```
mAC3-FL      mprnqgfsdpeysaeysaeysvslpsdpdrgvgrtheisvrnsgsclclprfmrltfvpe   60
mAC3-AT      ------------------------------------------------------------   0

mAC3-FL      slenlyqtyfkrqrhetllvlvvfaalfdcyvvvmcavvfssdklaplmvagfglvldii   120
mAC3-AT      ------------------------------------------------------------   0

mAC3-FL      lfvlckkgllpdrvsrkvvpyllwllisaqifsylglnfsrahaasdtvgwqaffvfsff   180
mAC3-AT      ----------------------------------------------------mwmgf------   5
                                                                  * .*

mAC3-FL      itlplslspiviisvvscvvhtlvlgvtvaqqqqdelegmqllreilanvflylcaiivg   240
mAC3-AT      ----------------------ltgelrvcqeaggrrnggrrslkilanvflylcaiivg   43
                                  *.  : *.*:  :. :* :   :***************
```

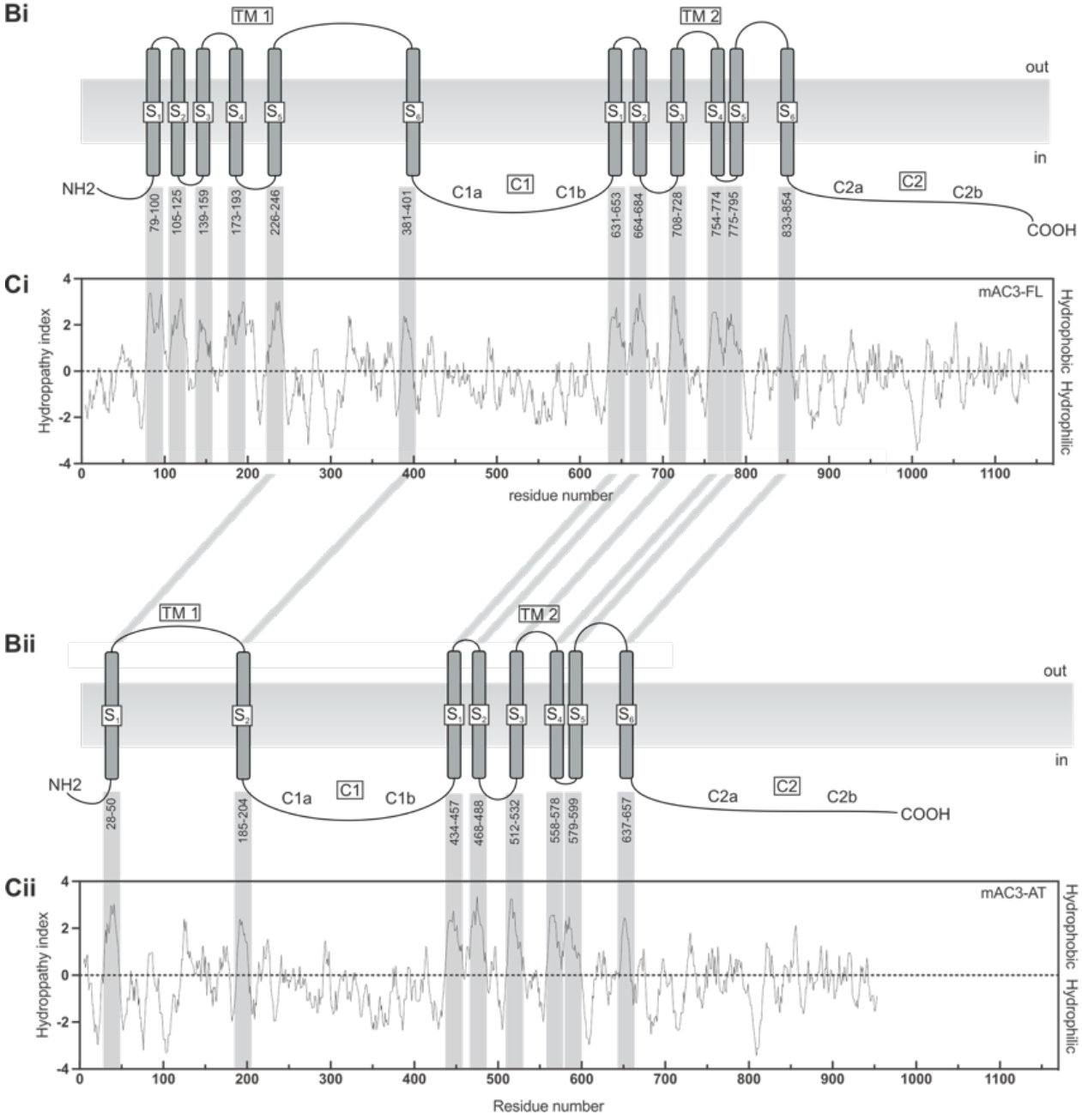

Figure 3: Alignment of the protein sequence AC3-FL *vs.* AC3-AT and Kyte-Doolittle plots of mAC3-FL and mAC3-AT protein sequences. A The N-terminus for both protein sequences has been aligned using Clustal Omega (EMBL-EBI). (identical amino acid residues are indicated with *, conserved with : or .). **B** Putative transmembrane segments (S_n) of AC3-FL **(Bi)** or AC3-AT **(Bii)** are indicated as grey boxes across the lipid bilayer. The position of amino acids predicted to be localized in a transmembrane segment is numbered underneath each box. The black line represents the amino acid chain of AC3-FL **(Bi)** or AC3-AT **(Bii)**. Cytoplasmic domains C1 and C2 with their respective subdomains C1a, C1b, and C2a, C2b following each transmembrane domain (TM) are indicated. **C** Kyte-Doolittle hydrophobicity plots of AC3-FL (primary accession number: Q8VHH7) **(Ci)** and AC3-AT **(Cii).** Each membrane-spanning domain is 21 residues in length. AC3-FL is predicted to have 2 TM with 6 transmembrane segments each (TM1: 79-100, 105-125, 139-159, 173-193, 226-246, 381-401, TM2: 631-653, 664-684, 708-728, 754-774, 775-795 and 833-853) and AC3-AT 2 TM, with TM1 consisting of 2 membrane-spanning segments (28-50, 185-204) and TM2 consisting of 6 membrane-spanning segments (434-457, 468-488, 512-532, 558-578, 579-599, 637-657). The represented data were obtained utilizing the ExPASy ProtScale analysis tool, using a window size of 9 residues, a window edge relative weight value of 100% and the linear weight variation model.

The N-terminally truncated AC3-AT is composed of 948 amino acids. At the N-terminus, the sequence of amino acids in AC3-AT is distinct from AC3-FL (**Figure 3 A**). According to Kyte-Doolittle topology prediction (**Figure 3 Cii**), AC3-AT exposes a cytosolic N-terminus followed by a transmembrane domain, which comprises only two membrane-spanning segments. The remaining part of the protein is identical to AC3-FL: the cytoplasmic loop containing the C1 catalytic domain, the TM2 domain, the cytoplasmic loop containing the C2 catalytic domain, and the intracellular C terminus (**Figure 3 B and C**).

1.5 Interaction of the transmembrane domain and protein dimerization is crucial for trafficking and functional assembly of adenylyl cyclases

According to structure prediction, AC3-AT contains a distinct intracellular N-terminus (**Figure 3 A**) followed by TM1, consisting of only two membrane-spanning segments, whereas AC3-FL contains an intracellular N-terminus followed by TM1, which encompasses a block of six membrane-spanning segments. Using AC truncations, it has been shown that the presence and interaction of both TM1 and TM2 are required for protein transport to the plasma membrane (Gu et al., 2001). As AC3-AT lacks the majority

of TM1, we hypothesize that the interaction between TM1 and TM2 is disturbed and, thereby, transport to the plasma membrane is impaired.

Furthermore, it is known that the cytosolic domains C1 and C2 must dimerize to form the interface for ATP-binding and, ultimately, the site for catalytic activity and regulation by G-proteins (Sunahara et al., 1996; Zhang et al., 1997). However, more recent studies show that the interaction between the two transmembrane domains TM1 and TM2 promotes the intramolecular dimerization of C1 and C2 (**Figure 4**) (Gu et al., 2001). Therefore, transmembrane adenylyl cyclases are activated when the two catalytic domains C1 and C2 interact, which is promoted by the interaction between the two transmembrane domains (Gu et al., 2001).

Physiologically, the C1 and C2 interaction is evoked when the G-protein subunit $G_{\alpha s}$ binds to the C1 subunit, promoting the interaction with C2. Pharmacologically, the interaction of C1 and C2 is stimulated by forskolin. AC3-AT contains both C1 and C2, but whether the structural conformation changes that are needed to promote C1-C2 interaction upon $G_{\alpha s}$ or forskolin stimulation are preserved in AC3-AT, particularly because the majority of the first transmembrane domain is missing, is not known. Even though AC3-AT contains both catalytic subunits, we hypothesize that its ability to synthesize cAMP is impaired because the majority of TM1 is missing.

Adenylyl cyclases form active proteins as dimers (**Figure 4**). It has been shown that they can form either homo- or heterodimers and that protein dimerization is crucial for transport from the ER to the plasma membrane (Baragli et al., 2008; Cooper and Crossthwaite, 2006; Ding et al., 2005; Gu et al., 2002; Gu et al., 2001). Dimerization is facilitated by intermolecular interaction via the hydrophobic domains, i.e., via TM2 (Gu et al., 2002).

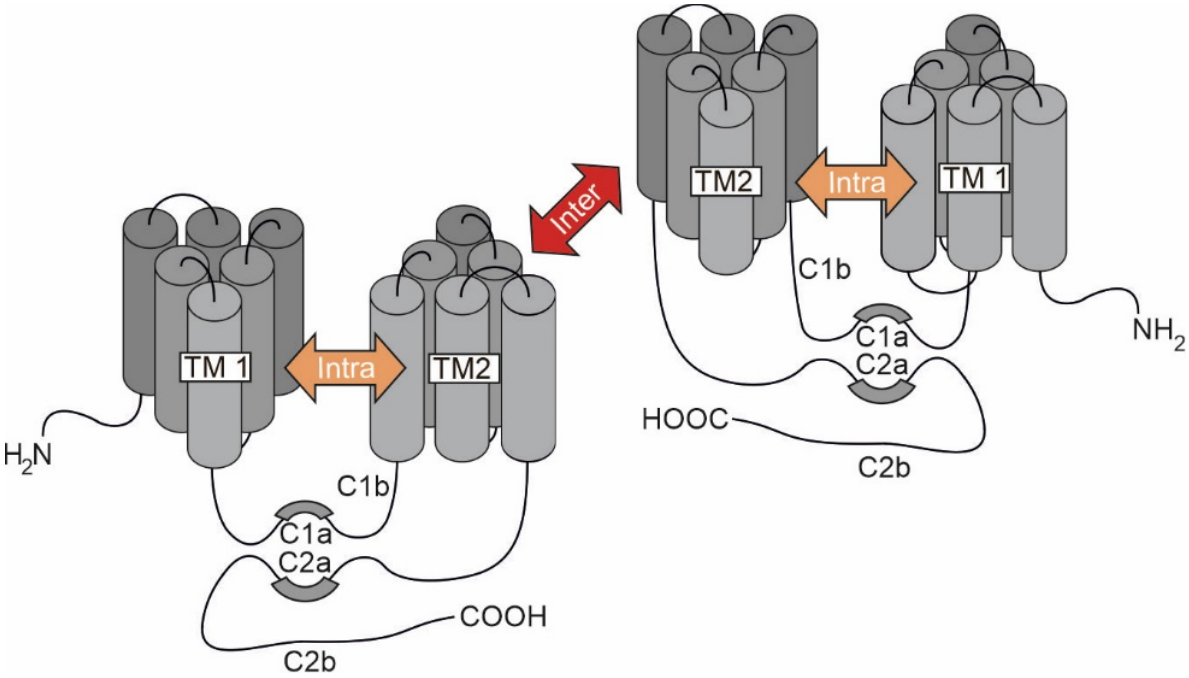

Figure 4: Intramolecular association and intermolecular interaction of adenylyl cyclases. Adapted from Cooper and Crossthwaite, Trends in Pharmalogical Sciences, 2006.

Gu and colleagues proposed that the full function of a dimeric arrangement necessitates the integrity of the entire complex, implying that an inactive subunit would have a detrimental impact on collective enzymatic activity in a dominant negative fashion. Therefore, Gu and colleagues engineered truncated mutants of *Adcy8* by deleting part of the C1 region. cAMP levels were measured in stimulated HEK293 cells, which were transfected with wild-type *Adcy8* only or co-transfected with both wild-type *Adcy8* and the *Adcy8* truncated mutant. It was shown that the presence of the truncated mutant suppressed the activity of wild-type AC8. This finding is congruent with the assembly of multimeric complexes of AC8 (Gu et al., 2002).

Whether the presence of AC3-AT exerts a similar effect on AC3-FL activity is not known. Based on these findings, we hypothesize that AC3-AT forms heterodimers with AC3-FL, which in turn affects the function of AC3-FL.

1.6 Aim of this thesis

How cold-induced *Adcy3-at* expression and function change cellular cAMP signaling and its role in regulating thermogenic signaling in BAT is not known. Therefore, I aimed to

1.) generate and characterize AC3-AT and AC3-FL-specific antibodies to verify expression in heterologous systems and ultimately protein expression pattern *in vivo,*

2.) determine the subcellular localization of AC3-AT and AC3-FL, and

3.) analyze AC3-AT and AC3-FL activity using cAMP fluorescent assays.

2. Materials and methods

All solutions were prepared using double-distilled water (ddH_2O). Sterile filtering of solutions was achieved by autoclavation for 20 min at 121 °C or using 0.22 µm pore filter membranes in a vacuum filtration.

2.1 Materials and reagents

2.1.1 Devices

The devices used for experiments performed in this thesis are shown in **Table 1**.

Table 1: Devices

Device	Manufacturer	Reference
3 mm (1/8“) Tapered Micro Tip	Sonics & Materials Inc., Newtown, USA	630-0418
Centrifuge 5425	Eppendorf AG, Hamburg Germany	5405IQ214642
Centrifuge 5430 R	Eppendorf AG, Hamburg Germany	5428JJ530672
Coupler	Sonics & Materials Inc., Newtown, USA	630-0421
Converter Model CV26	Sonics & Materials Inc., Newtown, USA	CV00026
CO_2 Incubator MCO-230AICUV	PHC Corporation, Tokyo, Germany	191060150
DynaMag™-Spin Magnetic Particle Concentrator	Invitrogen Dynal AS, Oslo, Norway	123.20D
EVOS™ FL	Thermo Fisher Scientific, Waltham, USA	AMF4300
FLUOstar® Omega	BMG Labtech GmbH, Ortenberg, Germany	S/N 415 2082
Freezer (-20 °C)	Liebherr International AG	n.a.
Fridge (4 °C)	Liebherr International AG	n.a.

Device	Manufacturer	Reference
Hinged spacer plates	Bio-Rad Laboratories, Hercules, USA	#1654173
Hot Plate A3	LABOTECT GmbH, Rosdorf, Germany	15668
Infors HT shaking incubator	Infors, Bottmingen, Switzerland	S-000133247-002
Mini-PROTEAN Tetra Cell System	Bio-Rad Laboratories, Hercules, USA	#1658001EDU
Mini-PROTEAN® Comb, 10 well, 1.5 mm thick, 66 µL	Bio-Rad Laboratories, Hercules, USA	#1653365
Mr. Frosty™ freezing container	Thermo Fisher Scientific, Waltham, USA	5100-0001
NanoDrop™ 2000 Spectrophotometer	Thermo Fisher Scientific, Waltham, USA	91-ND-2000
Neubauer counting chamber	Paul Marienfeld, Lauda-Königshofen, Germany	0640010
Power Supply EV Series EV2310	Carl Roth, Karlsruhe, Germany	A545.1
ROCKER 2D digital	IKA Werke GmbH, Staufen, Germany	100670258
Safety cabinet Scanlaf Mars 1200 Runner	LaboGene, Lillerod, Denmark	703620
Semi-dry blotter	Carl Roth, Karlsruhe, Germany	T788.1
SeroPAL™ Electronic Serological Pipette Controller	Luna Nanotech, Markham, Canada	SEP100S
Ultra Low Temperature Freezer MDF-DU502VHW-PE	PHC Corporation, Tokyo, Japan	19070257
Ultra-Low Temperature Freezer MDF-C2156VANW	PHC Corporation, Tokyo, Japan	19100105
Vibra-Cell™ High Intensity Ultrasonic Processor	Sonics & Materials Inc., Newtown, USA	432-0133

Device	Manufacturer	Reference
Vortex-Genie® 2	Scientific Industries, Inc., Bohemia, USA	2E5-254267
VWR® Tube Rotator with 36 X 1	Andwin Scientific, Tryon, USA	NC9854190
Water bath WBT 12	meding Lab, Freital Germany	2284719

2.1.2 Software

The software used for experiments performed in this thesis is shown in **Table 2**.

Table 2: Software

Software	Version	Supplier
BioRender	2023	Science Suite Inc., Toronto, Canada
CiliaQ Plugin	v0.1.5	Kindly provided by Jan Niklas Hansen
ClustalOmega	1.2.2	Des Higgins, Fabian Sievers, Conway Institute, UCD, Dublin, Ireland
CorelDraw	2023 (25)	Corel Corporation, Ottawa, Canada
EndNote X9	X9.3.3	Clarivate Analytics, London, UK
ExPasy - ProtScale	n.a.	SIB Swiss Institute of Bioinformatics, Lausanne, Switzerland
Fiji/ ImageJ	v2.3.051	Broad Institute, Inc., Cambridge, USA
GraphPad Prism 9	9.3.0	Dotmatics, Boston, USA
MotiQ Thresholder	n.a.	Kindly provided by Jan Niklas Hansen
Office 365	16.80	Microsoft Inc., Redmond, USA
SpermQ preparator Plugin	n.a.	Kindly provided by Jan Niklas Hansen

2.1.3 Consumables

The consumables used for experiments performed in this thesis are shown in **Table 3**.

Table 3: Consumables

Product	Company	Reference
0.22 µm filter membranes	Merck Millipore, Billerica, USA	GSWP02500
1 mL CryoTube™ vials	Thermo Fisher Scientific, Waltham, USA	377224
10 cm CELLSTAR® plasticware	Greiner bio-one, Kremsmünster, Austria	664 160
13 mm glass coverslips	Paul Marienfeld, Lauda-Königshofen, Germany	117530
24-well CELLSTAR® plasticware	Greiner bio-one, Kremsmünster, Austria	662 160
6-well CELLSTAR® plasticware	Greiner bio-one, Kremsmünster, Austria	657 160
96-well CELLSTAR® plasticware	Greiner bio-one, Kremsmünster, Austria	655 180
1.5 mL reaction tube with attached cap	Greiner bio-one, Kremsmünster, Austria	616201
2 mL reaction tube with attached cap	Greiner bio-one, Kremsmünster, Austria	623201
Falcon® conical tube 15 mL	VWR, Radnor, USA	734-0451
Falcon® conical tube 50 mL	VWR, Radnor, USA	734-0448
Nunc™ multiplate (4-well plate)	Thermo Fisher Scientific, Waltham, USA	176740
UltraCruz® cell scrapers (39 cm), sterile	Santa Cruz Biotechnology, Dallas, USA	sc-395250

2.1.4 Kits

The kits used for experiments performed in this thesis are shown in **Table 4**.

Table 4: Kits

Product	Company	Catalog #
CatchPoint™ cAMP Fluorescent Assay Kit	Molecular Devices, San Jose, USA	#R8089
NucleoBond® Xtra Midi	Macherey-Nagel, Düren, Germany	740410.100
Pierce™ BCA Protein Assay Kit	Thermo Scientific™	23225
Pierce™ Cell Surface Biotinylation and Isolation Kit	Thermo Scientific™	A44390

2.1.5 Reagents

The reagents used for experiments performed in this thesis are shown in **Table 5**.

Table 5: Reagents

Product	Manufacturer	Reference
2-Mercaptoethanol (β-ME)	Sigma Aldrich, St. Louis, USA	M3148-100ML
2-Propanol (Isopropanol)	Carl Roth, Karlsruhe, Germany	CN09.3
3-isobutyl-1-methylxantine (IBMX)	Applied biosystems, Waltham, USA	A0695
Acrylamide 4K solution	Applied biosystems, Waltham, USA	A1672,0500
Ammonium persulfate (APS)	Sigma Aldrich, St. Louis, USA	A3678
Aqua-Poly/ Mount	Tebi-Bio, Le Perray-en-Yvelines, France	#07918606-20
Bromphenolblue	Sigma Aldrich, St. Louis, USA	B0126

Product	Manufacturer	Reference
Bovine serum albumin (BSA)	Thermo Fisher Scientific, Waltham, USA	B14
Calcium chloride ($CaCl_2$)	Carl Roth, Karlsruhe, Germany	CN93.1
ChemiBlocker	Merck Millipore, Billerica, USA	2170
Dimethyl Sulfoxide (DMSO)	Sigma Aldrich, St. Louis, USA	D45450
Disodium hydrogen phosphate (Na_2HPO_4)	Merck Millipore, Billerica, USA	119753
Dithiothreitol (DTT)	Sigma Aldrich, St. Louis, USA	43815
Dulbecco's phosphate-buffered saline (DPBS)	Gibco, Amarillo, USA	14190-094
Egtazic acid (EGTA)	Sigma Aldrich, St. Louis, USA	324626
Ethanol (EtOH)	Carl Roth, Karlsruhe, Germany	P075.5
Ethylene diamine tetra acetic acid (EDTA)	Sigma Aldrich, St. Louis., USA	E5134
Forskolin	Sigma Aldrich, St. Louis, USA	# SLBP3308V
G418 (Geneticin)	Thermo Fisher Scientific, Waltham, USA	11811
Glucose	Carl Roth, Karlsruhe, Germany	X997.2
Glutamic acid monopotassium salt monohydrate ($C_5H_8KNO_4$)	Sigma Aldrich, St. Louis, USA	G1501-100G
Glycerol	Sigma Aldrich, St. Louis, USA	G2289
Glycine for molecular biology	applied biosystems, Waltham, USA	A1067,5000

Product	Manufacturer	Reference
HEPES	Carl Roth, Karlsruhe, Germany	X997.2
Hydrogen peroxide (H_2O_2)	Carl Roth, Karlsruhe, Germany	0034.1
Isoprenaline hydrochloride (Isoproterenol)	Sigma Aldrich, St. Louis, USA	I5627
Magnesium chloride ($MgCl_2$)	Carl Roth, Karlsruhe, Germany	KK36.2
Methanol (MeOH)	Carl Roth, Karlsruhe, Germany	8388.6
Monosodium phosphate (NaH_2PO_4)	Sigma Aldrich, St. Louis, USA	S3139
Nonidet® P40 (NP-40)	Thermo Fisher Scientific, Waltham, USA	PIER85124
Paraformaldehyde, 16% w/v aq. Solvent, methanol free (PFA)	Alfa Aesar, Landau, Germany	43368
Poly-L-Lysine Hydrochloride (PLL)	Sigma Aldrich, St. Louis, USA	P1399
Potassium acetate ($C_2H_3KO_2$)	Sigma Aldrich, St. Louis, USA	529543
Potassium chloride (KCl)	Carl Roth, Karlsruhe, Germany	P017.2
Potassium dihydrogen phosphate (KH_2PO_4)	Carl Roth, Karlsruhe, Germany	3904.2
Sodium chloride (NaCl)	Carl Roth, Karlsruhe, Germany	HN00.2
Sodium hydroxide (NaOH)	Carl Roth, Karlsruhe, Germany	6771.1
Sodium dodecylsulfate (SDS), pellets	Carl Roth, Karlsruhe, Germany	8029.4
Sodium Pyruvate 100 mM (100x)	Gibco, Amarillo, USA	11360-039

Product	Manufacturer	Reference
TEMED	Applied biosystems, Waltham, USA	A1148
Tris-base	Merck Millipore, Billerica, USA	648310-M
Tris-HCl	Carl Roth, Karlsruhe, Germany	9090.3
Triton-X100	Applied biosystems, Waltham, USA	3051.3
Trypsin-EDTA (0.05%)	Gibco, Amarillo, USA	25300062
Tween® 20	Sigma Aldrich, St. Louis, USA	P9416

2.1.6 Cell culture materials

The cell culture materials used for experiments performed in this thesis are shown in **Table 6**.

Table 6: Cell culture material

Product	Manufacturer	Reference
Dulbecco's Modified Eagle Medium F-12 Nutrient Mixture (Ham)	Gibco, Amarillo, USA	31331-028
Fetal Bovine Serum (FCS)	BIOCHROM, Berlin, Germany	S 0115
Lipofectamine™ 2000 Reagent	Invitrogen, Waltham, USA	11668-027
MEM GlutaMAX™ Supplement	Gibco, Amarillo, USA	41090036
MEM Non-Essential Amino Acids Solution (NEAA) (100x)	Gibco, Amarillo, USA	11140-035
Opti-MEM® Reduced Serum Medium	Gibco, Amarillo, USA	11058-021
PBS, pH 7.4	Thermo Fisher Scientific, Waltham, USA	10010023
Polyethylenimine (PEI)	Sigma Aldrich, St. Louis, USA	408727

2.1.7 Antibodies

2.1.7.1 Primary antibodies

The following primary antibodies were used for immunocytochemical staining (ICC) and Western blot analysis (WB). (**Table 7**).

Table 7: Primary antibodies used for ICC and WB analysis

Antibody	kDa	Species	Type	Dilution		Producer	Reference
				ICC	WB		
β-Tubulin 2.1	55	ms	mAb	-	1:10000	Sigma	T4026
AC3 (C Terminus)	130	rb	pAb	1:200	1:500	Thermo Scientific	PA5-35382
AC3 (N Terminus)	130	rt	mAb	1:200	-	Kindly provided by Heinz Gerd Körschen	n.s.
Calnexin	90	rb	pAb	1:500	-	Sigma	C4731
Calnexin	90	ms	mAb	1:500	-	Abcam	ab31290
CRO 3B10	76	ms	mAb	1:100	1:500	Kindly provided by Heinz Gerd Körschen	n.s.
Flag M2	-	ms	mAb	-	1:1000	Sigma	F1804
HA (R001 3F10)	-	rt	mAb	1:1000	1:5000	EKr	n.s.
KOR-AEY2	130	rb	pAb	1:500	1:2000	Davids Biotechnologie	n.s.
RFP	-	rb	pAb	-	1:1000	Rockland Inc.	600-401-379

2.1.8 Secondary antibodies

The following secondary antibodies were used for immunocytochemical staining (ICC) and Western blot analysis (WB) (**Table 8**).

Table 8: Secondary antibodies used for ICC and WB analysis

Antigen	Antibody	Species	Type	Dilution		Producer	Catalog #
				ICC	WB		
ms	ms Alexa 488	gt	pAb	1:400	-	Thermo Scientific	A11029
ms	ms Cy 3	dk	pAb	1:500	-	Dianova	715-155-151
ms	ms Cy 5	dk	pAb	1:500	-	Dianova	715-175-151
ms	IRDye 680RD	dk	pAb	-	1:20,000	LI-COR Biosciences	926-68072
ms	IRDye 800CW	dk	pAb	-	1:20,000	LI-COR Biosciences	926-32212
rb	rb Alexa 488	gt	pAb	1:500	-	Thermo Scientific	A11034
rb	rb Alexa 647	dk	pAb	1:500	-	Dianova	711-605-152
rb	rb Cy 3	dk	pAb	1:250	-	Dianova	711-165-152
rb	IRDye 680RD	dk	pAb	-	1:20,000	LI-COR Biosciences	926-32223
rb	IRDye 800CW	dk	pAb	-	1:20,000	LI-COR Biosciences	926-32213
rt	rt Alexa 488	dk	pAb	1:500	-	Dianova	712-545-153
rt	IRDye 680 LT	gt	pAb	-	1:20,000	LI-COR Biosciences	926-32229

Antigen	Antibody	Species	Type	Dilution		Producer	Catalog #
rt	IRDye 800CW	gt	pAb	-	1:20,000	LI-COR Biosciences	926-32219

2.1.9 Fluorescent dyes

The following fluorescent dye was used for immunocytochemistry (ICC) (**Table 9**).

Table 9: Dyes used for ICC

Dye	Dilution	Producer	Catalog #
4',6-Diamidino-2-Phenylindol (DAPI)	1:10000	Life Technologies, Thermo Fisher Scientific, Waltham, USA	D1306

2.2 Escherichia coli culture

2.2.1 *Escherichia coli* strains

The *Escherichia coli* (*E. coli*) strain XL1-Blue (#200249, Stratagene, California, USA) was used for cloning.

2.2.2 Generation of competent *E. coli* cells

E. coli transformation via $CaCl_2$ was carried out following an adapted protocol derived from the method described by Mandel and Higa (1970). The *E. coli* cells were grown in a flask with 50 mL Lysogeny broth (LB)-medium (Carl Roth, Karlsruhe, Germany, X968.1) in a shaking incubator at 37 °C. Once the culture attained an optical density (OD) of 0.4 at 600 nm, equivalent to a cell density of 2 x 10^8 cells/ mL, the E. coli cells were placed on ice for 30 minutes before being centrifuged at 5,000 x g for 10 min at 4 °C. After the LB-medium was poured off, the remaining pellet was resuspended in 5 mL ice-cold 0.1 M $CaCl_2$ containing 25 % glycerol (v/v). After an incubation time of 2 h on ice, the cells were distributed in 100 µL aliquots into 1.5 mL tubes, then snap-frozen with liquid nitrogen, and stored at -80 °C until further use.

2.2.3 Transformation of competent *E. coli* cells using $CaCl_2$

1 µL of plasmid DNA was mixed with 5 µL 10x CM buffer (100 mM $CaCl_2$/ 400 mM $MgCl_2$). The mixture was filled up to 50 µL with ddH_2O. 50 µL competent *E. coli* cells were thawed on ice and mixed with DNA. While the mixture was incubated on ice for 20 min, a H_2O water bath was set to reach 42 °C and LB medium was placed in the bath to warm up. Subsequently, the cells were placed for 1 min in the water bath at 42 °C. After the heat-shock, the cells were immediately put back on ice for 10 min. Subsequently, 150 µL of room temperature LB-medium without antibiotics was added to the cells, which were then regenerated for 30 to 45 min at 37 °C on a shaker. The bacterial suspension was then plated on LB-Agar plates containing the appropriate antibiotic (100 µg/ mL ampicillin, Sigma Aldrich, St. Louis, USA, A5354). The plates were incubated overnight at 37 °C. The following morning, single colonies were picked and incubated in 5 mL LB-medium at 37 °C on an orbital shaker.

2.2.4 Small-scale (Mini) plasmid preparation via alkaline extraction method

The transformed bacteria were employed for the extraction of amplified plasmids using alkaline lysis in a Mini prep according to the protocol of Birnboim and Doly (1979). 1.5 mL of the overnight culture was transferred to a fresh Eppendorf tube and centrifuged for 30 to 60 sec at 20,000 x g at RT. The supernatant was removed, and the pellet was resuspended in solution I (**Table 10**) by vortexing or vigorous pipetting. Next, 60 µL solution II (**Table 10**) was added and mixed by gently vortexing the tube to lyse the cells. Subsequently, 75 µL solution III (**Table 10**) was added and mixed by gently vortexing the tube to denature the proteins. The sample was centrifuged for 5 to 7 min at 17,600 x g at 4 °C. The supernatant was carefully transferred to a fresh Eppendorf tube. The plasmid DNA was precipitated by adding 550 µL 100 % ethanol. The solution was centrifuged for 2 to 3 min at 17,600 x g at 4 °C and the pellet was washed with 500 µL 70 % ethanol. After centrifugation, the ethanol was removed, and the DNA pellet was allowed to dry shortly at 37 °C. The DNA pellet was then dissolved in 20 µL TE buffer. To verify amplification of the plasmid DNA and plasmid integrity, a test digest was performed via agarose gel electrophoresis.

Table 10: Solutions used for alkaline lysis of bacteria to isolate plasmid DNA

Solution I	Solution II	Solution III
25 mM Tris/ HCl pH 8.0	0.2 M NaOH	3 M CH_3CO_2K pH 4.8
10 mM EDTA	1% (w/v) SDS	
50 mM glucose		

2.2.5 Large-scale (Midi) plasmid DNA preparation

Plasmid DNA extractions from *E. coli* cultures were conducted utilizing the NucleoBond™ Xtra Midi kit according to the manufacturer's protocol. For Midi preparation from a 5 mL overnight culture, the *E. coli* cells were pelleted by centrifugation at 6,000 x g for 15 min at 4 °C and the supernatant was discarded completely. The cell pellet was then resuspended by pipetting the cells up and down or vortexing in 8 mL resuspension buffer supplemented with RNase A, ensuring that no clumps remained in the suspension. The cells were lysed by adding 8 mL of lysis buffer to the suspension and the mixture was incubated for 5 min at room temperature (RT). The column filter was then equilibrated by applying 12 mL equilibration buffer onto the rim of the column filter in a circular motion. The column was allowed to empty by gravity flow. Next, 8 mL neutralization buffer was added to the suspension and immediately loaded onto the equilibrated filter column and the column was allowed to empty by gravity flow. The column was washed by applying 5 mL equilibration buffer onto the rim of the column filter in a circular motion. After the filter was removed from the column, a second washing step was performed by adding 8 mL wash buffer. The plasmid DNA was recovered by adding 5 mL elution buffer, precipitated through addition of 3.5 mL RT isopropanol, which was followed by thorough vortexing. Next, the precipitate was centrifuged at 15,000 x g for 45 min at 4 °C and washed once with RT ethanol (70 %). The suspension was then centrifuged at 15,000 x g for 10 to 15 min at RT. The ethanol was carefully removed completely, and the pellet was air-dried at RT. The DNA pellet was then dissolved in an appropriate volume of TE buffer. To verify amplification of the plasmid DNA and plasmid integrity a test digest was performed via agarose gel electrophoresis.

2.3 Mammalian cell culture

2.3.1 Buffers and media used for cell culture

The cell lines used and their respective culture media are listed in **Table 11**. Cells were managed in safety cabinets under sterile conditions for both maintenance and transfection procedures. All cell lines were cultured on 10 cm or 6-well plates, maintained in medium containing 10 % FCS, and kept in an incubator under conditions of 5 % CO_2 and 37 °C at 95 % humidity.

Table 11: Cell lines

Cell line	Producer	Reference	Growth medium
CHO K1	European Collection of Cell cultures	85051005	F12 + 10 % FCS
CHO K1 AC3-FL-HA	Lara-Marie Vagliano (generated during this study)	n.s.	F12 + 10 % FCS
CHO K1 AC3-AT-HA	Lara-Marie Vagliano (generated during this study)	n.s.	F12 + 10 % FCS
CHO mCherryCAAX	Kindly provided by Lea Wobig	n.s.	F12 + 10 % FCS
CHO TM	Sibion biosciences GmbH	0906001TM	F12 + 10 % FCS
HEK-293	American Type Culture Collection (ATCC)	CRL1573	MEM Glutamax 10 % FCS 1 % NEAA (x100)

For subculture routine, sub-confluent cultures (70-80 %) were split twice a week according to the following protocol: Cultured cells were washed once with 5 mL phosphate buffered saline (PBS; **Table 12**) and detached from the plate floor by incubation with 1 mL Trypsin (0.05 % + EDTA) for 5-10 min on a hot plate at 37 °C. Trypsinization was stopped by adding 9 mL growth medium. Then, cell counting was conducted by adding Trypan Blue Stain (0.4 %) (Gibco, Amarillo, USA, 15250-061) and utilizing a Neubauer counting chamber. Cultured cells were seeded at a dilution depending on the growth speed of the respective cell line. Cells older than passage 15 were discarded.

Table 12: Phosphate buffered saline (PBS)

PBS
137 mM NaCl
2.7 mM KCl
6.5 mM Na_2HPO_4
1.5 mM KH_2PO_4
adjust to pH 7.4
sterilize by autoclaving

2.3.2 Cell freezing

To preserve cells for long-term storage, cultured cells were cryopreserved in their respective media supplemented with 10 % dimethyl sulfoxide (DMSO) following the outlined protocol: Cultured cells were washed with PBS and trypsinized, as described above. $1*10^6$ cells were centrifuged at 300 x g for 5 min to obtain a cell pellet. The supernatant was aspirated, and the cell pellet was resuspended in 1 mL DMSO-containing culture medium. The cell suspension was then transferred to a cryotube. The vials were placed inside a freezing container and frozen at -80°C overnight, with a steady temperature decrease of 1 °C per minute. The following morning, the cryotubes were transferred to liquid nitrogen cell storage (-196 °C) for long-term preservation.

2.3.3 Cell recovery

Thawing of 1 mL frozen cell suspension in cryotubes was carried out at 37 °C in a water bath, followed by direct transfer into a Falcon tube containing 20 mL pre-warmed cell culture medium. To eliminate DMSO, cells were centrifuged at 300 x g for 5 minutes at RT. The resulting pellet was resuspended in 20 mL cell culture medium and evenly distributed across two 10 cm cell culture dishes for maintenance. The cells were allowed to attach for one day in an incubator at 37 °C with 5 % CO_2, and then their medium was replaced with fresh, complete medium.

2.3.4 Transient transfection using polyethyleneimine

To achieve transient transfection using polyethyleneimine, the cells were plated one day prior to transfection to ensure they reached 90 % confluency at the time of transfection. For each transfection sample, as indicated in **Table 13,** plasmid DNA was diluted in Opti-MEM® Reduced Serum Medium in a fresh Eppendorf tube. For each transfection sample, as indicated in **Table 13**, branched polyethyleneimine (PEI) stock (1 µg/µL) was added to obtain a final concentration of 20 ng PEI per µL OptiMem. The mixture was incubated for 10 min at RT. The cell culture medium was replaced by the respective medium, which contained only 2 % FCS instead of 10 % FCS. After incubation, the DNA/PEI mix was added dropwise to the plate/ well, and cells were maintained at 37 °C/5 %-CO_2 for 24 to 48 h before analysis.

Table 13: Pipetting scheme for transient transfection using PEI

Culture vessel	Surface area per well (cm^2)	DNA (µg)	OptiMem (µL)	PEI (µg)	Volume of plating medium (µL)
4-well	2	0.5	50	1	200
6-well	10	2.35	235	5	940
5 cm	20	4.5	450	9	1800
10 cm	60	9.5	950	19	3800

2.3.5 Transient transfection using Lipofectamine™ 2000

To achieve transient transfection using Lipofectamine™ 2000, cells were seeded on a plate one day prior to transfection to ensure 90-95 % confluency at the time of transfection. For each transfection sample, as indicated in **Table 14**, DNA and Lipofectamine™ 2000 were diluted in Opti-MEM® Reduced Serum Medium, separately. After gentle mixing and an incubation time of 5 min at RT, the diluted Lipofectamine™ 2000 was combined with the diluted DNA. This mixture was incubated for 20 min at RT and then added to the cells. After incubation for 4-6 h at 37 °C/5 % CO_2 the growth medium was replaced with fresh, complete medium.

Table 14: Pipetting scheme for transient transfection using Lipofectamine™ 2000

Culture vessel	Surface area per well (cm^2)	Volume of plating medium (µL)	DNA (µg) and dilution volume (µL)	Lipofectamine™ 2000 (µg) and dilution volume (µL)
96-well	0.3	100	0.2 in 25	0.25 in 25
4-well	2	500	0.8 in 50	1.0 in 50
5 cm	20	5000	0.2 in 25	10 in 500
10 cm	60	15000	0.2 in 25	30 in 1.500

2.3.6 Generation of stable cell lines

For generating stable cell lines expressing AC3-FL-HA or AC3-AT-HA, initially CHO-K1 cells were transiently transfected using PEI, as described above, with a mammalian expression vector pcDNA3.1(+) containing a cytomegalovirus (CMV) promotor, a Kozak consensus sequence, an HA-tagged *Adcy3-fl* or *Adcy3-at*, and a neoR selective resistance gene (neomycin resistance, neoR). In the morning preceding the experiment $1.5x10^5$ cells were seeded onto a 5 cm plate. As a control, a 5 cm plate with non-transfected (NT) cells was also included in the forthcoming selection process.

One day after transfection, the cells were harvested by trypsinization. The obtained cell suspension was seeded at dilutions of 1:10, 1:100, and 1:1000 in fresh 10 cm plates. 24 h later the selection for transfected cells with the antibiotic G418 (geneticin, selection concentration: 1200 ng/ml) was started. G418 is an aminoglycoside antibiotic that acts by blocking translational elongation. The neomycin resistance in the transfected vector encodes for an aminoglycoside phosphotransferase that can oppress the action of the geneticin by phosphorylating it. Thereby, if the vector is successfully introduced into the cells, the cells can become G-418-resistant cells.

After starting the selection process, the medium of the cells was changed every 2-3 days to maintain the concentration of G418 and to remove dead cells. The non-transfected cells mostly died off in the course of two weeks after starting the selection. After approximately

2 weeks, the initially transfected cells were harvested, and only 20 and 200 cells were seeded onto fresh 10 cm plates. The cells were kept in a medium containing 1200 ng/ml of G418. The colonies forming on these plates were then picked and tested for the expression of the respective protein in Western blot analysis (WB) and immunocytochemistry (ICC).

2.3.7 Poly-L-lysine coating of glass coverslips

To optimize cell adhesion, cover slips (13 mm) were coated with poly-L-lysine (PLL). Cover slips were placed in a multi-well plate (4-well plate). 500 µL of 0.1 mg/mL PLL per well was added. After 30 min of incubation at RT, the wells were washed once with PBS. After aspirating the PBS, the coated glass cover slips were either used directly and cells were seeded onto the cover slip or the coated glass cover slips were stored in the dark at 4 °C until further usage.

2.4 Immunocytochemistry

2.4.1 Fixation of cells

For fixation of the cells, the medium was removed, cells were washed with PBS, and fixed with paraformaldehyde (PFA) for 10 min at RT. To remove the PFA, fixed cells or cell-free plasma membrane sheets were washed three times in PBS and either stored at 4 °C in PBS until further usage or directly used for immunocytochemical staining.

2.4.2 Immunocytochemical staining

Samples that did not undergo ultrasound treatment were blocked in 5 % Chemiblocker / 0.5 % TritonX-100 in PBS for 30 min; sonicated samples were blocked in 5 % Chemiblocker in PBS. The sample was then incubated for 60 min with the primary antibody prepared in the respective blocking solution. After the removal of the primary antibody, the cells were washed three times with PBS. The sample was then incubated for 45 min in the dark with the secondary antibody, which was prepared in the respective blocking solution in addition to DAPI (1:10.000 of 5 µg/µL stock in H_2O). After washing the sample three times in PBS, the coverslip was mounted with Aqua Poly/Mount. Slides were

then stored at 4 °C for at least 12 h. Imaging was conducted utilizing one of the following confocal laser scanning microscopes: Olympus FV1000, Nikon Eclipse Ti, or Leica SP8 with Lightning. All procedures were carried out at RT.

2.4.3 Preparation of cell-free plasma membrane sheets

One day after transfection, medium was removed from cells and ice-cold sonication (**Table 15**) buffer was added. The cells were kept on ice until sonification. The coverslips were transferred from the wells to a glass bowl containing 5 mL of ice-cold sonication buffer, which was prepared according to the protocol established by Sieber et al. (2006). The high-intensity ultrasonic processor was assembled by adding a tapered microtip of 3 mm diameter to the coupler-converter assembly. To ensure maximum energy transfer, the sonication device was tuned beforehand. The distance from the coverslip to the end of the microtip was set to 3 mm. Cells were then subjected to ultrasound treatment by applying up to three 100 ms ultrasound pulses of 10-25 % intensity, depending on the type and the confluency of the cells grown on the coverslip. After sonication, a cell-free crater on the coverslip was clearly visible.

Table 15: Sonication buffer used for generating cell free plasma membrane sheets

1x Sonication buffer
120 mM $C_5H_8KNO_4$
20 mM CH_3CO_2K
10 mM HEPES
10 mM EGTA
adjust to pH 7.2

2.4.4 Quantification of fluorescence intensity in cell-free plasma membrane sheets

Analysis of fluorescence intensity in cell-free plasma membrane sheets was performed using custom-written ImageJ plugins (designed by Jan Niklas Hansen) for user-dependent membrane sheet selection, image segmentation, and quantification. To avoid preferential selection, membrane Sheets were selected for analysis in the mCherryCaaX image. First, a Gaussian blur (σ = 2) was performed on the original mCherryCaaX (basal plasma

membrane sheet) image and Calnexin (ER-membrane) image (using the SpermQ Preparator plugin (Hansen et al., 2018)). mCherryCaaX or Calnexin images derived from the previous step were automatically segmented to binary images by application of an intensity threshold, which was calculated ("Huang"- or "Otsu" -algorithm, respectively, using MotiQ Thresholder (Hansen et al., 2022)) individually for each membrane sheet. Binary single-cell images obtained in the previous step were then semi-automatically subtracted, using the Image Calculator, ImageJ ($BIN(mCherryCAAX) - BIN(Calnexin)$). The average fluorescence intensity of the HA image was then analyzed (using the CiliaQ plugin (Hansen et al., 2021)) within the 16-bit converted mask.

2.5 Protein biochemistry

2.5.1 Protein lysates of cultured cells

Transfected cells were washed once with 5 mL PBS. Utilizing a cell scraper, cells were harvested from either a 10 cm plate or a 5 cm plate in either 3 mL or 1 mL PBS, respectively. Then, the cells were centrifuged at 500 g for 3 min at 4 °C. The cell pellet was resuspended in total lysis buffer (**Table 16**) containing a mammalian protease inhibitor cocktail (mPic, Sigma Aldrich, St. Louis, USA, P8340-1ML) in a 1:500 dilution. Depending on the size of the cell pellet, the amount of total lysis buffer added varied between 50 µL and 200 µL. Cells were lysed for 30 min at 4 °C. After centrifugation at 10.000 x g for 10 min at 4 °C the supernatant containing the solubilized protein was transferred to a fresh tube and stored at 4 °C. Protein concentration was determined in a bicinchoninic (BCA) test.

Table 16: Total lysis buffer used for cell lysis

1x Total lysis buffer
10 mM Tris/ HCl pH 7.6
140 mM NaCl
1 mM EDTA
1% (v/v) TritonX-100
1:500 mPic

2.5.2 Bicinchinonic (BCA) test

The Pierce® bicinchoninic (BCA) Protein Assay Kit was used for detection and quantitation of total protein, determined by a color change of the sample solution from green to purple, which is proportional to the concentration of protein in the sample. This assay combines two reactions. In an alkaline BCA solution, the peptide bonds of proteins in the sample reduce Cu^{2+} ions from copper (II) sulfate, which is contained in the BCA solution, to Cu^{+}. Then, two molecules of BCA chelate with one Cu^{+}. This purple-colored complex absorbs light at a wavelength of 562 nm.

A bovine serum albumin (BSA) dilution series ranging from 0.125 µg/ µL to 2 µg/µL was included in the assay serving as a protein standard for forthcoming interpolation of the protein concentration of each sample. 1:10 and 1:20 dilutions of the sample in total lysis buffer were prepared. Next, 10 µL of the diluted sample or standard were, in duplicates, inserted into each well on a 96-well plate. BCA reagent B was added to reagent A at a dilution of 1:50 and 190 µL of diluted BCA solution was inserted into each well. After 30 min of incubation at 37 °C, the absorption at 562 nm was measured in the FluoStar plate reader. The absorption values of the standard were plotted against the respective standard concentration to create a standard curve. The absorption values of the unknown sample were then interpolated using this curve to calculate protein concentrations in the sample.

2.5.3 SDS-Page

2.5.3.1 SDS-Gels

Electrophoretic separation of proteins according to their molecular weight was achieved via denaturing sodium dodecyl sulfate (SDS) polyacrylamide gel electrophoresis (PAGE). The separating gel (10 % or 12.5 %) and stacking gel (5 %), were prepared according to the pipetting scheme shown in **Table 17**. SDS sample buffer was added to protein samples (diluted to 1x; **Table 18**). If not stated otherwise, boiling at 95 °C for 5 min was omitted. Electrophoretic separation was performed at a current of 15 mA per gel in a minigel chamber filled with SDS running buffer (diluted to 1x; **Table 18**).

Table 17: Pipetting scheme to cast gels for SDS-PAGE

Component	Stacking gel (5 %)	Separating gel (10 %)	Separating gel (12.5 %)
1.5 M Tris/ HCl	0.5 mL (pH 6.8)	1.5 mL (pH 8.8)	1.5 mL (pH 8.8)
10% SDS	20 µL	60 µL	60 µL
10% APS	40 µL	40 µL	40 µL
TEMED	3.5 µL	4 µL	4 µL
Acrylamide/ Bisacrylamide 30% solution (37.5:1)	340 µL	2 mL	2.5 mL
ddH_2O	1.12 mL	2.42 mL	1.95 mL

Table 18: SDS sample buffer and SDS running buffer

SDS sample buffer (4x)	SDS running buffer (20x)
200 mM Tris/ HCl pH 6.8	250 mM Tris
8 % (w/v) SDS	1 % SDS
5 % (v/v) β-mercaptoethanol	1.92 M glycine
50 % (v/v) glycerol	
0.04 % (w/v) bromphenol blue	

2.5.3.2 Protein marker

5-10 µL of prestained AppliChem VI (11-245 kDa) protein ladder (AppliChem, Darmstadt, Germany, A8889) were loaded per lane as a protein standard, against which to measure the molecular weight of the respective protein.

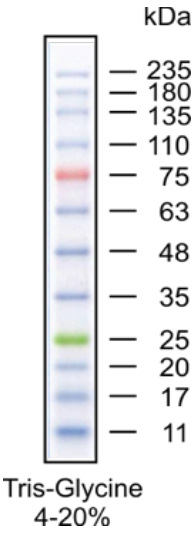

Figure 5: Protein standards used for SDS-PAGE. Images were taken and modified from the A8889 data sheet (AppliChem).

2.5.3.3 Western blot analysis

Proteins separated by SDS-PAGE were transferred onto a polyvinylidene difluoride membrane (PVDF membrane Immobilon-P, Merck Millipore, Billerica, USA, IPFL00010) via traditional semi-dry Western blotting. For the electrophoretic protein transfer, the membrane was activated in methanol (MeOH) first and then stripped in anode buffer II (**Table 19**). The SDS-gel and PVDF membrane were placed between filter papers, which were stripped in either anode buffer I, anode buffer II, or cathode buffer (**Table 19**), and stacked in a specific order, which is shown in **Figure 6.** The stacked transfer components were then inserted between flat-plate electrodes. A current of 2.4 mA was applied per cm^2 PVDF membrane (8 x 9 cm PVDF membrane) for 50 minutes in total.

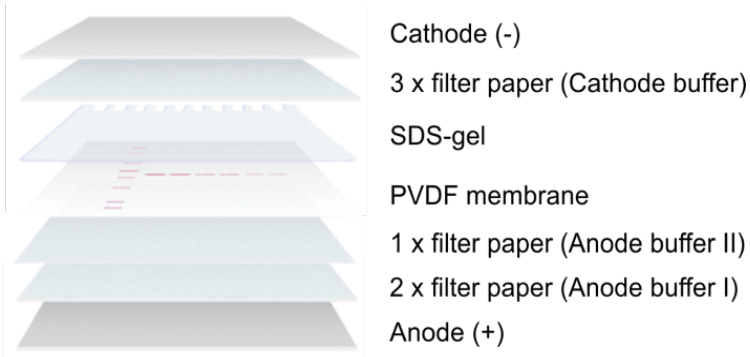

Figure 6: Setup for electrophoretic protein transfer. Image modified from: BioRad Protein Blotting Methods – Electrophoretic transfer setup.

Table 19: Buffers used for protein transfer onto PVDF membranes

Anode buffer I	Anode buffer II	Cathode buffer
0.3 M Tris pH 10.4	25 mM Tris pH 10.4	25 mM Tris pH 9.4
20 % (v/v) MeOH	20 % (v/v) MeOH	20 % (v/v) MeOH
		0.04 M glycerin

2.5.3.4 Immunostaining of immobilized proteins

Before blocking unspecific binding sites, the membrane was activated in MeOH and washed in PBS (**Table 20**). Blocking was performed using a blocking solution containing Odyssey® blocking buffer (LI-COR Biosciences, Lincoln, USA 927-40000) for 30 min at RT. The membrane was then incubated overnight at 4 °C or for 1 h at room temperature with the primary antibody directed against the protein of interest. The primary antibody was prepared in a blocking solution (**Table 21**). Next, the non-bound antibody was removed by washing the membrane thrice for 20 min in 10 mL PBS-T (**Table 20**) at RT. The membrane was then incubated for 1 h at RT with the secondary antibody prepared in blocking solution (**Table 21**). The specificity of the secondary antibody was chosen depending on the species in which the primary antibody was generated. Again, the non-bound antibody was removed by washing the membrane thrice for 20 min in 10 mL PBS-T. Then the membrane was transferred to 10 mL PBS for 2 x 5 min.

Table 20: PBS and PBS-T washing buffer for immunostaining of immobilized proteins

PBS washing buffer (1x)	PBS-T washing buffer (1x)
130 mM NaCl	PBS washing buffer
7 mM Na_2HPO_4	0.05 % (v/v) Tween 20
3 mM NaH_2PO_4	
adjust to pH 7.4	
sterilize by autoclaving	

Table 21: Blocking solutions for primary and secondary antibody

Blocking solution: primary antibody	Blocking solution: secondary antibody
PBS-T washing buffer	PBS-T washing buffer
50 % (v/v) Odyssee Blocking Buffer (PBS)	50 % (v/v) Odyssey Blocking Buffer (PBS)
	0.01 % SDS

2.6 Biotinylation assay

Transfected cells, cultivated on a 10 cm plate, were subjected to biotinylation using the Pierce™ Cell Surface Biotinylation and Isolation Kit according to the manufacturer's protocol. Initially, cells were washed twice with 5 mL of ice-cold PBS. 7 mL of the biotinylation reagent Sulfo-NHS-SS-Biotin (0.25 mg/mL prepared in PBS), was then added to the cells. After 30 min of incubation at 4 °C on a rocking platform, the biotinylation reaction was quenched with 500 µL quenching solution. Cells were scraped from the plate using a cell scraper, and the plate was rinsed with 2.5 mL of 1x Tris-buffered saline (TBS) (**Table 16**).

Table 22: Tris-buffered saline used for biotinylation assay

1x TBS
150 mM NaCl
20 mM Tris-HCl
adjust to pH 7.6
sterilize by autoclaving

The harvested cells were centrifuged at 500 x g for 3 min at RT. The supernatant was removed, and the cell pellet was resuspended in 5 mL TBS and, again, centrifuged at 500 x g for 3 min at RT. The cell pellet was resuspended in 300 µL total lysis buffer (**Table 16**) containing mPic in a 1:500 dilution. To improve solubilization efficiency, sonication of the sample for 30 sec every 10 min and vortexing every 5 min was performed during lysis.

After 30 min, the total protein lysate was centrifuged at 10.000 x g for 2 min at 4 °C. The clarified supernatant, which contained the solubilized protein, was transferred to a new tube. Protein concentration was determined in a BCA test.

300 µL of NeutrAvidin Agarose Slurry was added to a column. The column was then equilibrated by adding 300 µL wash buffer and centrifuging at 1000 x g for 1 min at RT. The total protein lysate was added to the column, which was incubated overnight end-over-end at 4 °C. The next day, the column was centrifuged at 1000 x g for 1 min at RT, and the flow-through fraction was collected. The column was then washed three times with 500 µL of wash buffer containing mPic at a 1:500 dilution, collecting each wash fraction after centrifugation at 1000 x g for 1 min at RT. For elution, 200 µL of SDS sample buffer (4x) without bromphenol blue (**Table 18**) containing 50 mM dithiothreitol (DTT) was added to the column, which was then incubated end-over-end for 60 min at RT. After centrifugation of the column at 1000 x g for 2 min at RT, the eluate was collected, and a trace amount of bromphenol blue (0.04 %) was added. After elution, the beads were scraped off the column. 80 µL of standard SDS sample buffer (4x) were added to the beads, which were then boiled and centrifuged at 1000 x g for 2 min at RT (**Figure 7**). SDS sample buffer (4x) was added to 40 µL of total protein lysate, flow-through, and wash samples. Western blot analysis was then conducted following the protocol shown above.

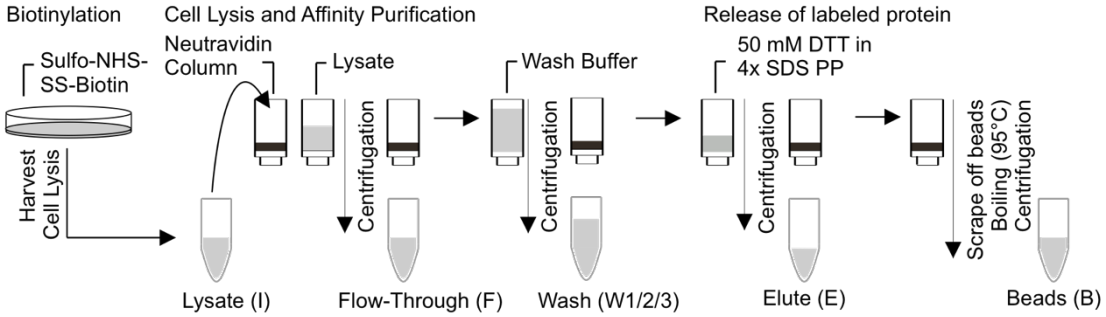

Figure 7: Biotinylation assay workflow. The total protein lysate is transferred to a NeutrAvidin column, where biotinylated protein binds to avidin with high affinity. After overnight incubation, the column is centrifuged, and the non-bound protein is collected in the flow-through fraction. After three washing steps, labeled protein is released using SDS-page sample buffer containing 50 mM dithiothreitol (DTT). After elution, beads are scraped off the agarose matrix and boiled in conventional 4x SDS-sample buffer.

Table 23: Elution buffer (4x) without bromophenol blue

Elution buffer (4x)
200 mM Tris/ HCl pH 6.8
8 % (w/v) SDS
5 % (v/v) β-mercaptoethanol
50 % (v/v) glycerol
50 mM DTT

2.6.1 Densitometric analysis with ImageJ

The Odyssey Imaging detection system (LI-COR Biosciences) was used to visualize the presence of the protein of interest in the respective sample. The output tiff file was transformed to grayscale, and image curves were adjusted. The image view was converted to 8-bit color graphics. Densitometric quantification of biotinylation assay Western blot signals was performed using ImageJ. The protein band with the biggest width was used as a reference for defining a rectangular region of interest (ROI) around the protein band. For each protein band, a profile plot was obtained. The profile plots showed the density of the respective band, with an intense band resulting in a higher peak and a faint band resulting in a wider peak. A baseline was drawn at the bottom of each peak. The integral (area), measured in arbitrary units (AU), was calculated for each profile plot (**Figure 8**).

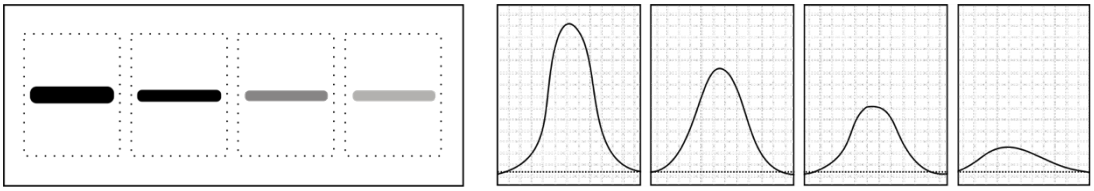

Figure 8: Quantifying Western blot signals using ImageJ

The obtained area value for each band (input, flow-through, wash 1/2/3, eluate, and beads) was multiplied by the ratio between the total volume of the respective sample (see above) and the loaded volume (40 µL). Normalization was then performed by dividing the area of each band by the calculated area of the input (total lysate) control band.

2.7 Co-immunoprecipitation using magnetic beads

CHO K1 cells grown in 10 cm dishes stably expressing AC3-FL-HA and transfected with AC3-AT-Flag or mCherry were subjected to butyrate treatment with sodium butyrate (0.5 M) at a dilution of 1:100 for six hours after transfection to boost protein expression. The cells were then incubated at 37 °C, 5 % CO_2 for 24 hours. The cells were then washed twice with 5 mL of ice-cold PBS, harvested, and pelleted by centrifugation at 500 x g for 5 min and resuspended in 400 µL lysis buffer (**Table 23**). Proper lysis of the cells was achieved by vigorous pipetting during the 1-hour incubation time. Cell debris was then removed by centrifugation at 10.000 x g for 5 minutes at 4 °C. The supernatant was harvested, and protein concentration was determined using a BCA assay. 545 µg of cell lysate was filled up with lysis buffer to a total volume of 545 µL, to obtain a lysate with a concentration of 1 µg/ µL. 45 µL of this lysate with 15 µL of standard SDS sample buffer were used as the input sample for western blot analysis. The buffer of 75 µL Anti-FLAG® M2 Magnetic Beads (Sigma Aldrich, St. Louis, USA, M8823) was removed using a magnet. The anti-Flag magnetic beads were then equilibrated using 375 µL of equilibration buffer (**Table 23**). The supernatant after magnetic separation was removed. The resin was then equilibrated using 375 µL of lysis buffer. The supernatant after magnetic separation was removed. 500 µg of cell lysate in a total volume of 500 µL was added to the beads and incubated at 4 °C, over-night, end-over-end mixing. 45 µL of the supernatant after magnetic separation was used as a non-bound sample for western blot analysis with 15 µL of standard SDS sample buffer. The beads were then washed four times with 300 µL wash buffer (**Table 23**). 45 µL wash sample with 15 µL of standard SDS sample buffer were used of each washing step for western blot analysis. The bound protein was eluted in 150 µL of 0.1 M glycine (pH 3.0). Following magnetic separation, the supernatant was directly transferred to 25 µL of 1 M Tris (pH 8.0) for neutralization. 45 µL of the final eluate and 15 µL of standard SDS sample buffer were used for western blotting.

Table 24: Lysis, equilibration, and wash buffer used for co-immunoprecipitation

Lysis buffer (1x)	Equilibration buffer (1x)	Wash buffer (1x)
20 mM Tris/HCl pH 8.0	10 mM Tris/ HCl pH 7.4	20 mM Tris/HCl pH 8.0
137 mM NaCl	150 mM NaCl	137 mM NaCl
2 mM EDTA		2 mM EDTA
1 % NP40		0.2 % NP40
1:500 mPic		1:500 mPic

2.8 cAMP fluorescent assay

cAMP formation in CHO K1 WT cells and cells stably expressing AC3-FL or AC3-AT was assessed using the CatchPoint™ cAMP Fluorescent Assay Kit. The cells were plated in PLL-coated 96 well plates and grown overnight in an incubator at 37 °C with 5 % CO_2. On the day of the assay, lyophilized cAMP calibrator for the cAMP standard curve was dissolved in 5 mL assay buffer. Then, the cAMP calibrator curve was prepared, covering a concentration range of 0 to 10 µM.

The reagents for the following conditions were prepared in ES buffer (**Table 24**): (1) DMSO, 2 µM Forskolin alone, and 2 µM Forskolin + 100 µM IBMX; (2) DMSO, and 1 µM Isoproterenol. The culture medium was removed from the 96 well plate, and 100 µL of fresh, pre-warmed ES buffer was added to the wells. The ES buffer was then removed, and 150 µL ES buffer containing the reagents was added to the wells. After an incubation time of 30 min on a tumbler at RT, the reaction was stopped by adding 50 µL of lysis buffer. For proper lysis of the cells, the mixture was pipetted up and down. The lysate was incubated for 10 min on a tumbler at RT. During the incubation time, the working concentration of the antibody and HRP conjugate was prepared. The HRP-cAMP conjugate was diluted in a ratio of 1:4 in assay buffer. Likewise, the anti-cAMP antibody was diluted in a ratio of 1:4 in assay buffer. After 10 min of incubation, 40 µL of each sample (or calibrator) was added in duplicates on the antibody covered assay plate. A dilution buffer-only control was included. Then, 40 µL anti-cAMP antibody was added to each well. The mixture was incubated on a tumbler for 5 min. Subsequently, 40 µL of HRP-cAMP conjugate was added to each well, followed by an incubation time of 2 h at

RT on a tumbler. Shortly before the end of the incubation time, the Stoplight red solution was prepared, which was kept protected from light at all times. For the preparation of the Stoplight red solution, 100x stock substrate was diluted in substrate buffer at a ratio of 1:100, and 3 % H_2O_2 was added. After the incubation time of 2 hours, the samples were aspirated and washed 4 times with 200 µL wash buffer. Then, 100 µL stoplight solution was added to each well. The plate was covered and incubated for at least 10 min at RT on a tumbler, while kept in the dark. The fluorescence intensity was measured at 590 nm following excitation at 530 nm using the FluoStar plate reader. Lastly, the protein concentration of the total lysates was determined using the BCA assay.

Table 25: Extracellular solution (ES) buffer

ES buffer (1x)
120 mM NaCl
5 mM KCl
2 mM $MgCl_2$
10 mM HEPES
10 mM glucose in H_2O
Adjust to pH 7.4 using 1 M NaOH

3. Results

3.1 Generation and characterization of isoform-specific AC3 antibodies

Cold-induced epigenetic changes in the *Adcy3-fl* gene in brown adipose tissue result in the expression of a truncated transcript, *Adcy3-at*. To distinguish between AC3-FL and -AT expression *in vivo,* isoform-specific antibodies are needed.

To this end, monoclonal antibodies were generated in collaboration with Dr. Regina Feederle, Helmholtz Center Munich, and polyclonal antibodies were generated with David Biotechnologies, Regensburg. The epitopes used for antibody generation are localized at the N-terminus of AC3-FL and AC3-AT, where the two proteins show the least similarity (see **Figure 9**, sequence alignment using Clustal Omega, EMBL-EBI)**.** Unfortunately, both monoclonal and polyclonal antibodies could only be generated against the epitope for AC3-FL but not AC3-AT. In my thesis, I have characterized the specificity of the polyclonal antibody (KOR-AEY2).

```
mAC3-FL      mprnqgfsdpeysaeysaeysvslpsdpdrgvgrtheisvrnsgsclclprfmrltfvpe   60
mAC3-AT      ------------------------------------------------------------   0

mAC3-FL      slenlyqtyfkrqrhetllvlvvfaalfdcyvvvmcavvfssdklaplmvagfglvldii   120
mAC3-AT      ------------------------------------------------------------   0

mAC3-FL      lfvlckkgllpdrvsrkvvpyllwllisaqifsylglnfsrahaasdtvgwqaffvfsff   180
mAC3-AT      -----------------------------------------------------mwmgf------   5
                                                                  * .*

mAC3-FL      itlplslspiviisvvscvvhtlvlgvtvaqqqqdelegmqllreilanvflylcaiivg   240
mAC3-AT      ----------------------ltgelrvcqeagqrrnggrrslkilanvflylcaiivg   43
                                  *.  : *.*:  :. :* :   :***************

...


mAC3-FL      alamkdtltninnqsfnnfmlrigmnkggvlagvigarkphydiwgntvnvasrmestgv   1080
mAC3-AT      alamkdtltninnqsfnnfmlrigmnkggvlagvigarkphydiwgntvnvasrmestgv   883
             ************************************************************

mAC3-FL      mgniqvveetqvilreygfrfvrrgpifvkgkgelltfflkgrdrpaafpngssvtlphq   1140
mAC3-AT      mgniqvveetqvilreygfrfvrrgpifvkgkgelltfflkgrdrpaafpngssvtlphq   943
             ************************************************************

mAC3-FL      vvdnpypydvpdya       1154
mAC3-AT      vvdnpypydvpdya       957
             **************
```

Figure 9: Amino-acid sequence alignment of mAC3-FL and mAC3-AT. The N and C termini for both sequences have been aligned using Clustal Omega (EMBL-EBI). Identical amino acid residues are indicated with *, conserved with . or :. The epitopes used for antibody generation are highlighted in grey (AC3-FL) or yellow (AC3-AT).

3.1.1 Characterization by Western blot analysis

To verify the specificity of the antibody by Western blot, AC3-FL-HA or AC3-AT-Flag were transiently expressed in human embryonic kidney (HEK293) cells, and protein expression was analyzed using antibodies against hemagglutinin (HA) (**Figure 10A**)- or Flag-tag (**Figure 10B**). When using the standard electrophoresis protocol, protein migration in the gel seemed to be impeded, and proteins were detected at a higher molecular weight than their calculated molecular weights of 130 kDa (AC3-FL) and 108 kDa (AC3-AT) (**Figure 10i**). Thus, both proteins seemed to aggregate under standard conditions. Thus, I changed the protocol and omitted boiling the total protein lysate. In turn, the proteins could be detected at their calculated molecular weight (**Figure 10ii**). However, AC3-AT separated into multiple bands.

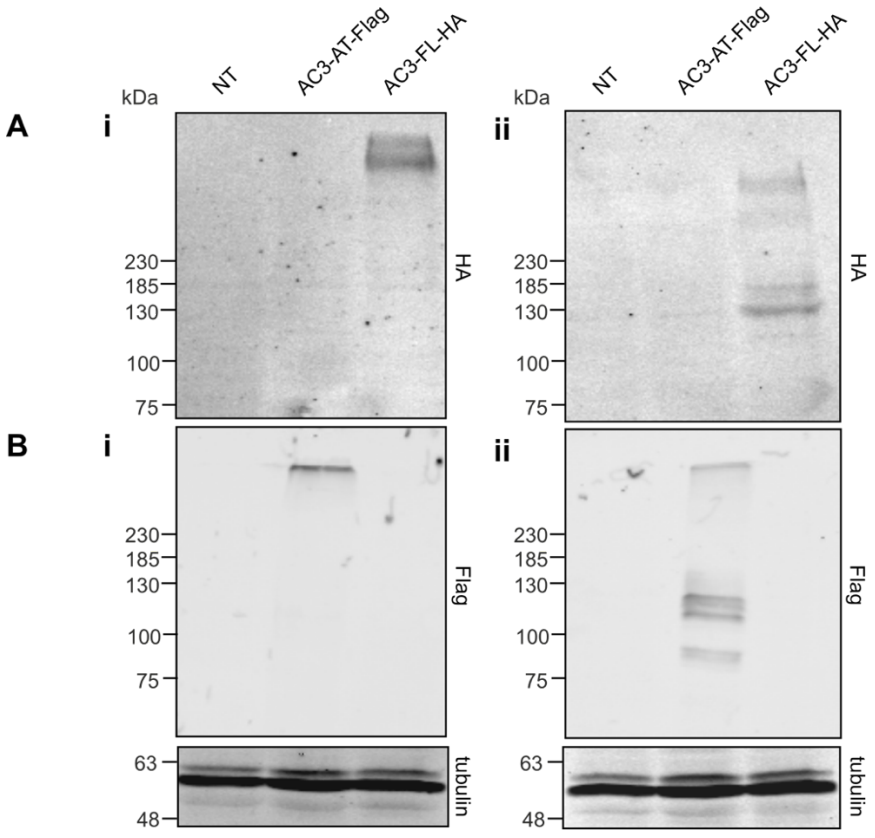

Figure 10: AC3-AT and AC3-FL aggregate upon boiling. Western blot analysis of total protein lysates (60 µg) from HEK293 expressing AC3-AT-Flag or AC3-FL-HA. Protein was either boiled **(i)** or not boiled **(ii)**. Non-transfected cells (NT) were used as controls. Proteins were labeled with an anti-Flag antibody **(A)** or an anti-HA antibody **(B)**. Beta-tubulin was used as a loading control.

Using the optimized protocol, I tested the specificity of the polyclonal antibody (KOR-AEY2) by Western blot and could show that the antibody exclusively detected the full-length, but not the truncated isoform (**Figure 11A**). As a control, AC3-FL-HA and AC3-AT-Flag were detected using an antibody against their respective tags.

The Western blot protocol was extended by separating the total protein lysate into the membrane and cytosolic protein fractions (**Figure 11B**). Both AC3-FL and AC3-AT were detected in the membrane, but not in the cytosolic protein fraction. Additionally, the membrane protein fraction was treated with peptide-N-glycosidase F (PNGaseF), an enzyme that removes post-translational glycosylation. Western blot analysis revealed that, upon removing glycosylation, the protein migrated further in the gel. Moreover, AC3-AT separated into fewer bands compared to the glycosylated protein sample.

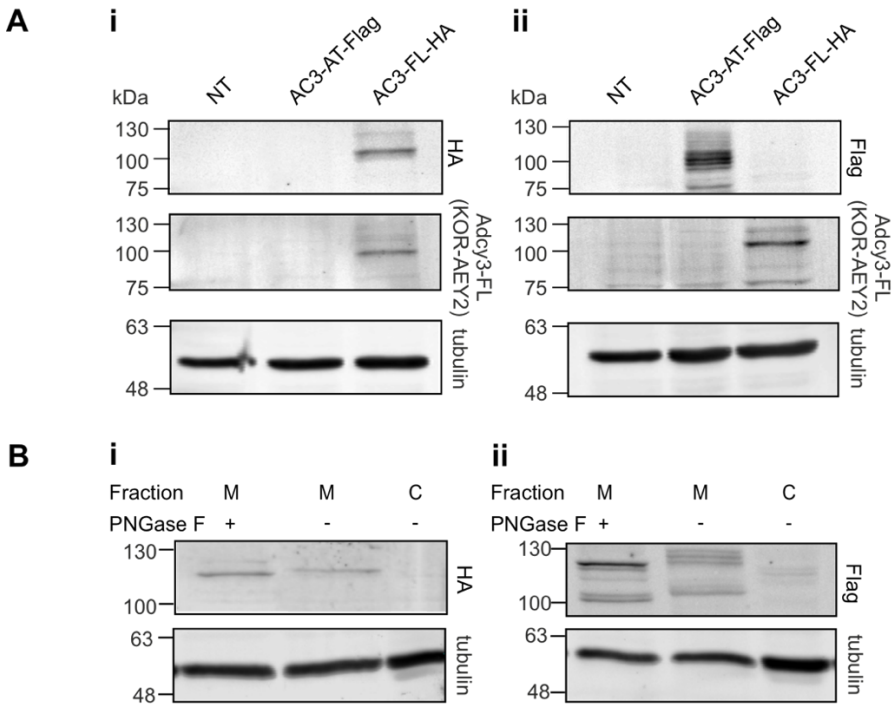

Figure 11: AC3-FL-specific antibody characterization. (A) Western blot analysis of HEK293 total protein lysates from non-transfected cells (NT), cells transiently transfected with *mAdcy3-at-Flag*, or *mAdcy3-fl-HA*. 60 µg protein per lane was loaded; proteins were labeled with an anti-HA **(i)**, anti-Flag **(ii)** or an AC3-FL-specific (KOR-AEY2) antibody. Beta tubulin was used as a loading control. **(B)** Western blot analysis of membrane proteins isolated from HEK293 cells expressing mAC3-FL-HA **(i)** or mAC3-AT-Flag **(ii)**; 20 µg of membrane proteins (M) and 13.5 µg of cytosolic proteins **(C)** were loaded. Membrane proteins were treated without (-) or with (+) peptide-N-glycosidase F (PNGaseF) to reduce glycosylation.

3.1.2 Characterization by immunocytochemistry

In addition, the expression of AC3-FL and AC3-AT and the specificity of the KOR-AEY2 antibody were analyzed in transiently transfected HEK293 cells by immunocytochemistry. To this end, AC3-FL and AC3-AT were expressed with mCherry in a 2A-peptide-mediated mechanism (**Figure 12**) (AC3-FL-HA-2A-mCherry or AC3-AT-Flag-mCherry) in stoichiometric amounts to the respective AC and, thereby, served as a control.

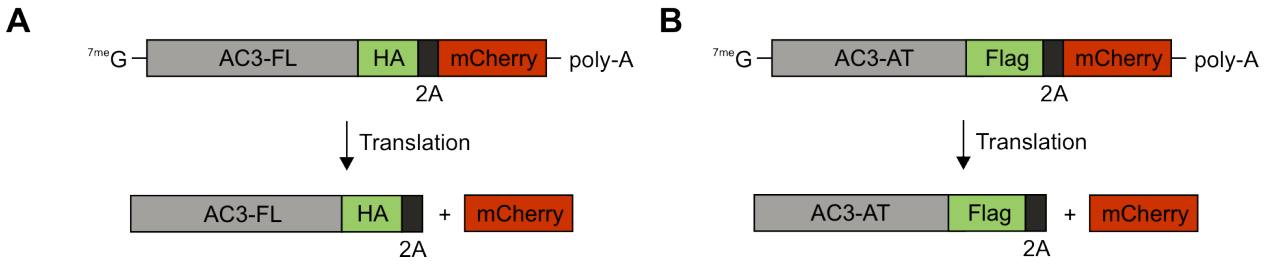

Figure 12: Expression of AC3 isoforms and mCherry using a 2A-peptide-mediated mechanism. From one RNA, two separate proteins are expressed in stoichiometric amounts: AC3-FL-HA and mCherry (A) or AC3-AT-Flag and mCherry (B). 2A peptide-mediated cleavage begins after translation. Precisely, the peptide bond between the proline and the glycine in the C-terminus of the A2 peptide is cleaved.

In mCherry-positive cells, the AC3-FL-specific antibody detected AC3-FL but not AC3-AT (**Figure 13**), which is in accordance with the results obtained by Western blot analysis.

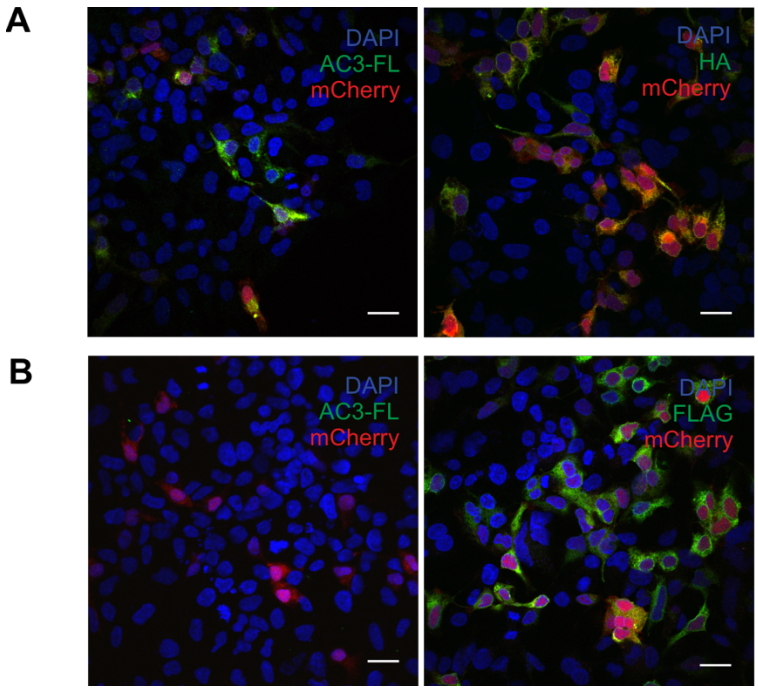

Figure 13: Immunocytochemical characterization of the AC3-FL-specific antibody. HEK293 cells expressing either AC3-FL-HA **(A)** or AC3-AT-Flag **(B)** and co-expressing mCherry in a 2A-peptide-mediated mechanism were stained with the AC3-FL-specific KOR-AEY2 antibody and with an anti-Flag or anti-HA antibody as controls (green). mCherry fluorescence is indicated in red. DAPI (blue) was used to label the cell nuclei. Scale bar: 10 µm.

3.2 Subcellular localization of AC3-FL versus AC3-AT

Transmembrane adenylyl cyclases form dimers in the endoplasmic reticulum and are then incorporated into the plasma membrane. AC3-AT lacks the majority of the first transmembrane domain, which might impair dimerization and/or plasma membrane transport. Therefore, the subcellular localization of AC3-FL versus AC3-AT, in particular the localization in the plasma membrane, was analyzed by different techniques.

3.2.1 Analyzing plasma membrane localization using a biotinylation assay

For this assay, Sulfo-NHS-SS-Biotin, a membrane-impermeable, amide bond-forming, and cleavable biotinylation reagent, was added to intact cells, labeling the ε-amino group of accessible lysine residues within extracellular domains of proteins in the plasma membrane **(Figure 14A)**. The following work steps are shown in **Figure 14B**: The biotin labeling reaction was quenched by the addition of a buffer containing primary amines. The

cells were then harvested and lysed. The total protein lysate was applied to a column, where labeled proteins were purified via the Biotin-NeutrAvidin interaction. After centrifugation, the non-bound proteins were collected in the flow-through fraction. Labeled proteins were eluted using SDS-page sample buffer containing dithiothreitol (DTT), a reducing agent that breaks the disulfide bond within the spacer arm of the biotinylation reagent. To prevent contamination of the eluate with proteins unspecifically binding to the agarose matrix, several washing steps were included before elution. After elution, beads were scraped off the agarose matrix and boiled in standard SDS-sample buffer. Subjecting cells, which express AC3-FL or AC3-AT, to this assay will reveal whether the proteins are localized in the plasma membrane.

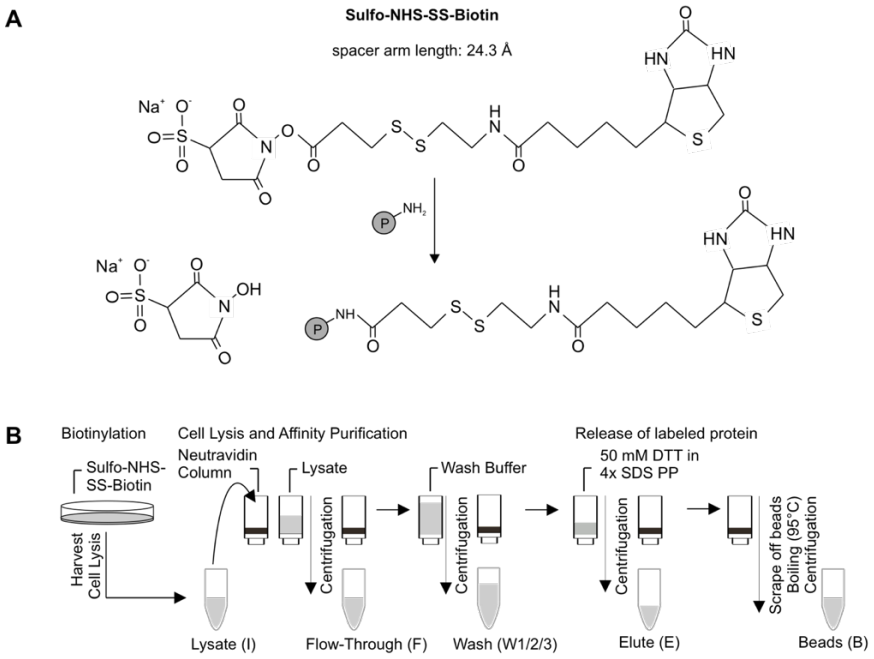

Figure 14: Labeling of cell surface proteins using Sulfo-NHS-SS-Biotin. (A) When added to intact cells, the Sulfo-N-hydroxysuccinimid (Sulfo-NHS) ester linked to the biotin via an extended spacer arm, containing a cleavable disulfide bond, reacts with the ε-amino group of lysine residues within extracellular domains of proteins (P) on the cell surface. As a result, an amide bond is formed. The reaction proceeds at pH 7-9 in an aqueous solution and can be quenched by the addition of buffers containing primary amines, competing with the biotin labeling reaction. **(B)** Quenching of the labeling reaction is followed by harvest lysis of the cells. The total protein lysate is transferred to a NeutrAvidin column, where biotinylated protein binds to avidin with high affinity. After overnight incubation, the column is centrifuged, and the non-bound protein is collected in the flow-through fraction. After three washing steps, labeled protein is released using SDS-page sample buffer containing 50 mM dithiothreitol (DTT). After elution, beads are scraped off the agarose matrix and boiled in conventional 4x SDS-sample buffer.

Two negative control proteins were included in the assay: (1) mCherry to ensure that the biotinylation reagent does not label cytosolic protein, and (2) LAPD-HA, an independent, HA-tagged protein, to detect unspecific protein binding to the agarose matrix. As a positive control, the transmembrane protein CNGA2-TM-HA, a cyclic nucleotide-gated ion channel, was included. HEK293 cells were transiently transfected with the respective constructs and subjected to the biotinylation assay (**Figure 15**). mCherry was detected by an anti-RFP antibody; CNGA2-TM-HA and LAPD-HA were detected using an antibody against the HA-tag.

Western blot analysis revealed that the negative control protein mCherry was expressed (**Figure 15A, (I)**) and otherwise only detected the flow-through fraction (**Figure 15A, (F)**), which is in accordance with its localization in the cytoplasm. Similarly, LAPD-HA was expressed (**Figure 15B, (I)**) and most of the protein was retrieved in the flow-through fraction (**Figure 15B, (F)**). A small amount of protein was pulled down in the wash fraction (**Figure 15B, (W1)**), indicating unspecific binding to the agarose matrix. No protein was detected in the eluate (**Figure 15B, E)**). CNGA2-TM-HA was expressed (**Figure 15C, (I)**) and was detected in the eluate (**Figure 15C, (E)**), which suggests specific binding of the protein to the NeutrAvidin column. Moreover, CNGA2-TM-HA was also retrieved in the flow-through fraction (**Figure 15C, (F)**) in larger amounts than in the eluate, indicating that only a small amount of the total CNGA2-TM-HA protein was incorporated into the plasma membrane and was, therefore, biotinylated. This could be due to transient transfection and strong and artificial overexpression of the protein, resulting in accumulation in the endoplasmic reticulum, which might cause an overload of the protein transport into the plasma membrane.

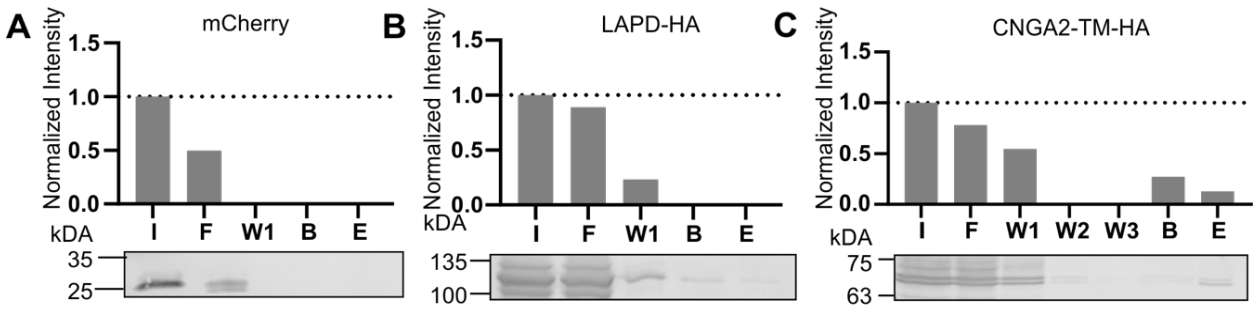

Figure 15: Biotinylation assay of control proteins. Western blot analyses of total protein lysates of HEK293 cells expressing mCherry **(A)**, LAPD-HA **(B)**, or CNGA2-TM-HA **(C)**. Cells were treated with the biotinylation reagent Sulfo-NHS-SS-Biotin, harvested, and lysed (sample I). 300 µL lysate was transferred to a column containing NeutrAvidin-agarose-resin and incubated overnight end-over-end mixing. The column was centrifuged, and the flow-through (sample F) was collected. The column was washed three times (samples W1, W2, W3) with 500 µL wash buffer, and the labeled protein was eluted (sample E) using 200 µL 4x SDS sample buffer containing 50 mM dithiothreitol (DTT). After elution, beads of the agarose matrix were scraped off the column, boiled in 100 µL 4x SDS probe buffer, and centrifuged (sample B). 40 µL of the collected samples were loaded. Results from densitometric analysis of n = 1 are plotted above each respective band. Values were normalized to the respective input sample (($Area_{Fraction}$* $Volume_{total}$/ $Volume_{loaded}$)/$Area_{Input}$).

Next, the biotinylation assay was performed using HEK293 cells transiently transfected with *Adcy3-fl-HA* or *Adcy3-at-HA* (**Figure 16**). Western blot analysis indicated that both proteins were expressed (**Figure 16A and B, (I)**), but neither AC3-FL-HA nor AC3-AT-HA was retrieved in the eluate (**Figure 16A and B, (E)**). However, this might be due to low protein expression in transiently transfected cells (remark: brightness and contrast of Western blot images had to be adjusted to make the bands visible). Thus, I aimed to generate cell lines stably expressing AC3-FL-HA or AC3-AT-HA.

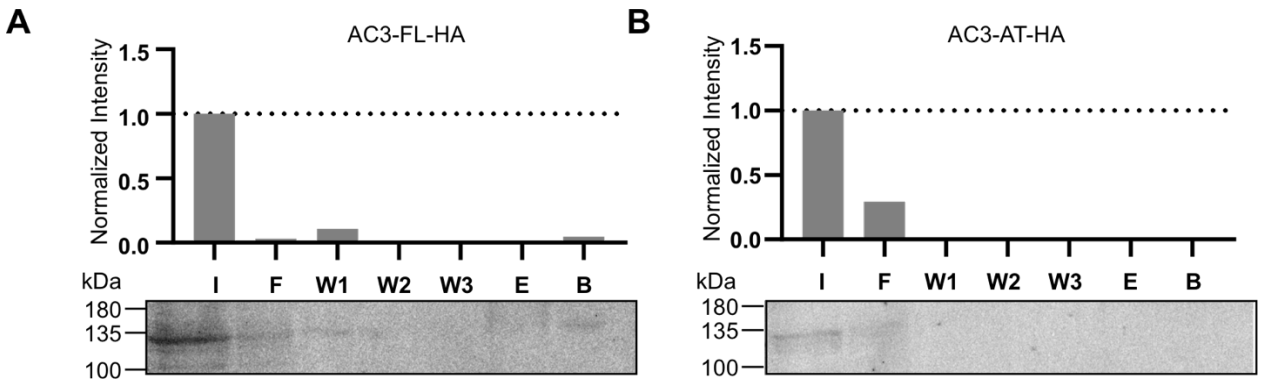

Figure 16: Biotinylation assay of HEK293 expressing AC3-FL-HA or AC3-AT-HA. Western blot analysis of total protein lysates of HEK293 cells expressing AC3-FL-HA **(A)** or AC3-AT-HA **(B)**. Cells were treated with the biotinylation reagent Sulfo-NHS-SS-Biotin, harvested, and lysed (sample I). 300 µL lysate was transferred to a column containing NeutrAvidin-agarose-resin and incubated overnight end-over-end mixing. The column was centrifuged, and the flow-through (sample F) was collected. The column was washed three times (samples W1, W2, W3) with 500 µL wash buffer, and the labeled protein was eluted (sample E) using 200 µL 4x SDS sample buffer containing 50 mM dithiothreitol (DTT). After elution, beads of the agarose matrix were scraped off the column, boiled in 100 µL 4x SDS probe buffer, and centrifuged (sample B). 40 µL of the collected samples were loaded. Results from densitometric analysis of n = 1 are plotted above each respective band. Values were normalized to the respective input sample. $((Area_{Fraction}* Volume_{total}/ Volume_{loaded})/Area_{Input})$.

To generate stable cell lines, CHO K1 cells were transfected with AC3-FL-HA or AC3-AT-HA. After antibiotic selection and expansion of clones, protein expression was analyzed by immunocytochemistry (**Figure 17A**) and Western blot (**Figure 17B**). Immunostaining was performed with an antibody against the HA tag. Both analyses revealed that either AC3-FL-HA or AC3-AT-HA were expressed. However, immunocytochemical analysis showed that not all cells expressed AC3-FL-HA or AC3-AT-HA. Furthermore, expression levels between the cells varied. Thus, the selected cell lines were rather polyclonal than monoclonal.

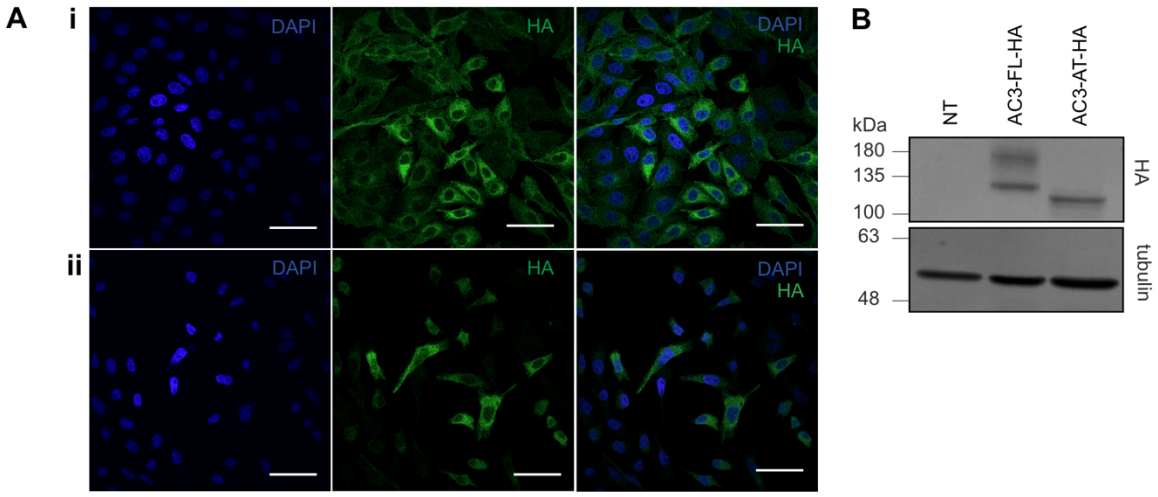

Figure 17: Expression of AC3-FL and AC3-AT in CHO K1 stable cell lines [A12] and [F7]. (A) CHO K1 cells stably expressing AC3-FL-HA **(i)** or AC3-AT-HA **(ii)** were labeled with an antibody against the HA-tag (green). DAPI (blue) is used to label the DNA. Merged images are shown on the right. Scale bar: 40 µm. **(B)** Western blot analysis using 35 µg total protein lysates from CHO K1 cells stably expressing AC3-FL-HA or AC3-AT-HA; non-transfected cells were used as controls. Protein lysates were incubated with an anti-HA antibody. Beta-tubulin served as a loading control.

Next, the biotinylation assay was performed using CHO K1 cells stably expressing AC3-FL-HA or AC3-AT-HA (**Figure 18, Aii and iv**). CHO K1 cells stably expressing CNGA2-TM (CHO TM cell line) or transiently transfected with mCherry were included as controls (**Figure 18, Ai and iii**). Western blot analysis revealed that the negative control protein mCherry was expressed (**Figure 18, Aiii, (I)**) and most of the protein was retrieved in the flow-through fraction (**Figure 18, Aiii (F)**), and no protein was detected in the eluate (**Figure 18, Aiii, (E)**). CNGA2-TM-HA was expressed (**Figure 18, Ai (I)**) and detected in the eluate (**Figure 18, Ai, (E)**), which is in accordance with its localization in the plasma membrane. AC3-AT-HA was expressed at higher levels in stable cell lines (**Figure 18B, Aiv (I)**) than in transiently transfected cells (**Figure 16B, (I)**) and similar to the negative control protein mCherry, AC3-AT-HA was mostly retrieved in the flow-through fraction (**Figure 18, Aiv (F)**) and only minor amounts were detected in the eluate (**Figure 18, Aiv (E)**). AC3-FL-HA was expressed (**Figure 18, Aii (I)**) and, in contrast to AC3-AT-HA, was also detected in the eluate (**Figure 18, Aii (E)**), indicating localization of the protein in the plasma membrane.

Densitometric analysis was performed for the different protein bands representing mCherry, AC3-AT-HA, CNGA2-TM, and AC3-FL-HA (**Figure 18, Ai-iv**). The ratios eluate/ input for each protein are shown in **Figure 18B**. The ratio (eluate/ input) between mCherry and AC3-AT-HA was not different. However, the ratio of CNGA2-TM and AC3-FL-HA was significantly higher than the negative control mCherry and also higher than for AC3-AT-HA. In addition, the ratio for CNGA2-TM and AC3-FL-HA was not significantly different, demonstrating that indeed, AC3-FL-HA localizes to the plasma membrane, whereas AC3-AT-HA does not.

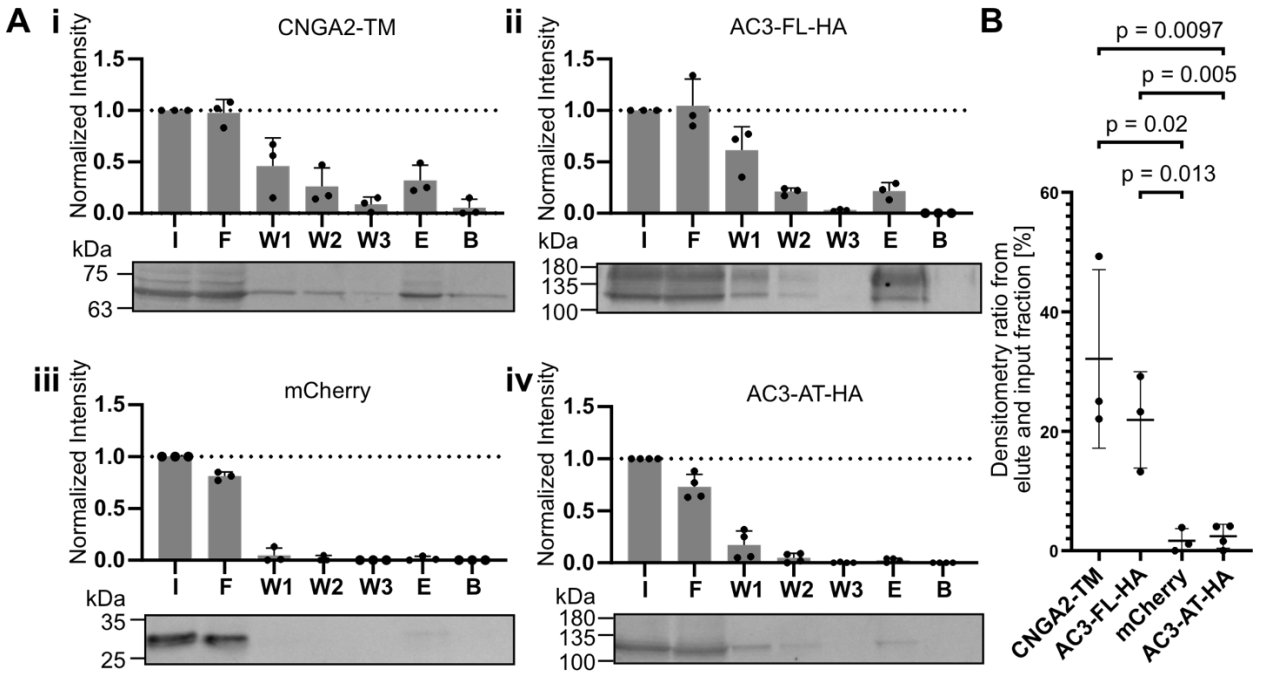

Figure 18: AC3-AT is not localized in the plasma membrane. As published by Khani et al. (2024). **(A)** Representative Western blot analysis of total protein lysates isolated from CHO K1 cells stably expressing CNGA2-TM **(i)**, transiently transfected with *pcDNA3.1zeo_mCherry* **(iii)**, stably expressing AC3-FL-HA **(ii)**, or AC3-AT-HA **(iv)**. Cells were treated with the biotinylation reagent Sulfo-NHS-SS-Biotin, harvested, and lysed (sample I). 300 µL lysate was transferred to a column containing a NeutrAvidin-agarose-resin and incubated end-over-end overnight. The column was centrifuged and the flow-through (sample F) was collected. The column was washed three times (samples W1, W2, W3) with 500 µL wash buffer, labeled protein was eluted (sample E) using 200 µL 4x SDS sample buffer containing 50 mM dithiothreitol (DTT). After elution, beads of the agarose matrix were scraped off the column, boiled in 100 µL 4x SDS probe buffer and centrifuged (sample B). 40 µL of the collected samples were loaded. Results from densitometric analysis of n = 3 (CNGA2-TM, mCherry, AC3-FL-HA) and n = 4 (AC3-AT-HA) are plotted above the respective samples. Values were normalized to the respective input sample. ($(Area_{Fraction}$* $Volume_{total}$/ $Volume_{loaded})/Area_{Input}$). Mean + S.D. are indicated. Densitometric ratio of elute and input samples [%] shown in **(B)**. Mean ± S.D. are indicated; p-values were calculated with unpaired two-tailed Student's t-test.

To examine whether AC3-AT alters AC3-FL transport to the plasma membrane by forming heterodimers, the biotinylation assay was performed using CHO K1 cells stably expressing AC3-FL-HA and transiently expressing mCherry (control) or AC3-AT-Flag-2A-mCherry (**Figure 19**).

Western blot analysis revealed that AC3-FL-HA was expressed (**Figure 19A, (I)**) and was also detected in the eluate when being coexpressed with AC3-AT-Flag-2A-mCherry (**Figure 19B, (E)**) or mCherry (**Figure 19A, (E)**). However, densitometric analysis revealed that in the presence of AC3-AT-Flag, significantly smaller amounts of AC3-FL-HA were retrieved in the eluate compared to the control condition in the presence of mCherry (**Figure 19C**). This demonstrates that, indeed, AC3-AT impairs the transport of AC3-FL to the membrane.

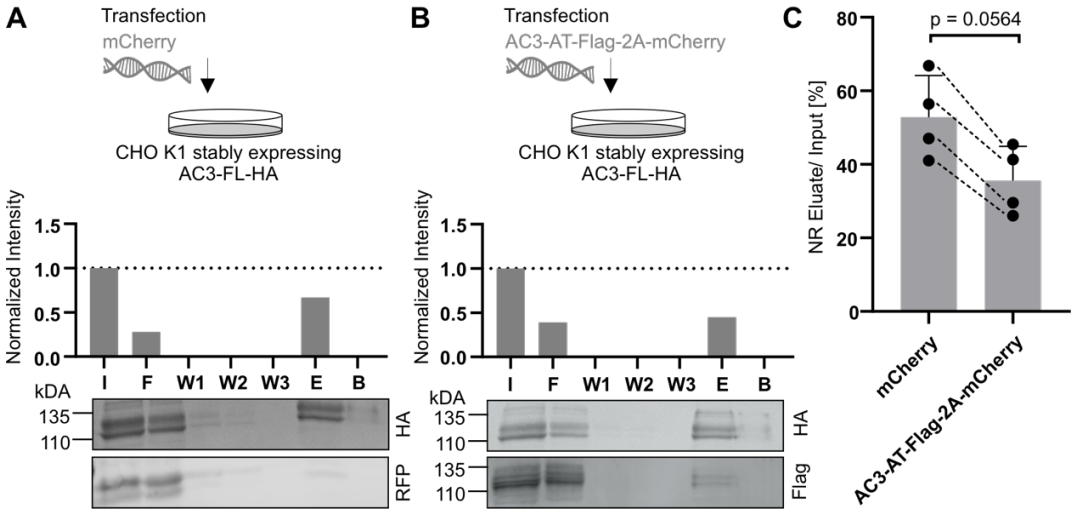

Figure 19: AC3-AT alters AC3-FL plasma membrane localization. As published by Khani et al. (2024). Representative Western blot analysis of total protein lysates isolated from CHO K1 cells stably expressing AC3-FL-HA or, transiently expressing **(A)** mCherry or **(B)** AC3-AT-Flag-2A-mCherry. Cells were treated with the biotinylation reagent Sulfo-NHS-SS-Biotin, harvested, and lysed (sample I). 300 µL lysate was transferred to a column containing a NeutrAvidin-agarose-resin and incubated end-over-end overnight. The column was centrifuged and the flow-through (sample F) was collected. The column was washed three times (samples W1, W2, W3) with 500 µL wash buffer, labeled protein was eluted (sample E) using 200 µL 4x SDS sample buffer containing 50 mM dithiothreitol (DTT). After elution, beads of the agarose matrix were scraped off the column, boiled in 100 µL 4x SDS probe buffer and centrifuged (sample B). 40 µL of the collected samples were loaded. Result from densitometric analysis is plotted above the respective samples. Values were normalized to the respective input sample. ((AreaFraction* Volumetotal/ Volumeloaded)/AreaInput). Densitometric ratio of elute and input samples [%] of n = 4 shown in **(C)**. The trend for paired experiments is indicated with a dotted line. Mean ± S.D. are indicated; p-value was calculated with unpaired two-tailed Student's t-test.

3.2.2 Analyzing protein-protein interaction using co-immunoprecipitation

My results demonstrated that in the presence of AC3-AT, AC3-FL membrane trafficking is impaired. It is known that transmembrane adenylyl cyclases form dimers in the endoplasmic reticulum and are then incorporated into the plasma membrane. Therefore, the ability of AC3-FL and AC3-AT to dimerize was assessed using co-immunoprecipitation (**Figure 20**).

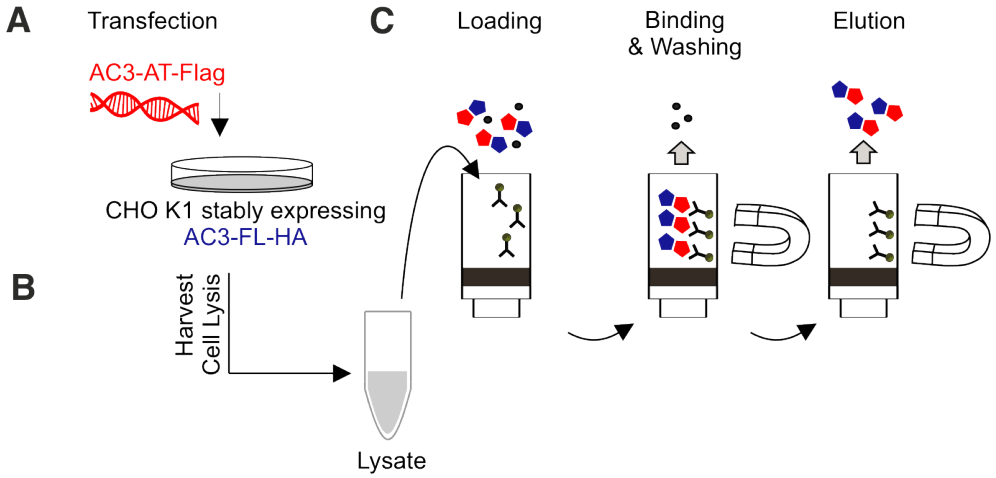

Figure 20: Co-immunoprecipitation of AC3-AT-Flag and AC3-FL-HA using anti-Flag magnetic beads. (A) Co-expression of AC3-AT-Flag and AC3-FL-HA in CHO K1 cells. (B) Total protein lysates were prepared and (C) added onto equilibrated magnetic beads bound with anti-FLAG antibodies, incubated end-over-end overnight, then washed. The bound protein was eluted with 1 M glycine at pH 3.0.

To analyze the protein-protein interaction of AC3-FL and AC3-AT, CHO K1 cells stably expressing AC3-FL-HA were transiently transfected with AC3-AT-Flag or mCherry (**Figure 21**). These cells were then subjected to the Flag-Trap co-immunoprecipitation assay. Western blot analysis revealed that AC3-FL-HA was expressed (**Figure 21, INPUT, 1 and 2**) and was also detected in the eluate when being coexpressed with AC3-AT-Flag (**Figure 21, IP, 1**), but not detected in the eluate when being coexpressed with mCherry (**Figure 21, IP, 2**) This demonstrates that, indeed, AC3-AT and AC3-FL dimerize *in vitro*.

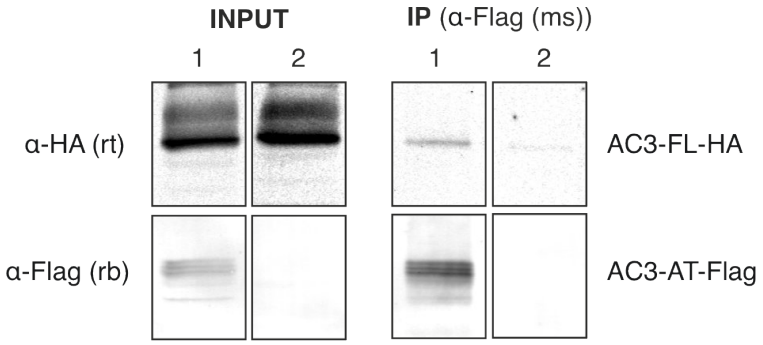

Figure 21: Co-immunoprecipitation of AC3-FL-HA and AC3-AT-Flag. As published by Khani et al. (2024). Representative Western blot analysis of the input fraction (INPUT) and immunoprecipitates (IP) collected during co-immunoprecipitation of AC3-FL-HA and AC3-AT-Flag performed using anti-Flag magnetic beads. For co-immunoprecipitation, CHO K1 cells stably expressing AC3-FL-HA were transiently transfected with (1) *pcDNA3.1 Adcy3-at-Flag* or (2) *zeo_mCherry*. Protein lysates of transfected cells were prepared. 500 µg total protein in a total volume of 500 µL were loaded on equilibrated anti-Flag M2 (mouse) magnetic beads (75 µL (= 1 x CV) bead slurry was used) and incubated end-over-end overnight. After incubation, the non-bound supernatant was removed from the beads, which were then washed four times with 5 x CV washing buffer. Immunoprecipitated protein was eluted using 2 x CV 0.1 M glycine pH 3.0 and neutralized in 25 µL 1 M Tris/HCl pH 8.0. In Western Blot analysis, 45 µg of total protein lysates were loaded as input (INPUT) and 45 µL of supernatant from non-bound, washing, immunoprecipitate (IP) and bead fraction were analyzed. AC3-FL-HA and AC3-AT-Flag were detected using Flag (rabbit) - and HA-specific antibodies, respectively.

3.2.3 Analyzing plasma membrane localization using cell-free plasma membrane sheets

To analyze the localization of transmembrane proteins in the plasma membrane using an independent, imaging-based approach, unroofing experiments were performed. Here, cells were treated with ultrasound (sonication), whereby the majority of the cell is removed and only the basal plasma membrane that is attached to the coverslip is left behind (cell-free plasma membrane sheet) (**Figure 22**). In combination with antibody labeling, the localization of proteins in the plasma membrane can be analyzed.

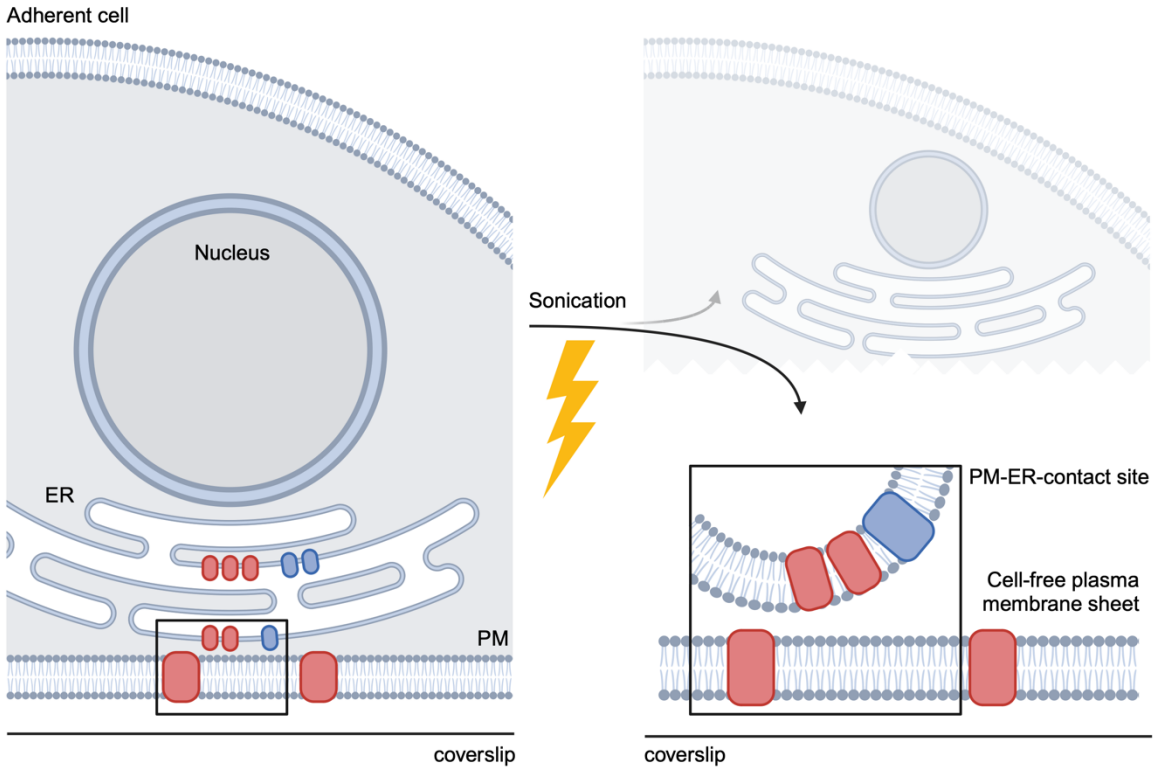

Figure 22: Generation of cell-free plasma membrane sheets. The majority of a cell grown on a glass coverslip is removed by ultrasound treatment, which leaves only the basal plasma membrane (cell-free plasma membrane sheet). Distal parts of the ER membrane fused to the plasma membrane (plasma membrane- endoplasmic reticulum contact sites) remain attached to the plasma membrane after sonication.

Also here, CNGA2-TM was included as a positive control. CNGA2-TM-HA was transiently expressed in HEK293 cells, which were then sonicated, fixed, and labeled with a CNGA2-TM-specific antibody (CRO 3B10) and an antibody against the HA-tag. In addition, sheets were labeled with an anti-Calnexin antibody, as Calnexin is a transmembrane protein of the endoplasmic reticulum (ER), which served as a control to label membrane sheets containing ER membranes (**Figure 23**). The Calnexin staining displayed a pattern of prominent spots (**Figure 23, top row, cell-free plasma membrane sheet, image on the left**), most likely representing plasma membrane- endoplasmic reticulum (PM-ER) contact sites (**Figure 23, top row, cell-free plasma membrane sheet, image on the left, arrows**). CRO 3B10- and HA-staining largely overlapped (**Figure 23, bottom right**). The majority of labeled CNGA2-TM-HA was evenly distributed in a sharply outlined structure

(**Figure 23, top right, top middle**), indicating the plasma membrane. CNGA2-TM-HA was also localized to the prominent spots resembling the Calnexin staining pattern (**Figure 23, arrows**). These spots most likely represent CNGA2-TM-HA accumulating in the ER membrane due to overexpression.

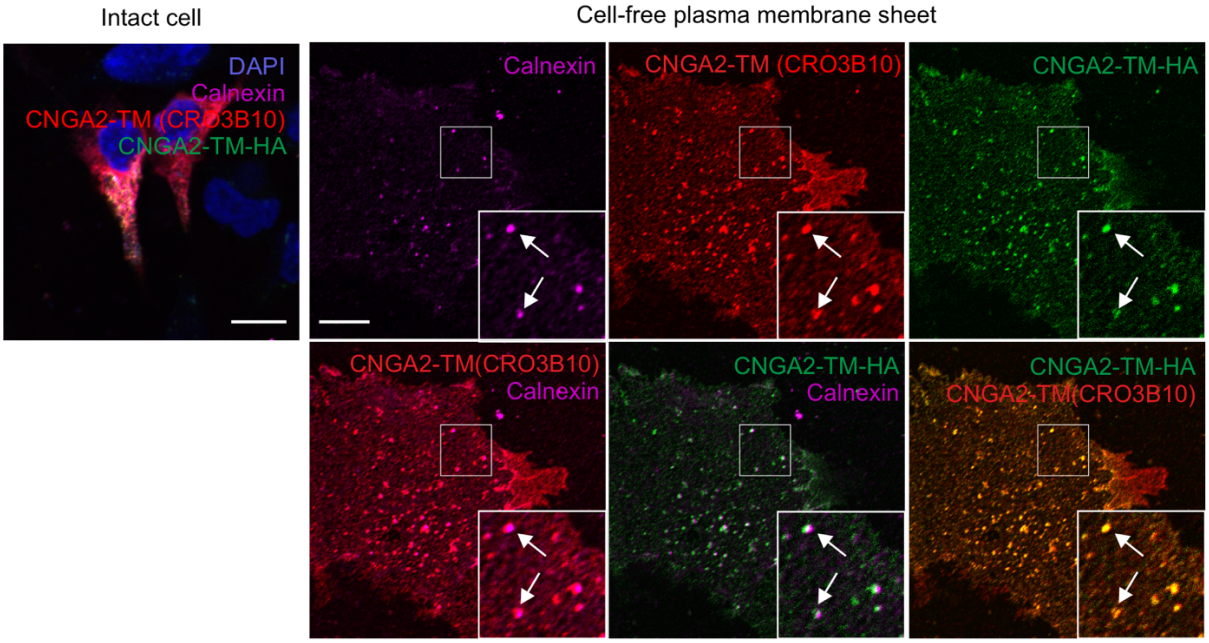

Figure 23: Generation of cell-free plasma membrane sheets in HEK293 expressing CNGA2-TM. HEK293 cells transiently transfected with CNGA2-TM-HA were sonicated and fixed with 4% PFA. Immunocytochemical staining with an anti-Calnexin antibody (ER-marker, magenta), a CNGA2-TM-specific antibody (red), and an anti-HA antibody (green) was performed. An intact cell is shown on the left; a cell-free plasma membrane sheet is shown on the right; single channels are shown at the top; merged images are in the bottom row. White boxes are shown as a magnified view at the bottom-right. Arrows point to endoplasmic reticulum-plasma membrane (ER-PM) contact sites. The results are representative of three replicates. Scale bar: 10 µm.

To identify the plasma membrane sheets more clearly, HEK293 cells were transiently co-transfected with mCherryCaaX, expressing a prenylated mCherry, which inserts into the plasma membrane and serves as a plasma membrane marker. The cells were sonicated, fixed, and labeled with an anti-Calnexin antibody (ER-marker) and an antibody against the HA-tag to analyze the localization of CNGA2-TM-HA (**Figure 24**). The mCherryCaaX fluorescence was detected in a sharply outlined region **(Figure 24, cell-free plasma membrane sheet, top right)** cell devoid of ER contact sites, labeled by the anti-Calnexin

antibody (**Figure 24, asterixes**), thus representing the cell-free plasma membrane sheet. The mCherryCaaX fluorescence largely overlapped with the HA staining (**Figure 24, bottom middle**), indicating that the CNGA2-TM-HA also resides in the plasma membrane.

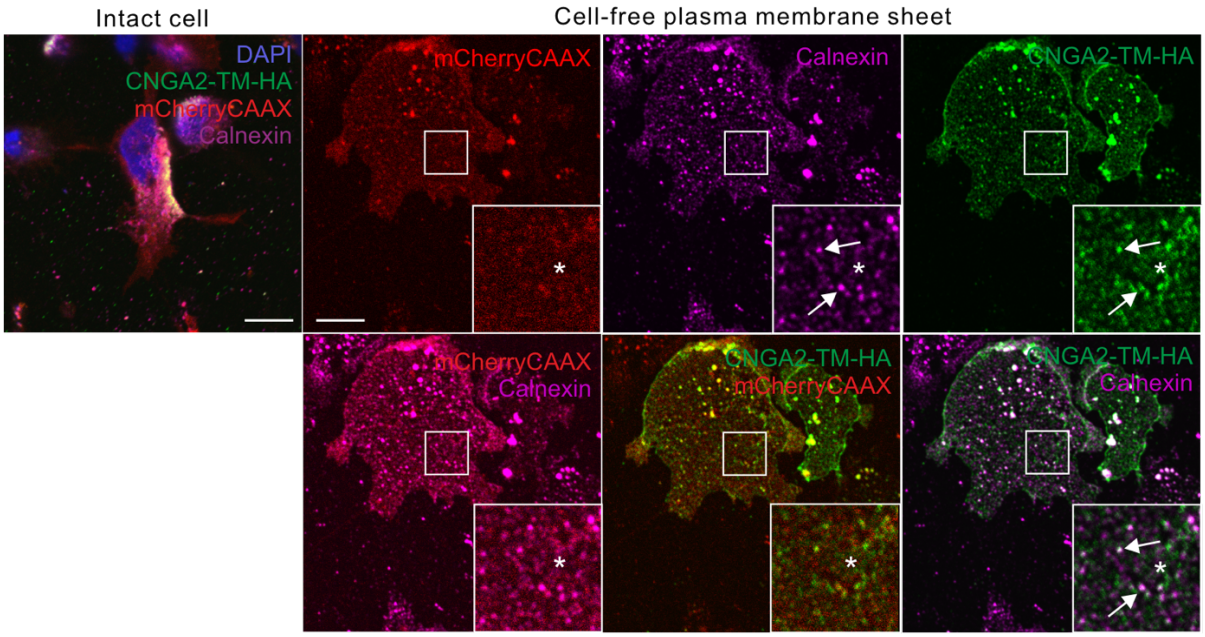

Figure 24: Counterstaining of plasma membrane and ER membrane. HEK293 cells transiently transfected with CNGA2-TM-HA and CherryCAAX were sonicated and fixed with 4 % PFA. Immunocytochemical staining with an anti-Calnexin antibody (ER-marker, magenta) and an anti-HA antibody (green). mCherryCAAX fluorescence is indicated in red. An intact cell is shown on the left, a cell-free plasma membrane sheet is shown on the right, single channels are shown at the top, and merged images are shown at the bottom row. White boxes are shown as a magnified view at the bottom right. Arrows point to endoplasmic reticulum-plasma membrane (ER-PM) contact sites; asterixes indicate contact-free sites within the membrane sheet. The results are representative of three replicates. Scale bar: 10 µm.

To analyze the localization of AC3-FL-HA or AC3-AT-HA in the plasma membrane, CHO K1 cells stably expressing mCherryCaaX (obtained from Lea Wobig, Caesar, Bonn), were transiently transfected with CNGA2-TM-HA, AC3-FL-HA, or AC3-AT-HA (**Figure 25**). Cells were sonicated, fixed, and labeled with an anti-Calnexin antibody (ER-marker) and an antibody against the HA-tag to localize CNGA2-TM-HA or the respective AC.

The Calnexin staining displayed a pattern of prominent spots **(Figure 25, A, B and C cell-free plasma membrane sheet, top middle)**, which were scattered randomly across an

area, also showing evenly distributed endogenous mCherryCaaX fluorescence, clearly indicating ER-plasma membrane contact sites **(Figure 25, arrows)**. The CNGA2-TM-HA (**Figure 25A, cell-free plasma membrane sheet, top right**) and the AC3-FL-HA (**Figure 25B, cell-free plasma membrane sheet, top right**) staining largely overlapped with the mCherryCaaX fluorescence **(Figure 25A and B, cell-free plasma membrane sheet, bottom middle)**, indicating that both CNGA2-TM-HA and AC3-FL-HA reside in the plasma membrane. Both also showed prominent spots in a pattern resembling Calnexin staining **(Figure 25A and B, cell-free plasma membrane sheet, bottom right)**, most likely representing the protein accumulating in the ER due to overexpression. However, AC3-AT-HA was not detected within the area of evenly distributed mCherryCaaX fluorescence **(Figure 25C, cell-free plasma membrane sheet, bottom middle)**. Instead, AC3-AT was only detected in the prominent spots resembling the Calnexin staining (**Figure 25C, cell-free plasma membrane sheet, bottom right**), suggesting that AC3-AT does not localize to the membrane but might be stuck in the ER membrane.

As a control, CHO K1 cells stably expressing mCherryCaaX were sonicated, fixed, and labeled with an anti-Calnexin antibody (ER-marker) and an antibody against the HA-tag. The average HA fluorescence intensity due to non-specific binding was quantified (**Figure 25D, empty**) and compared with the average HA fluorescence intensity in plasma membrane sheets positive for CNGA2-TM-HA, AC3-FL-HA, or AC3-AT-HA. The average HA fluorescence of CNGA2-TM-HA and AC3-FL-HA within plasma membrane sheets was higher than the intensities measured for AC3-AT-HA and the background (“empty”) average HA fluorescence intensity (**Figure 25D**).

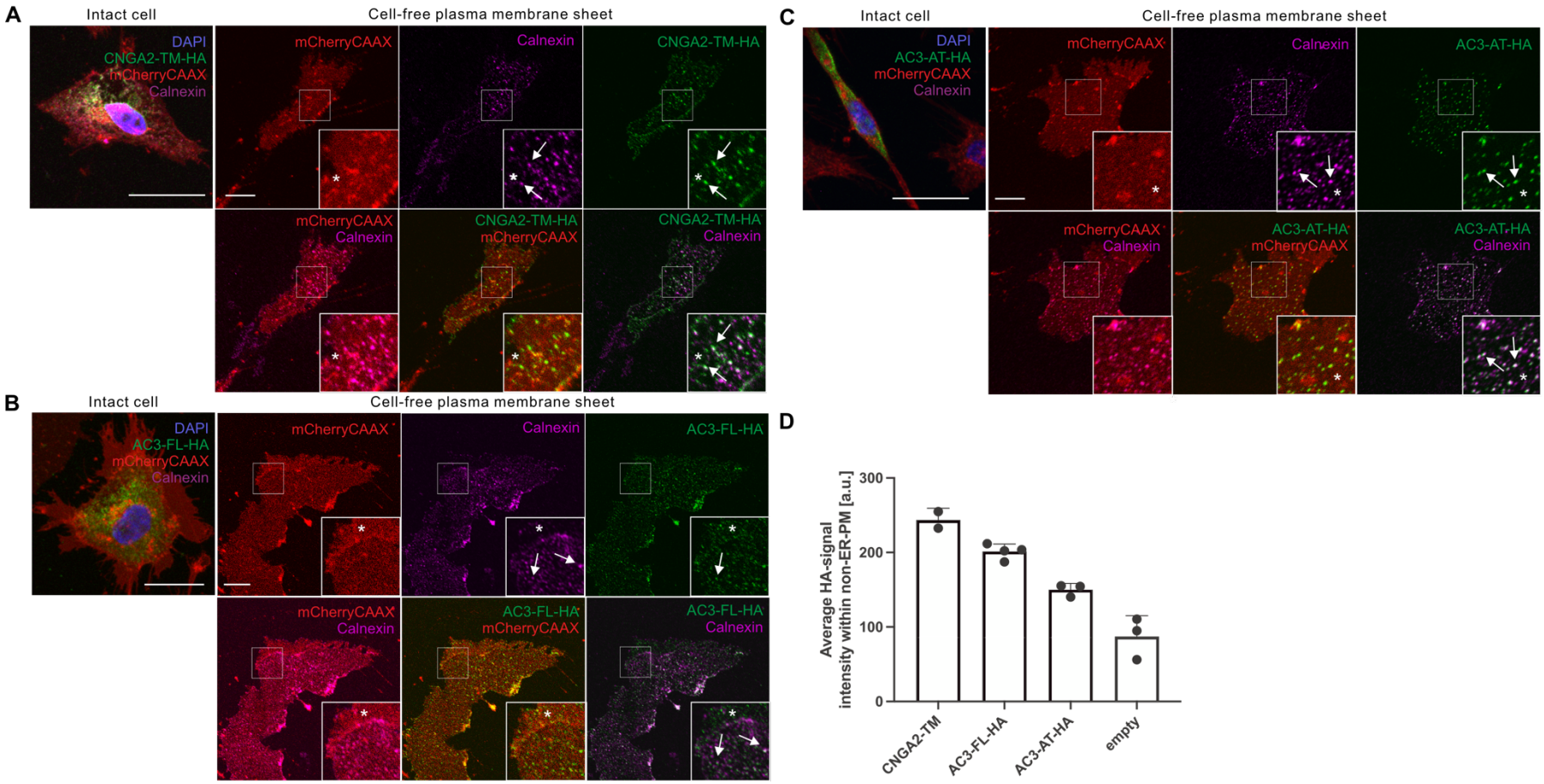

Figure 25: AC3-FL-HA and AC3-AT-HA are detected in cell-free plasma membrane sheets. CHO K1 cells stably expressing mCherryCAAX and transiently transfected with CNGA2-TM-HA (A), AC3-FL-HA (B) or AC3-AT-HA (C) were sonicated and fixed with 4% PFA. Afterwards, immunocytochemical staining with an anti-Calnexin antibody (ER-marker, magenta) and an anti-HA antibody (green) was performed. mCherryCAAX fluorescence is indicated in red. An intact cell is shown on the left, a cell-free plasma membrane sheet on the right; single channels are shown at the top, merged images at the bottom row. White boxes are shown as a magnified view on the bottom-right. Arrows point to endoplasmic reticulum plasma-membrane (ER-PM) contact sites; asterixes indicate contact-free parts within the membrane sheet. Scale bar: 10 µm. (D) Quantification of the average HA-signal intensity within contact-free parts of the membrane sheet. Data shown as mean + S.D. and are representative of n = 2 (CNGA2-TM-HA), n = 4 (AC3-FL-HA) and n = 3 (AC3-AT-HA, empty) replicates.

To verify that the transient expression of AC3-AT-HA does not interfere with its localization in the plasma membrane, the same experiments were performed using CHO K1 cells stably expressing AC3-FL-HA or AC3-AT-HA that were transiently transfected with mCherryCaaX (**Figure 26**).

The Calnexin staining displayed a pattern of prominent spots scattered randomly across an area (**Figure 26A and B, cell-free plasma membrane sheet, top middle**), showing evenly distributed endogenous mCherryCaaX fluorescence (**Figure 26A and B, cell-free plasma membrane sheet, top left**), indicating a plasma membrane sheet. The AC3-FL-HA staining largely overlapped with the mCherryCaaX fluorescence (**Figure 26A, cell-free plasma membrane sheet, bottom middle**), indicating that AC3-FL-HA resides in the plasma membrane. AC3-FL-HA showed prominent spots resembling Calnexin staining (**Figure 26A, cell-free plasma membrane sheet, bottom right, arrows**), most likely representing AC3-FL-HA accumulating in the ER due to overexpression.

Again, AC3-AT-HA was not localized in the area of evenly distributed mCherryCaaX fluorescence (**Figure 26B, cell-free plasma membrane sheet, bottom middle**). Instead, AC3-AT was only detected in the prominent spots resembling the Calnexin staining (**Figure 26B, cell-free plasma membrane sheet, bottom right**), demonstrating that AC3-AT does not localize to the membrane but only to PM-ER contact sites, which is in accordance with the results shown above in **Figure 25, C**.

Comparing the background (“empty”) HA fluorescence intensity with HA fluorescence intensity recorded within plasma membrane sheets from cells expressing AC3-FL-HA or AC3-AT-HA (**Figure 26, D**) revealed that AC3-FL-HA average HA fluorescence intensity was significantly higher compared to AC3-AT-HA and background (“empty”) average HA fluorescence intensity.

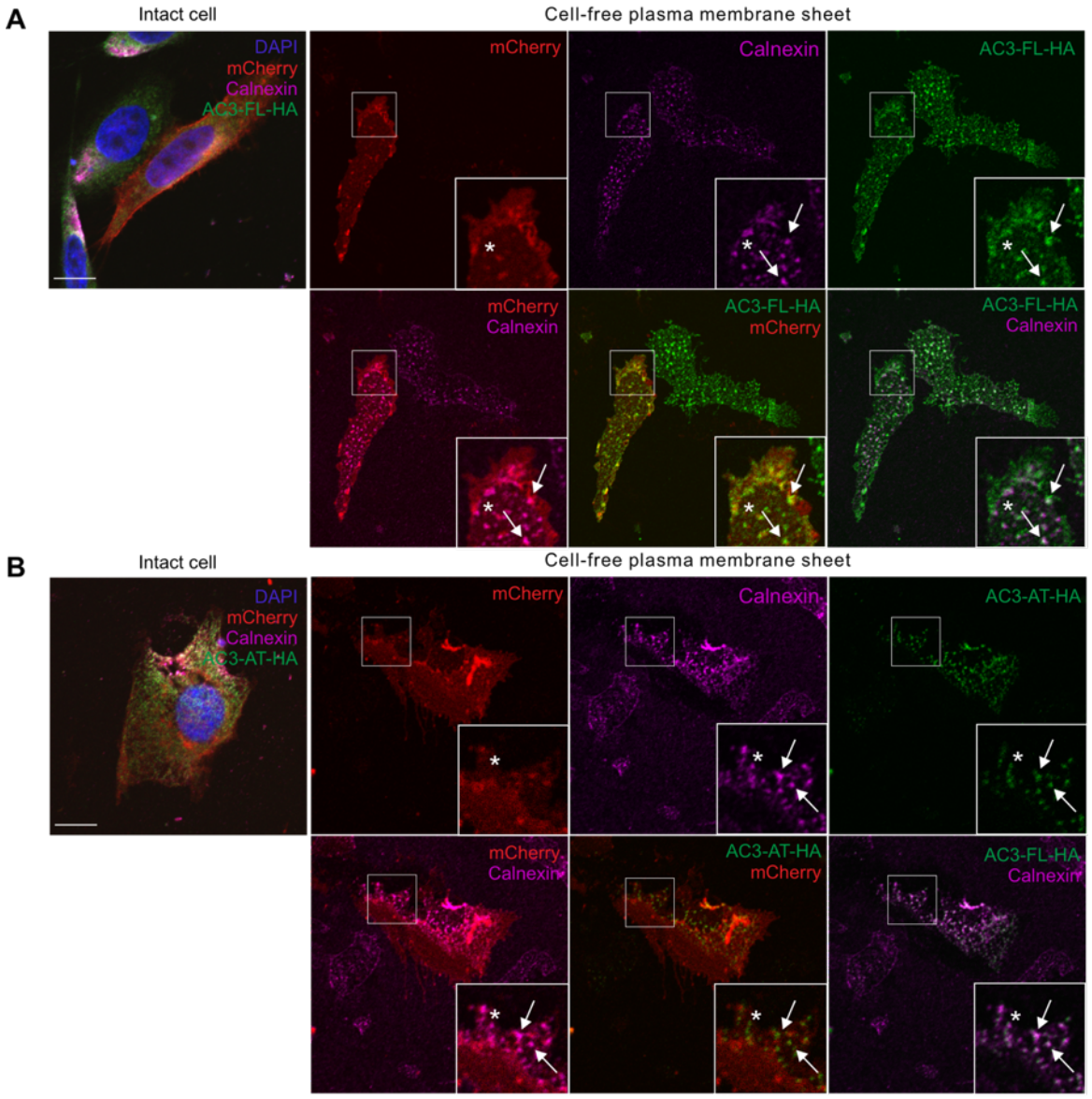
A
Intact cell
Cell-free plasma membrane sheet
DAPI
mCherry
Calnexin
AC3-FL-HA
mCherry
Calnexin
AC3-FL-HA
mCherry
AC3-FL-HA
mCherry
Calnexin
AC3-FL-HA
Calnexin
B
Intact cell
Cell-free plasma membrane sheet
DAPI
mCherry
Calnexin
AC3-AT-HA
mCherry
Calnexin
AC3-AT-HA
mCherry
Calnexin
AC3-AT-HA
mCherry
AC3-FL-HA
Calnexin

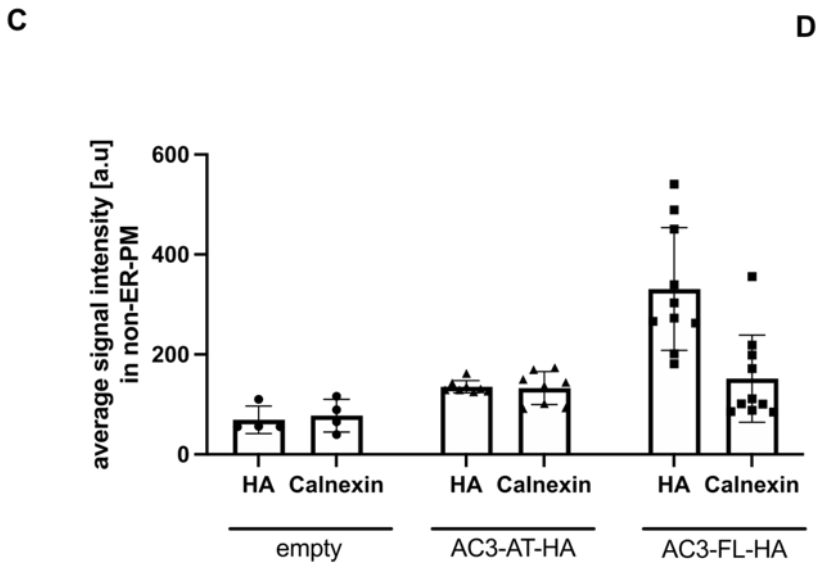
C
average signal intensity [a.u]
in non-ER-PM
600
400
200
0
HA
Calnexin
HA
Calnexin
HA
Calnexin
empty
AC3-AT-HA
AC3-FL-HA

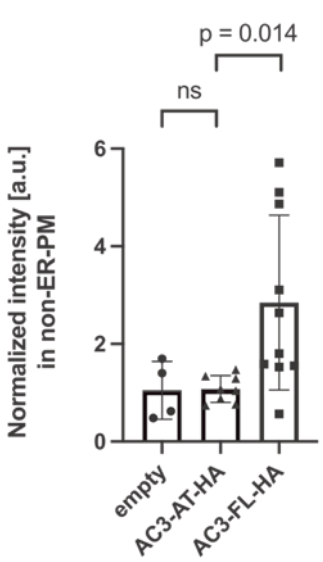
D
p = 0.014
ns
Normalized intensity [a.u.]
in non-ER-PM
6
4
2
0
empty
AC3-AT-HA
AC3-FL-HA

Figure 26: Localization of AC3-AT-HA in cell-free plasma membrane sheets is limited to PM-ER contact sites. As published by Khani et al. (2024). CHO K1 cells stably expressing AC3-FL-HA **(A)** or AC3-AT-HA **(B)** and transiently transfected with mCherry-CAAX were sonicated. Afterwards, immunocytochemical staining with an anti-Calnexin antibody (ER-marker, magenta) and an anti-HA antibody (green) was performed. mCherryCAAX fluorescence is indicated in red. Single channels are shown at the top, with merged images at the bottom row. White boxes are shown as a magnified view at the bottom-right. Arrows point to endoplasmic reticulum-plasma membrane (ER-PM) contact sites, and asterixes indicate contact-free parts within the membrane sheet. The results are representative of six replicates. Scale bar: 10 µm. **(C)** Quantification of the average HA signal intensity within contact-free parts of the membrane sheet. Data shown as mean + S.D. and are representative of n = 10 (AC3-FL-HA), n = 8 (AC3-AT-HA), and n = 4 (empty) replicates. **(D)** Quantification of normalized HA signal intensity within contact-free parts of the membrane sheet. Data shown as mean + S.D. and are representative of n = 10 (AC3-FL-HA), n = 8 (AC3 AT-HA), and n = 4 (empty) replicates. P-value was calculated with unpaired, two-tailed Student's t-test. ns: not significant.

3.3 Analyzing the enzymatic activity of AC3-FL versus AC3-AT

Transmembrane adenylyl cyclases are activated when the two catalytic domains C1 and C2 interact. C1-C2 dimerization is promoted by the interaction between the two blocks of transmembrane domains. AC3-AT contains both C1 and C2, but lacks the first block of transmembrane domains. Thus, it is not known whether conformational changes that are required to promote C1-C2 interaction are preserved in AC3-AT. Thus, the activity of AC3-AT in comparison to AC3-FL was analyzed.

Adenylyl cyclases can be pharmacologically activated using isoproterenol or forskolin (FSK). Isoproterenol is a β-adrenoceptor agonist, causing the G-protein subunit $G_{\alpha s}$ to bind to the C1 subunit, promoting the interaction with C2. In contrast, forskolin directly binds to the catalytic units, promoting the C1-C2 interaction (**Figure 27**).

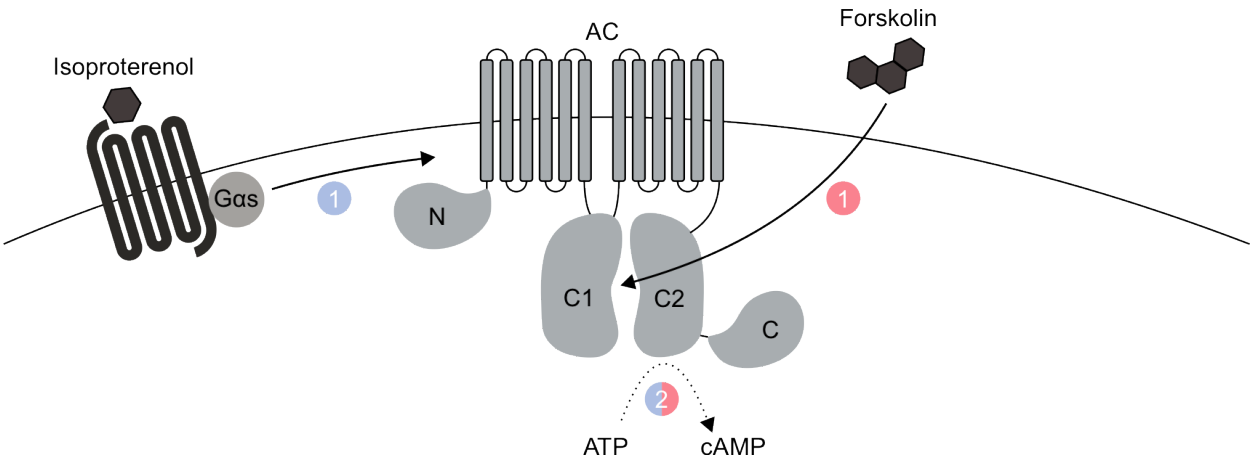

Figure 27: Mechanism of Action of Isoproterenol and Forskolin. Modified from Dessauer et al. (2017). Isoproterenol (blue) increases adenosine 3′, 5′-cyclic monophosphate (cAMP) levels through stimulation of a G-protein (Gαs)-coupled receptor (β-adrenoceptor), which subsequently activates adenylyl cyclases, whereas forskolin (red) causes a dimerization of the catalytic subunits C1 and C2 of the adenylyl cyclase, resulting in the conversion of adenosine triphosphate (ATP) to cAMP.

Total cAMP levels after stimulation with isoproterenol or forskolin were measured in CHO K1 cells using an ELISA (Enzyme-linked Immunosorbent Assay).

3.3.1 Analyzing the enzymatic activity upon stimulation with forskolin

Wild-type (WT) CHO K1, CHO K1 cells stably expressing AC3-FL-HA or AC3-AT-HA were treated with either 2 µM forskolin (FSK) alone, 2 µM FSK and 100 µM 3-Isobutyl-1-methylxanthin (IBMX), or dimethyl sulfoxide (DMSO) as a control for 30 minutes. Total protein lysates were prepared and transferred to an anti-cAMP-covered microplate. In the total protein lysates or standard, cAMP competes with a horseradish peroxidase (HRP)-cAMP conjugate for binding sites on the anti-cAMP antibody. Increasing amounts of cAMP in the respective samples decrease the amount of bound conjugate, thus decreasing measured HRP activity (**Figure 28**).

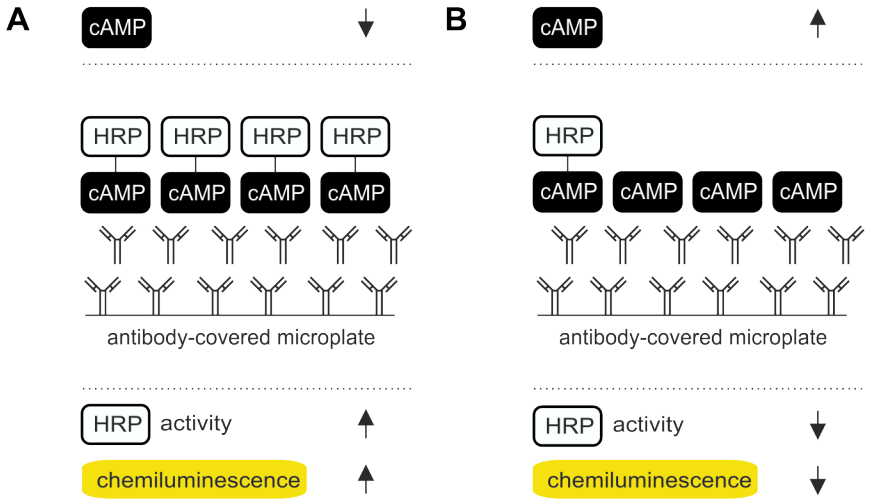

Figure 28: Principles of the ELISA-Assay. Image adapted from Molecular Devices. Total protein lysates were prepared and transferred to an anti-cAMP-covered microplate. In the total protein lysates or standard, cAMP competes with a horseradish peroxidase (HRP)-cAMP conjugate for binding sites on the anti-cAMP antibody. When the amounts of cAMP in the sample are small **(A)**, bigger amounts of HRP-cAMP conjugate are bound to the anti-cAMP antibody, thus increasing measured HRP activity. High amounts of cAMP in the respective samples **(B)** decrease the amount of bound conjugate, thus decreasing measured HRP activity.

To calculate cAMP amounts in the respective sample, the intensity of chemiluminescence was interpolated, and concentrations were determined according to the standard curve. The fold change in cAMP concentration was calculated by normalizing the values to the respective buffer control (DMSO) and plotted with or without normalization to the respective protein amount in **Figure 29, A and 29, B**.

FSK stimulation increased total cAMP levels in WT cells (**Figure 29, A or B, WT, FSK**), which reflects the activation of endogenous adenylyl cyclases. Total cAMP levels in cells expressing AC3-FL-HA were significantly increased compared to WT cells (**Figure 29, A or B, AC3-FL, FSK**), demonstrating that the over-expressed AC3-FL-HA can be stimulated by FSK. However, there was no significant increase in total cAMP levels in cells stably expressing AC3-AT-HA (**Figure 29, A or B, AC3-AT, FSK**), indicating that AC3-AT is not active.

Stimulation with FSK and IBMX further increased total cAMP levels in WT cells compared to FSK alone (**Figure 29, A and B, WT, FSK and IBMX**), reflecting the activation of endogenous adenylyl cyclases (FSK) and the inhibition of phosphodiesterases (IBMX). Total cAMP levels in cells expressing AC3-FL-HA were significantly increased compared

to WT cells (**Figure 29, A and B, AC3-FL, FSK and IBMX**). However, there was no significant increase in total cAMP levels in cells expressing AC3-AT-HA, indicating that AC3-AT is not active.

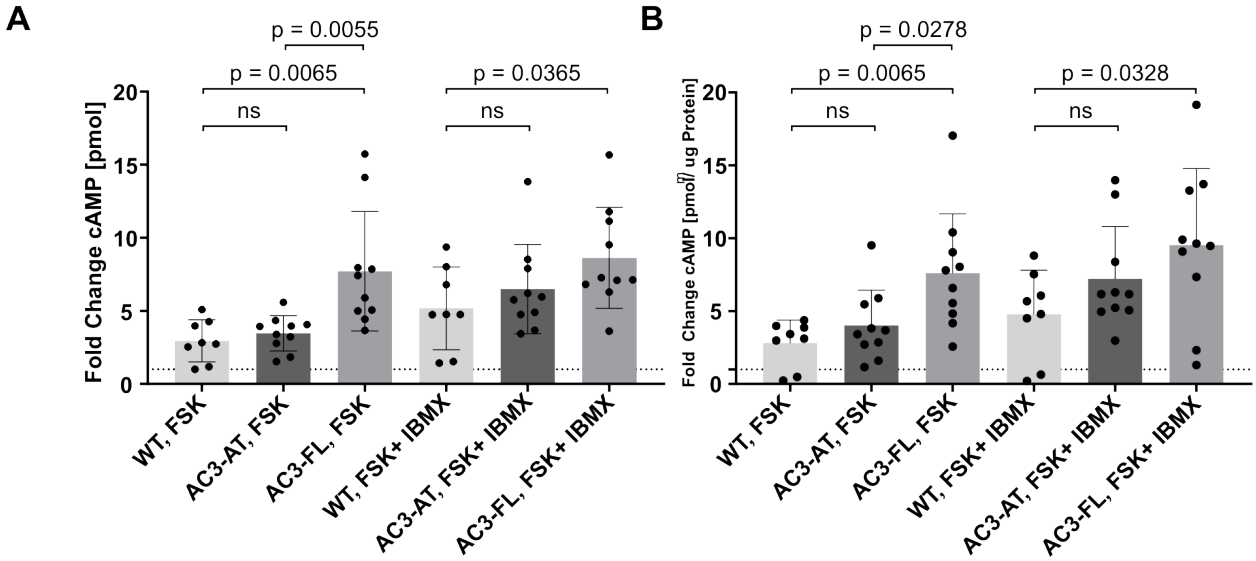

Figure 29: Quantification of intracellular cAMP levels using ELISA. As published by Khani et al. (2024). A chemiluminescence-based cAMP assay was performed by adding the buffer control DMSO, 2 µM Forskolin (FSK), or 2 µM FSK and 100 µM 3-isobutyl-1-methylxanthine (IBMX) for 30 min to CHO K1 wild-type (WT) or CHO K1 cells stably expressing AC3-AT-HA or AC3-FL-HA. Chemiluminescence is measured on a FluoStar fluorescence microplate reader. Values were normalized to the respective buffer control. **(A)** Fold change of absolute cAMP levels [pmol]. **(B)** Fold change of cAMP levels normalized to the respective amount of total protein. Mean ± S.D. for n = 4 (wild-type) and n = 5 (AC3-FL, AC3-AT) experiments are indicated. Statistical analyses were performed using an unpaired, two-tailed Student's t-test. ns: not significant.

3.3.2 Analyzing the enzymatic activity upon stimulation with isoproterenol

The same experiments were performed using WT, CHO K1 cells stably expressing AC3-FL-HA, or AC3-AT-HA that were treated for 15 min with 1 µM isoproterenol (Iso) or ES buffer as a control. The fold change of cAMP levels with or without normalization to the respective amount of protein in the sample is plotted in **Figure 30, A and B**.

Isoproterenol stimulation increased the total cAMP concentration in WT cells, which reflects the activation of endogenous adenylyl cyclases (**Figure 30, A and B, WT, Iso**). Total cAMP levels in cells expressing AC3-FL-HA were significantly increased compared to WT cells (**Figure 30, A, AC3-FL, Iso**), demonstrating that AC3-FL-HA is sensitive to activation by $G_{\alpha s}$. However, there was no significant increase in total cAMP levels in cells

stably expressing AC3-AT-HA (**Figure 30, A and B, AC3-AT, Iso**), indicating that AC3-AT is not activated by $G_{\alpha s}$ proteins. Furthermore, total cAMP levels in cells stably expressing AC3-AT-HA were decreased compared to total cAMP levels in total protein lysates of WT cells, suggesting that overexpression of AC3-AT-HA inhibits the basal activity of endogenous adenylyl cyclases.

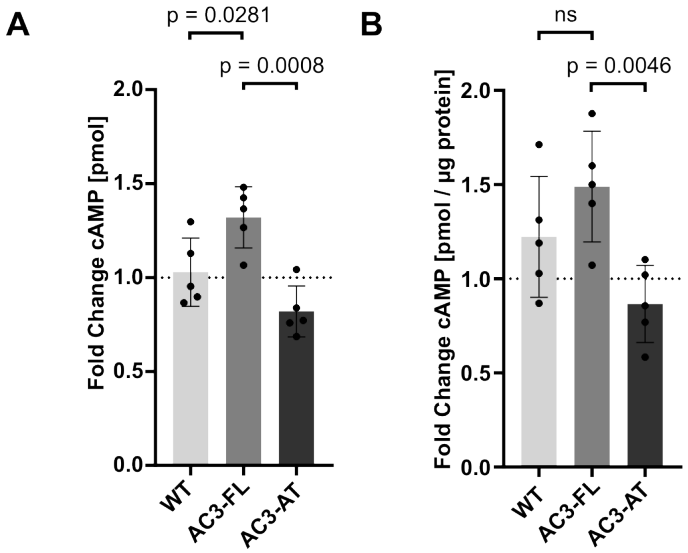

Figure 30: AC3-AT exerts a dominant negative effect on endogenous adenylyl cyclases. As published by Khani et al. (2024)**.** A chemiluminescence-based cAMP assay was performed by adding ES buffer control or 1 µM isoproterenol (Iso) for 15 min to CHO K1 wild-type (WT) and CHO K1 cells stably expressing AC3-FL-HA or AC3-AT-HA. Chemiluminescence is measured on a FluoStar fluorescence microplate reader. All values were normalized to the respective buffer control. **(A)** Fold change of absolute cAMP levels in pmol. **(B)** Fold change of cAMP levels normalized to the respective amount of total protein. The mean ± S.D. for n = 5 separate experiments is indicated. Statistical analyses were performed using unpaired, two-tailed Student's t-test. ns: not significant.

4. Discussion

Here, I investigated the cellular function of the truncated AC3-AT protein. I could demonstrate that AC3-FL, but not AC3-AT, localizes to the plasma membrane. Furthermore, I showed that AC3-AT is catalytically inactive, demonstrating that the truncation renders AC3-AT inactive. I could also demonstrate that AC3-AT heterodimerizes with AC3-FL *in vitro*. Moreover, AC3-AT impaired the transport of AC3-FL to the plasma membrane, which could, in turn, reduce AC3-FL levels in the plasma membrane, resulting in reduced global cAMP production in the cell. In summary, my results indicate that the expression of a truncated AC3 protein isoform provides a mechanism to curb intracellular cAMP signaling in brown adipocytes.

4.1 Regulating intracellular cAMP homeostasis and downstream signaling

Different mechanisms have evolved to regulate intracellular cAMP signaling. They operate at the GPCR level, continuing at the AC level, and unceasingly also at cAMP and PKA levels.

One thoroughly studied example of limiting GPCR signaling and ultimately reducing intracellular cAMP levels is the desensitization and receptor internalization of GPCRs upon repeated or prolonged stimulation. When bound by agonists, G protein-coupled receptors (GPCRs) are phosphorylated by G-protein-coupled receptor kinases (GRKs). (Pitcher et al., 1998). Ubiquitously expressed β-arrestins bind phosphorylated GPCRs (Lefkowitz and Shenoy, 2005). For short-term desensitization, arrestin-binding physically obstructs G-protein coupling to the GPCR, whereby the GPCR becomes resistant to repeated stimuli and, therefore, less sensitive. For long-term desensitization, arrestins function as endocytotic adapters, linking the GPCRs to the clathrin-coated pit machinery. More specifically, β-arrestins facilitate the endocytosis of GPCRs by serving as adaptors for β2 adaptin (AP2) and clathrin, directing them to clathrin-coated pits. The GPCRs are then targeted to lysosomes for degradation. Therefore, GPCRs not only become less sensitive but also the GPCR density in the plasma membrane decreases (Harden, 1983;

Lohse, 1993; Rajagopal and Shenoy, 2018). Loss of β-arrestin-dependent receptor internalization upon depletion of both β-arrestin isoforms in HEK293 cells lead to prolonged G-protein-dependent cAMP production and the response was further increased upon ligand binding (Jones et al., 2021). In line with this finding, inhibiting GRK activity by expressing a dominant negative mutant of GRK2 in CHO cells resulted in increased GPCR expression and higher cAMP responses (Horie and Insel, 2000).

Another thoroughly studied example of regulating GPCR trafficking are receptor expression enhancing proteins (REEPs), an evolutionally conserved family of six ER-shaping proteins (REEP1-6), which are common in various mammalian tissues (Fan et al., 2022). REEPs were originally identified in olfactory sensory neurons (Saito et al., 2004), where they increase ER trafficking of α_2-AR to the plasma membrane and thereby enhance total α_2-AR protein levels in the plasma membrane. This function is not limited to GPCR trafficking, but REEPs also seem to control AC trafficking. More specifically, *(i)* REEP6 is highly expressed in murine adipocytes, *(ii) Reep6* expression was upregulated during cold exposure, *(iii)* REEP6 knockout mice showed reduced levels of AC3 in BAT, and in turn, *(iv)* REEP6 knockout mice displayed an ablation of cold-induced thermogenesis and, in turn, showed increased susceptibility to weight gain (Son et al., 2022).

Downstream, intracellular cAMP levels are directly controlled by the activity of phosphodiesterases (PDEs). PDEs hydrolyze cAMP to 5'-AMP by cleavage of the 3',5'-phosphodiester bond in cAMP (Azevedo et al., 2014), which results in rapid termination of the signaling cascade and hence the downstream effects of cAMP. In the past, the cAMP second messenger was believed to diffuse freely in the cytosol (Hunter, 2000). However, this assumption upsets the notion that different adrenergic receptors expressed in the same cell, each evoking distinct physiological output signals, transduce signaling via the same second messenger. An emerging view is that cAMP diffusion is rather restricted to localized microdomains in certain subdomains of the cell (Kayser et al., 2022), generating compartmentalized cAMP signaling, which ensures the specificity of the cAMP response. One mechanism contributing to shaping cAMP microdomains are PDEs, which provide an enzymatic barrier to cAMP diffusion (Abrahamsen et al., 2004; Jurevicius et al., 2003; Mongillo et al., 2004; Mongillo and Zaccolo, 2006; Rich et al., 2001), creating a

nanometer-size domain around the place of cAMP origin (Anton et al., 2022; Bock et al., 2020), resulting in a selective activation of defined subsets of downstream effector targets (Di Benedetto et al., 2008). Accordingly, studies using FRET-based imaging techniques have shown that inhibition of PDEs disperses cAMP gradients (Terrin et al., 2006), pointing out the central role of PDEs in cAMP compartmentalization. An increase in spatial resolution of cAMP signaling events was achieved by means of advanced FRET-based imaging techniques using FRET sensors targeted to distinct subcellular subdomains (Surdo et al., 2017), contributing further evidence for the involvement of PDEs in compartmentalized cAMP signaling. Another crucial role in signaling compartmentalization is exerted by A-kinase-anchoring proteins (AKAPs), that not only tether PKA to specific subcellular localizations of PKA targets (Skroblin et al., 2010), but also to other components of the cAMP signaling cascade, such as GPCRs (Malbon, 2007) , ACs (Dessauer, 2009), and PDEs (Scott et al., 2013).

4.2 Expression of truncated protein isoforms – a common strategy to regulate cell and tissue function?

Alternative AC protein isoform expression has already been observed in vascular smooth muscle cells (VSMCs). VSMCs are the major cell type in blood vessel walls and play a fundamental role in the pathophysiology of atherosclerosis. Here, a crucial step is the transdifferentiation of VSMCs from contractile (differentiated, quiescent, non-migratory) to synthetic (dedifferentiated, proliferative, migratory) phenotypes. The molecular mechanisms underlying the transdifferentiation of VSMCs are not fully understood. The transdifferentiation of rat VSMCs to the synthetic phenotype is triggered by the proinflammatory cytokine interleukin 1β (IL-1β), which is secreted by macrophages infiltrating the vascular wall. This enables VSMCs to move from the medial to the intimal layer of the blood vessel (Ross et al. 1999, Lusis et al. 2000). The IL-1β signal is then potentiated by the production of prostaglandin E_2 (PGE_2) by VSMCs (Wen et al., 1998; Wohlfeil and Campbell, 1999; Yamamoto et al., 1999). In an autocrine manner, PGE_2 triggers VSMCs to transdifferentiate.

Transdifferentiation has been shown to be dependent on *de novo* expression of *Adcy8* in VSMCs (Clement et al., 2006; Keuylian et al., 2012), which in the contractile state only

express *Adcy 3*, *5*, and *6* (Webb et al. 2001, Ostrom et al. 2002). However, high levels of intracellular cAMP have been shown to inhibit the synthetic properties of transdifferentiated VSMCs and antagonize pathological vascular remodeling (McKean et al. 2015, Hewer et al. 2011). Vallin and colleagues identified that *de novo* expressed *Adcy8* in IL-1β-transdifferentiated VSMCs consists of four short AC8 protein isoforms derived from *Adcy8* splice variants (Vallin et al., 2018). All isoforms lacked the first five transmembrane domains (termed AC8E-H), and AC8E and AC8F represented the two isoforms exhibiting the highest levels of expression. Furthermore, AC8E-H isoforms were catalytically inactive and did not localize to the plasma membrane, suggesting that AC8E-H was retained in the rER. Using a FRET based approach, Vallin and colleagues demonstrated that AC8E-H downregulate cAMP production in IL1β transdifferentiated VSMCs. More specifically, they revealed that AC8E exerts a dominant negative effect on endogenous AC activity. Furthermore, they could show that AC8E and AC3 heterodimerize, and their data suggested that thereby, AC trafficking to the plasma membrane is diminished and, in turn, cAMP levels are reduced. These findings harmonize the *de novo* expression of AC8 with the diminished cAMP levels necessary for the emergence of synthetic VSMC characteristics (Vallin et al., 2018).

Accordingly, in my thesis, using two independent experimental approaches, I have demonstrated that AC3-FL localizes to the plasma membrane, whereas AC3-AT does not. This result is in line with the studies of Gu and colleagues, suggesting that two transmembrane clusters are necessary for the whole molecule to travel to the plasma membrane (Gu et al., 2001). Furthermore, I showed that AC3-AT is catalytically inactive (see 3.3.1), demonstrating that the truncation, even though it does not affect the catalytic domains, obliterates the enzymatic activity of AC3-AT. This is in accordance with other studies, which have shown that the interaction between the two transmembrane domains TM1 and TM2 promotes the intramolecular dimerization of C1 and C2, and thereby catalytic activity (Gu et al., 2001). My results also demonstrate that AC3-AT impairs the transport of AC3-FL to the membrane (see 3.2.1). Using co-immunoprecipitation, I showed that AC3-AT heterodimerizes with AC3-FL (see 3.2.2), which is in accordance with precedent studies demonstrating the formation of heteromeric assemblies between full-length ACs and engineered truncation mutants (Ding et al., 2005; Gu et al., 2001). In

summary, my results indicate that the expression of truncated AC protein isoforms provides a more general mechanism to regulate AC activity in brown adipocytes but also in VSMCs, as shown by others.

Further investigating the regulation of AC3-AT expression, Kornfeld and colleagues have shown that, in analogy to *Adcy3-at*, a 5'-terminally truncated mRNA isoform of *Ppargc1a* (termed *Ppargc1a-at*) was induced upon cold exposure, whereas the canonical *Ppargc1a* (*Ppargc1a-fl*) expression remained unchanged. As described above, *Ppargc1a* constitutes a key regulator in cold-induced BAT thermogenesis. Intriguingly, silencing *Ppargc1a-fl/ Ppargc1a-at* did not affect *Adcy3-fl* expression, but arrested *Adcy3-at* induction upon stimulation with CL316,234, a selective β_3-AR receptor agonist (Khani et al., 2024).

How the expression of these truncated protein isoforms is induced and regulated needs to be further studied. The Kornfeld lab has shown that upon cold induction, the H3K4me3 domain arises in the *Adcy3* gene in brown adipocytes, which marks a novel TSS located downstream of the original TSS in the 2nd intron of *Adcy3*. The novel TSS gives rise to the 5' truncated alternate transcript, *Adcy3-at*. How cold exposure induces the formation of H3K4me3 sites in the *Adcy3* gene is yet unclear. Epigenetic modification enzymes, like histone methyltransferases or histone demethylases, are widely recognized for their role in regulating the expression of many genes crucial for biological functions (Wang and Zhu, 2008). However, only a limited number of factors controlling these enzymes have been identified. One factor that has been identified to induce the expression of a histone demethylase is the transcription factor cAMP responsive element binding protein (CREB). More precisely, Li and colleagues have demonstrated that clenbuterol, a β_2-AR agonist, upregulates the β_2-AR/cAMP/PKA/p-CREB pathway, which in turn upregulates JHDM2a, a histone demethylase via direct binding of p-CREB to the CRE site in the JHDM2a promotor (Li et al., 2012). Accordingly, cold exposure could activate the β_3-AR signaling pathway upstream of specific histone methylases or demethylases and CREB may serve as an intermediary regulated by cAMP/PKA, triggering the induction of histone methylases or the inhibition of histone demethylases to facilitate an increase in H3K4me3 in the *Adcy3* gene.

4.3 The role of AC3 versus AC3-AT in BAT

Seminal studies by Granneman and colleagues have shown that in BAT, cold exposure and in turn, adrenergic stimulation not only trigger thermogenesis, but dramatically reorchestrate the expression of genes encoding for key molecular players involved in the thermogenic process, aiming to increase the functional capacity of BAT (Chaudhry et al., 1996; Granneman, 1995; Granneman and Bannon, 1989; Granneman and Lahners, 1992).

Transcriptome-wide gene expression changes in cold-exposed murine adipose tissues were monitored by the Kornfeld lab using RNA-sequencing, which showed that mRNA levels of *Adcy3* were specifically induced during cold exposure in BAT and inguinal WAT (iWAT), but not in epididymal WAT (eWAT). This finding is in accordance with earlier studies, proposing that *(i)* thermogenic adipocytes are only present in brown fat and subcutaneous, but not visceral white fat (Cohen and Spiegelman, 2016; Guo et al., 2021), and most importantly *(ii)* that AC3 represents a crucial component for proper cold-induced cAMP/ PKA signaling in thermogenic tissues (Granneman, 1995; Son et al., 2022). Furthermore, the Kornfeld lab analyzed *Adcy3* expression in previously published single-nucleus RNA-Seq (snRNA-seq) datasets from brown adipocytes, isolated from interscapular BAT (iBAT) (Sun et al., 2020) under thermoneutral *vs.* cold conditions. This revealed that *Adcy3* was lowly expressed under thermoneutral conditions, but its expression was induced upon cold exposure. This resembled the expression pattern for not only *Ucp1*, but also other known BAT-markers, such as *peroxisome proliferator-activated receptor gamma coactivator 1-alpha* (*PPARGC1A*) (Chang et al., 2018), encoding for the transcriptional coactivator PGC-1α, which increases e.g., mitochondrial biogenesis, and fatty acid oxidation, and thereby constitutes a key regulator in cold-induced BAT thermogenesis (Puigserver et al., 1998; Wu et al., 1999).

To further elucidate the role of *Adcy3* in brown adipose tissue, energy expenditure was measured in lean and obese pan-adipocyte-deficient *Adcy3* knockout mice. These were generated by crossing mice, expressing a Cre recombinase under the control of the *Adiponectin* (*Adipoq*)-promotor, with loxP-flanked *Adcy3* mice (*Adcy3-AdcKO*). Although cAMP levels in BAT of *Adcy3-AdcKO* mice were significantly reduced, energy expenditure

remained unchanged upon cold exposure. Only in the obese state after high fat diet (HFD) challenge, energy expenditure was reduced in *Adcy3-AdcKO* mice (Khani et al., 2024).

The Kornfeld lab has detected a novel, cold-inducible promotor in the *Adcy3* gene in BAT. This promotor gives rise to a 5' truncated *Adcy3* isoform, termed *Adcy3-at*. When interrogating their RNA-seq data separately for *Adcy3-fl* and *Adcy3-at*, Kornfeld and colleagues showed that, while elevated mRNA levels of *Adcy3-at* failed to appear during brown adipogenesis, mRNA levels of *Adcy3-at* were mainly induced in cold-exposed mature thermogenic adipocytes and constituted the main isoform during cold-exposure, pointing towards *Adcy3-at* playing a seminal role in mature thermogenic adipocytes (Khani et al., 2024).

As only *Adcy3-at*, and not *Adcy3,* expression is increased, the Wachten and Kornfeld labs further elucidated the role of AC3-AT and its effect on cAMP synthesis and energy metabolism *in vitro* and *in vivo*, by generating a mouse line only lacking *Adcy3-at* using CRISPR-Cas9-mediated gene deletion. First, cAMP levels in *Adcy3ΔAT* mice were measured after β-AR stimulation. It was shown that cAMP levels in brown adipocytes lacking mAC3-AT were increased after 24 h, but not 6 h of CL316,243 stimulation, which matched the kinetics of mAC3-AT expression, pointing towards mAC3-AT limiting cAMP synthesis after prolonged β-AR stimulation. Next, the role of mAC3-AT in regulating energy homeostasis was examined in lean mice. While food intake was increased, body weight remained unchanged and glucose tolerance was improved, suggesting negative energy balance in *Adcy3ΔAT* mice. To test, whether negative energy balance in *Adcy3ΔAT* mice was due to BAT gain-of-function, qPCR analysis was performed and revealed increased *Ppargc1a* and *Prdm16* expression, suggesting increased thermogenic activity in BAT of *Adcy3ΔAT* mice. Based on the induction of thermogenic genes in *Adcy3ΔAT* brown adipocytes, Khani and colleagues theorized that *Adcy3ΔAT* mice could be shielded from diet-induced obesity. Intriguingly, *Adcy3ΔAT* mice subjected to HFD feeding, were protected from HFD-induced gain in body weight. More precisely, obese mice deficient in AC3-AT exhibited enhanced glucose tolerance, comparable food intake, elevated oxygen consumption in both ambient and cold conditions, and heightened BAT activity assessed via subdermal thermometry telemetry probes. These findings suggest

that BAT gain-of-function is responsible for the negative energy balance seen in mice lacking *Adcy3-at* (Khani et al., 2024).

The phenotype of increased BAT activity and a state of negative energy balance observed in AC3-AT-deficient mice can be explained by AC3-AT constituting a suppressor of thermogenic activity in BAT. As demonstrated in this study, the presence of catalytically inactive AC3-AT leads to the heterodimerization of AC3-AT and AC3-FL and in turn, reduction of AC3-FL pools in the plasma membrane, subsequently causing diminished cAMP production within the cell. Consequently, this would result in reduced thermogenic activity. However, absence of AC3-AT results in a disinhibition of the thermogenic process, as pools of AC3-FL in the membrane would be increased and consequently, cAMP production uncurbed, finally leading to increased thermogenic activity.

4.4 Targeting BAT to tackle the obesity epidemic

There is significant interest in enhancing energy expenditure and promoting weight loss through pharmacological BAT activation. Various pharmacological agents increasing BAT activity at ambient temperatures have been tested in humans. According to their mode of action, the pharmacological agents used for drug-induced BAT activation have been grouped into four major classes (Mukherjee et al., 2016). The first two consist of sympathomimetic agents. In fact, studies in humans investigating the pharmacological activation of BAT thermogenesis to date have predominantly concentrated on sympathomimetic agents (Astrup et al., 1985; Carey et al., 2013; Cypess et al., 2012; Vosselman et al., 2012). Class one consists of drugs that are selective β3-AR agonists. Class two consists of drugs such as ephedrine, which increases endogenous NE release from SNS terminals and blocks NE reuptake, leading to increased synaptic NE concentration (Dulloo et al., 1991). Class three consists of drugs such as glitazones, which activate peroxisome proliferator-activated receptor gamma (PPARγ). Class four consists of natural products that act on various pathways within the adipocyte. It has been hypothesized that chronic treatment with ephedrine in humans induces thermogenesis in BAT, resulting in increased BAT activity. However, BAT activity was significantly reduced by chronic ephedrine treatment, which has been proposed to be due to decreased responsiveness of the β-AR to continuous stimulation with ephedrine, more precisely by receptor downregulation (Carey et al., 2015).

My study provides experimental evidence for a novel mechanism underlying the downregulation of cAMP signaling in brown adipocytes: During BAT thermogenesis, β-AR are activated, which in turn, activate adenylyl cyclases, whereby cAMP levels increase. In turn, CREB is phosphorylated by PKA and binds to CRE in the promotor region of specific histone methylases and demethylases, whereby their expression is regulated. I hypothesize that the methylases then catalyze the tri-methylation of H3K4 in the 2nd intron of *Adcy3*, whereby a novel TSS is generated, leading to the expression of the 5' truncated alternate transcript *Adcy3-at.* This catalytically dead isoform could act in a dominant negative fashion by dimerizing with endogenous full length ACs, retaining them in ER and, thereby, reducing global cAMP production in the cell, whereby further stimulation of β-AR does not result in further thermogenesis. This mechanism could also explain why BAT activity is reduced upon chronic ephedrine treatment, which would not only be due to receptor desensitization but also to AC3-AT upregulation.

5. Summary

Obesity has become one of the main public health issues in the 21st century. Targeting brown adipose tissue (BAT) activity, which is physiologically induced by cold temperatures, has been recognized as a potential therapeutic approach to tackle the obesity epidemic. Whereas the main molecular players of BAT activation have been identified, their precise regulation through, e.g., epigenetic modification, is not well understood. Recently, it was found that cold exposure leads to the formation of novel H3K4me3 sites in the *adenylyl cyclase 3* gene. In *Adcy3*, the H3K4me3 domain arising from cold induction marks a novel transcription start site, which gives rise to a 5' truncated alternate transcript (AT), termed *Adcy3-at*. However, the function of AC3-AT in BAT is unknown. Here, I demonstrate that AC3-FL, but not AC3-AT, localizes to the plasma membrane, suggesting that AC3-AT is retained in the endoplasmic reticulum. I also found that AC3-AT itself is catalytically inactive. I could demonstrate that AC3-AT heterodimerizes with AC3-FL. Moreover, I found that AC3-AT impairs the transport of AC3-FL to the plasma membrane, which reduces AC3-FL levels in the plasma membrane, resulting in lower cAMP production in the cell. In summary, my results indicate that the expression of truncated AC protein isoforms provides a mechanism to regulate intracellular cAMP signaling in brown adipocytes. I anticipate my research to be a starting point for more sophisticated pharmacological approaches to activate BAT and thereby tackle the obesity epidemic.

6. List of figures

7. List of tables

8. References

Abrahamsen H, Baillie G, Ngai J, Vang T, Nika K, Ruppelt A, Mustelin T, Zaccolo M, Houslay M, Tasken K. TCR- and CD28-mediated recruitment of phosphodiesterase 4 to lipid rafts potentiates TCR signaling. J Immunol. 2004; 173: 4847-4858

Altshuler-Keylin S, Shinoda K, Hasegawa Y, Ikeda K, Hong H, Kang Q, Yang Y, Perera RM, Debnath J, Kajimura S. Beige Adipocyte Maintenance Is Regulated by Autophagy-Induced Mitochondrial Clearance. Cell Metab. 2016; 24: 402-419

Anton SE, Kayser C, Maiellaro I, Nemec K, Moller J, Koschinski A, Zaccolo M, Annibale P, Falcke M, Lohse MJ, Bock A. Receptor-associated independent cAMP nanodomains mediate spatiotemporal specificity of GPCR signaling. Cell. 2022; 185: 1130-1142 e1111

Astrup A, Bulow J, Madsen J, Christensen NJ. Contribution of BAT and skeletal muscle to thermogenesis induced by ephedrine in man. Am J Physiol. 1985; 248: E507-515

Azevedo MF, Faucz FR, Bimpaki E, Horvath A, Levy I, de Alexandre RB, Ahmad F, Manganiello V, Stratakis CA. Clinical and molecular genetics of the phosphodiesterases (PDEs). Endocr Rev. 2014; 35: 195-233

Bakalyar HA, Reed RR. Identification of a specialized adenylyl cyclase that may mediate odorant detection. Science. 1990; 250: 1403-1406

Baragli A, Grieco ML, Trieu P, Villeneuve LR, Hebert TE. Heterodimers of adenylyl cyclases 2 and 5 show enhanced functional responses in the presence of Galpha s. Cell Signal. 2008; 20: 480-492

Barski A, Cuddapah S, Cui K, Roh TY, Schones DE, Wang Z, Wei G, Chepelev I, Zhao K. High-resolution profiling of histone methylations in the human genome. Cell. 2007; 129: 823-837

Bernstein BE, Kamal M, Lindblad-Toh K, Bekiranov S, Bailey DK, Huebert DJ, McMahon S, Karlsson EK, Kulbokas EJ, 3rd, Gingeras TR, Schreiber SL, Lander ES. Genomic maps and comparative analysis of histone modifications in human and mouse. Cell. 2005; 120: 169-181

Birnboim HC, Doly J. A rapid alkaline extraction procedure for screening recombinant plasmid DNA. Nucleic Acids Res. 1979; 7: 1513-1523

Blondin DP, Nielsen S, Kuipers EN, Severinsen MC, Jensen VH, Miard S, Jespersen NZ, Kooijman S, Boon MR, Fortin M, Phoenix S, Frisch F, Guerin B, Turcotte EE, Haman F, Richard D, Picard F, Rensen PCN, Scheele C, Carpentier AC. Human Brown Adipocyte Thermogenesis Is Driven by beta2-AR Stimulation. Cell Metab. 2020; 32: 287-300 e287

Bock A, Annibale P, Konrad C, Hannawacker A, Anton SE, Maiellaro I, Zabel U, Sivaramakrishnan S, Falcke M, Lohse MJ. Optical Mapping of cAMP Signaling at the Nanometer Scale. Cell. 2020; 182: 1519-1530 e1517

Braun K, Oeckl J, Westermeier J, Li Y, Klingenspor M. Non-adrenergic control of lipolysis and thermogenesis in adipose tissues. J Exp Biol. 2018; 221

Cali JJ, Zwaagstra JC, Mons N, Cooper DM, Krupinski J. Type VIII adenylyl cyclase. A Ca2+/calmodulin-stimulated enzyme expressed in discrete regions of rat brain. J Biol Chem. 1994; 269: 12190-12195

Cannon B, Nedergaard J. Brown adipose tissue: function and physiological significance. Physiol Rev. 2004; 84: 277-359

Carey AL, Formosa MF, Van Every B, Bertovic D, Eikelis N, Lambert GW, Kalff V, Duffy SJ, Cherk MH, Kingwell BA. Ephedrine activates brown adipose tissue in lean but not obese humans. Diabetologia. 2013; 56: 147-155

Carey AL, Pajtak R, Formosa MF, Van Every B, Bertovic DA, Anderson MJ, Eikelis N, Lambert GW, Kalff V, Duffy SJ, Cherk MH, Kingwell BA. Chronic ephedrine administration decreases brown adipose tissue activity in a randomised controlled human trial: implications for obesity. Diabetologia. 2015; 58: 1045-1054

Chang JS, Ghosh S, Newman S, Salbaum JM. A map of the PGC-1alpha- and NT-PGC-1alpha-regulated transcriptional network in brown adipose tissue. Sci Rep. 2018; 8: 7876

Chaudhry A, Muffler LA, Yao R, Granneman JG. Perinatal expression of adenylyl cyclase subtypes in rat brown adipose tissue. Am J Physiol. 1996; 270: R755-760

Chen Y, Cann MJ, Litvin TN, Iourgenko V, Sinclair ML, Levin LR, Buck J. Soluble adenylyl cyclase as an evolutionarily conserved bicarbonate sensor. Science. 2000; 289: 625-628

Christensen CR, Clark PB, Morton KA. Reversal of hypermetabolic brown adipose tissue in F-18 FDG PET imaging. Clin Nucl Med. 2006; 31: 193-196

Clement N, Glorian M, Raymondjean M, Andreani M, Limon I. PGE2 amplifies the effects of IL-1beta on vascular smooth muscle cell de-differentiation: a consequence of the versatility of PGE2 receptors 3 due to the emerging expression of adenylyl cyclase 8. J Cell Physiol. 2006; 208: 495-505

Cohen P, Spiegelman BM. Cell biology of fat storage. Mol Biol Cell. 2016; 27: 2523-2527

Collaboration NCDRF. Trends in adult body-mass index in 200 countries from 1975 to 2014: a pooled analysis of 1698 population-based measurement studies with 19.2 million participants. Lancet. 2016; 387: 1377-1396

Cooper DM. Regulation and organization of adenylyl cyclases and cAMP. Biochem J. 2003; 375: 517-529

Cooper DM, Crossthwaite AJ. Higher-order organization and regulation of adenylyl cyclases. Trends Pharmacol Sci. 2006; 27: 426-431

Cypess AM, Chen YC, Sze C, Wang K, English J, Chan O, Holman AR, Tal I, Palmer MR, Kolodny GM, Kahn CR. Cold but not sympathomimetics activates human brown adipose tissue in vivo. Proc Natl Acad Sci U S A. 2012; 109: 10001-10005

Cypess AM, Lehman S, Williams G, Tal I, Rodman D, Goldfine AB, Kuo FC, Palmer EL, Tseng YH, Doria A, Kolodny GM, Kahn CR. Identification and importance of brown adipose tissue in adult humans. N Engl J Med. 2009; 360: 1509-1517

Dawkins MJ, Scopes JW. Non-shivering thermogenesis and brown adipose tissue in the human new-born infant. Nature. 1965; 206: 201-202

Dessauer CW. Adenylyl cyclase--A-kinase anchoring protein complexes: the next dimension in cAMP signaling. Mol Pharmacol. 2009; 76: 935-941

Dessauer CW, Watts VJ, Ostrom RS, Conti M, Dove S, Seifert R. International Union of Basic and Clinical Pharmacology. CI. Structures and Small Molecule Modulators of Mammalian Adenylyl Cyclases. Pharmacol Rev. 2017; 69: 93-139

Di Benedetto G, Zoccarato A, Lissandron V, Terrin A, Li X, Houslay MD, Baillie GS, Zaccolo M. Protein kinase A type I and type II define distinct intracellular signaling compartments. Circ Res. 2008; 103: 836-844

Ding Q, Gros R, Chorazyczewski J, Ferguson SS, Feldman RD. Isoform-specific regulation of adenylyl cyclase function by disruption of membrane trafficking. Mol Pharmacol. 2005; 67: 564-571

Dulloo AG, Seydoux J, Girardier L. Peripheral mechanisms of thermogenesis induced by ephedrine and caffeine in brown adipose tissue. Int J Obes. 1991; 15: 317-326

Engelhard CA, Huang C, Khani S, Kasparek P, Prochazka J, Rozman J, Reguera DP, Sedlacek R, Kornfeld JW. Comprehensive Transcriptional Profiling and Mouse Phenotyping Reveals Dispensable Role for Adipose Tissue Selective Long Noncoding RNA Gm15551. Noncoding RNA. 2022; 8

Fan S, Liu H, Li L. The REEP family of proteins: Molecular targets and role in pathophysiology. Pharmacol Res. 2022; 185: 106477

Feinstein PG, Schrader KA, Bakalyar HA, Tang WJ, Krupinski J, Gilman AG, Reed RR. Molecular cloning and characterization of a Ca2+/calmodulin-insensitive adenylyl cyclase from rat brain. Proc Natl Acad Sci U S A. 1991; 88: 10173-10177

Ferguson GD, Storm DR. Why calcium-stimulated adenylyl cyclases? Physiology (Bethesda). 2004; 19: 271-276

Frontini A, Cinti S. Distribution and development of brown adipocytes in the murine and human adipose organ. Cell Metab. 2010; 11: 253-256

Gao BN, Gilman AG. Cloning and expression of a widely distributed (type IV) adenylyl cyclase. Proc Natl Acad Sci U S A. 1991; 88: 10178-10182

Glatt CE, Snyder SH. Cloning and expression of an adenylyl cyclase localized to the corpus striatum. Nature. 1993; 361: 536-538

Global BMIMC, Di Angelantonio E, Bhupathiraju Sh N, Wormser D, Gao P, Kaptoge S, Berrington de Gonzalez A, Cairns BJ, Huxley R, Jackson Ch L, Joshy G, Lewington S, Manson JE, Murphy N, Patel AV, Samet JM, Woodward M, Zheng W, Zhou M, Bansal N, Barricarte A, Carter B, Cerhan JR, Smith GD, Fang X, Franco OH, Green J, Halsey J, Hildebrand JS, Jung KJ, Korda RJ, McLerran DF, Moore SC, O'Keeffe LM, Paige E, Ramond A, Reeves GK, Rolland B, Sacerdote C, Sattar N, Sofianopoulou E, Stevens J, Thun M, Ueshima H, Yang L, Yun YD, Willeit P, Banks E, Beral V, Chen Z, Gapstur SM, Gunter MJ, Hartge P, Jee SH, Lam TH, Peto R, Potter JD, Willett WC, Thompson SG,

Danesh J, Hu FB. Body-mass index and all-cause mortality: individual-participant-data meta-analysis of 239 prospective studies in four continents. Lancet. 2016; 388: 776-786

Goodarzi MO. Genetics of obesity: what genetic association studies have taught us about the biology of obesity and its complications. Lancet Diabetes Endocrinol. 2018; 6: 223-236

Granneman JG. Expression of adenylyl cyclase subtypes in brown adipose tissue: neural regulation of type III. Endocrinology. 1995; 136: 2007-2012

Granneman JG, Bannon MJ. Neural control of the alpha-subunit of Gs messenger ribonucleic acid in rat brown adipose tissue. Endocrinology. 1989; 125: 2328-2334

Granneman JG, Lahners KN. Differential adrenergic regulation of beta 1- and beta 3-adrenoreceptor messenger ribonucleic acids in adipose tissues. Endocrinology. 1992; 130: 109-114

Grarup N, Moltke I, Andersen MK, Dalby M, Vitting-Seerup K, Kern T, Mahendran Y, Jorsboe E, Larsen CVL, Dahl-Petersen IK, Gilly A, Suveges D, Dedoussis G, Zeggini E, Pedersen O, Andersson R, Bjerregaard P, Jorgensen ME, Albrechtsen A, Hansen T. Loss-of-function variants in ADCY3 increase risk of obesity and type 2 diabetes. Nat Genet. 2018; 50: 172-174

Gruzdeva O, Borodkina D, Uchasova E, Dyleva Y, Barbarash O. Localization of fat depots and cardiovascular risk. Lipids Health Dis. 2018; 17: 218

Gu C, Cali JJ, Cooper DM. Dimerization of mammalian adenylate cyclases. Eur J Biochem. 2002; 269: 413-421

Gu C, Sorkin A, Cooper DM. Persistent interactions between the two transmembrane clusters dictate the targeting and functional assembly of adenylyl cyclase. Curr Biol. 2001; 11: 185-190

Guo DH, Yamamoto M, Hernandez CM, Khodadadi H, Baban B, Stranahan AM. Beige adipocytes mediate the neuroprotective and anti-inflammatory effects of subcutaneous fat in obese mice. Nat Commun. 2021; 12: 4623

Hanoune J, Defer N. Regulation and role of adenylyl cyclase isoforms. Annu Rev Pharmacol Toxicol. 2001; 41: 145-174

Hansen JN, Bruckner M, Pietrowski MJ, Jikeli JF, Plescher M, Beckert H, Schnaars M, Fulle L, Reitmeier K, Langmann T, Forster I, Boche D, Petzold GC, Halle A. MotiQ: an open-source toolbox to quantify the cell motility and morphology of microglia. Mol Biol Cell. 2022; 33: ar99

Hansen JN, Rassmann S, Jikeli JF, Wachten D. SpermQ(-)A Simple Analysis Software to Comprehensively Study Flagellar Beating and Sperm Steering. Cells. 2018; 8

Hansen JN, Rassmann S, Stuven B, Jurisch-Yaksi N, Wachten D. CiliaQ: a simple, open-source software for automated quantification of ciliary morphology and fluorescence in 2D, 3D, and 4D images. Eur Phys J E Soft Matter. 2021; 44: 18

Hanssen MJ, Hoeks J, Brans B, van der Lans AA, Schaart G, van den Driessche JJ, Jorgensen JA, Boekschoten MV, Hesselink MK, Havekes B, Kersten S, Mottaghy FM, van Marken Lichtenbelt WD, Schrauwen P. Short-term cold acclimation improves insulin sensitivity in patients with type 2 diabetes mellitus. Nat Med. 2015; 21: 863-865

Harden TK. Agonist-induced desensitization of the beta-adrenergic receptor-linked adenylate cyclase. Pharmacol Rev. 1983; 35: 5-32

Hatori M, Vollmers C, Zarrinpar A, DiTacchio L, Bushong EA, Gill S, Leblanc M, Chaix A, Joens M, Fitzpatrick JA, Ellisman MH, Panda S. Time-restricted feeding without reducing caloric intake prevents metabolic diseases in mice fed a high-fat diet. Cell Metab. 2012; 15: 848-860

Horie K, Insel PA. Retrovirally mediated transfer of a G protein-coupled receptor kinase (GRK) dominant-negative mutant enhances endogenous calcitonin receptor signaling in Chinese hamster ovary cells. GRK inhibition enhances expression of receptors and receptor mRNA. J Biol Chem. 2000; 275: 29433-29440

Hotamisligil GS. Inflammation, metaflammation and immunometabolic disorders. Nature. 2017; 542: 177-185

Hunter T. Signaling--2000 and beyond. Cell. 2000; 100: 113-127

Ikeda K, Maretich P, Kajimura S. The Common and Distinct Features of Brown and Beige Adipocytes. Trends Endocrinol Metab. 2018; 29: 191-200

Ishikawa Y, Katsushika S, Chen L, Halnon NJ, Kawabe J, Homcy CJ. Isolation and characterization of a novel cardiac adenylylcyclase cDNA. J Biol Chem. 1992; 267: 13553-13557

Ito S, Kuroshima A. [Distribution of brown adipose tissue in Japanese new-born infants]. Nihon Seirigaku Zasshi. 1967; 29: 660-661

Jones B, McGlone ER, Fang Z, Pickford P, Correa IR, Jr., Oishi A, Jockers R, Inoue A, Kumar S, Gorlitz F, Dunsby C, French PMW, Rutter GA, Tan T, Tomas A, Bloom SR. Genetic and biased agonist-mediated reductions in beta-arrestin recruitment prolong cAMP signaling at glucagon family receptors. J Biol Chem. 2021; 296: 100133

Jung SM, Sanchez-Gurmaches J, Guertin DA. Brown Adipose Tissue Development and Metabolism. Handb Exp Pharmacol. 2019; 251: 3-36

Jurevicius J, Skeberdis VA, Fischmeister R. Role of cyclic nucleotide phosphodiesterase isoforms in cAMP compartmentation following beta2-adrenergic stimulation of ICa,L in frog ventricular myocytes. J Physiol. 2003; 551: 239-252

Kajimura S, Spiegelman BM, Seale P. Brown and Beige Fat: Physiological Roles beyond Heat Generation. Cell Metab. 2015; 22: 546-559

Katsushika S, Chen L, Kawabe J, Nilakantan R, Halnon NJ, Homcy CJ, Ishikawa Y. Cloning and characterization of a sixth adenylyl cyclase isoform: types V and VI constitute a subgroup within the mammalian adenylyl cyclase family. Proc Natl Acad Sci U S A. 1992; 89: 8774-8778

Kayser C, Lohse MJ, Bock A. Real-Time Measurements of Intracellular cAMP Gradients Using FRET-Based cAMP Nanorulers. Methods Mol Biol. 2022; 2483: 1-13

Keuylian Z, de Baaij JH, Gueguen M, Glorian M, Rouxel C, Merlet E, Lipskaia L, Blaise R, Mateo V, Limon I. The Notch pathway attenuates interleukin 1beta (IL1beta)-mediated induction of adenylyl cyclase 8 (AC8) expression during vascular smooth muscle cell (VSMC) trans-differentiation. J Biol Chem. 2012; 287: 24978-24989

Khani S, Topel H, Kardinal R, Tavanez AR, Josephrajan A, Larsen BDM, Gaudry MJ, Leyendecker P, Egedal NM, Guller AS, Stanic N, Ruppert PMM, Gaziano I, Hansmeier NR, Schmidt E, Klemm P, Vagliano LM, Stahl R, Duthie F, Krause JH, Bici A, Engelhard CA, Gohlke S, Frommolt P, Gnad T, Rada-Iglesias A, Pradas-Juni M, Schulz TJ, Wunderlich FT, Pfeifer A, Bartelt A, Jastroch M, Wachten D, Kornfeld JW. Cold-induced expression of a truncated adenylyl cyclase 3 acts as rheostat to brown fat function. Nat Metab. 2024

Khannpnavar B, Mehta V, Qi C, Korkhov V. Structure and function of adenylyl cyclases, key enzymes in cellular signaling. Curr Opin Struct Biol. 2020; 63: 34-41

Kim TH, Barrera LO, Zheng M, Qu C, Singer MA, Richmond TA, Wu Y, Green RD, Ren B. A high-resolution map of active promoters in the human genome. Nature. 2005; 436: 876-880

Klepac K, Georgiadi A, Tschop M, Herzig S. The role of brown and beige adipose tissue in glycaemic control. Mol Aspects Med. 2019; 68: 90-100

Kouzarides T. Chromatin modifications and their function. Cell. 2007; 128: 693-705

Krupinski J, Lehman TC, Frankenfield CD, Zwaagstra JC, Watson PA. Molecular diversity in the adenylylcyclase family. Evidence for eight forms of the enzyme and cloning of type VI. J Biol Chem. 1992; 267: 24858-24862

Kusminski CM, Bickel PE, Scherer PE. Targeting adipose tissue in the treatment of obesity-associated diabetes. Nat Rev Drug Discov. 2016; 15: 639-660

Lefkowitz RJ, Shenoy SK. Transduction of receptor signals by beta-arrestins. Science. 2005; 308: 512-517

Leitner BP, Huang S, Brychta RJ, Duckworth CJ, Baskin AS, McGehee S, Tal I, Dieckmann W, Gupta G, Kolodny GM, Pacak K, Herscovitch P, Cypess AM, Chen KY. Mapping of human brown adipose tissue in lean and obese young men. Proc Natl Acad Sci U S A. 2017; 114: 8649-8654

Li Y, He J, Sui S, Hu X, Zhao Y, Li N. Clenbuterol upregulates histone demethylase JHDM2a via the beta2-adrenoceptor/cAMP/PKA/p-CREB signaling pathway. Cell Signal. 2012; 24: 2297-2306

Locke AE, Kahali B, Berndt SI, Justice AE, Pers TH, Day FR, Powell C, Vedantam S, Buchkovich ML, Yang J, Croteau-Chonka DC, Esko T, Fall T, Ferreira T, Gustafsson S, Kutalik Z, Luan J, Magi R, Randall JC, Winkler TW, Wood AR, Workalemahu T, Faul JD, Smith JA, Zhao JH, Zhao W, Chen J, Fehrmann R, Hedman AK, Karjalainen J, Schmidt EM, Absher D, Amin N, Anderson D, Beekman M, Bolton JL, Bragg-Gresham JL, Buyske S, Demirkan A, Deng G, Ehret GB, Feenstra B, Feitosa MF, Fischer K, Goel A, Gong J, Jackson AU, Kanoni S, Kleber ME, Kristiansson K, Lim U, Lotay V, Mangino M, Leach IM, Medina-Gomez C, Medland SE, Nalls MA, Palmer CD, Pasko D, Pechlivanis S, Peters MJ, Prokopenko I, Shungin D, Stancakova A, Strawbridge RJ, Sung YJ, Tanaka T, Teumer A, Trompet S, van der Laan SW, van Setten J, Van Vliet-Ostaptchouk JV, Wang Z, Yengo L, Zhang W, Isaacs A, Albrecht E, Arnlov J, Arscott GM, Attwood AP, Bandinelli S, Barrett A, Bas IN, Bellis C, Bennett AJ, Berne C,

Blagieva R, Bluher M, Bohringer S, Bonnycastle LL, Bottcher Y, Boyd HA, Bruinenberg M, Caspersen IH, Chen YI, Clarke R, Daw EW, de Craen AJM, Delgado G, Dimitriou M, Doney ASF, Eklund N, Estrada K, Eury E, Folkersen L, Fraser RM, Garcia ME, Geller F, Giedraitis V, Gigante B, Go AS, Golay A, Goodall AH, Gordon SD, Gorski M, Grabe HJ, Grallert H, Grammer TB, Grassler J, Gronberg H, Groves CJ, Gusto G, Haessler J, Hall P, Haller T, Hallmans G, Hartman CA, Hassinen M, Hayward C, Heard-Costa NL, Helmer Q, Hengstenberg C, Holmen O, Hottenga JJ, James AL, Jeff JM, Johansson A, Jolley J, Juliusdottir T, Kinnunen L, Koenig W, Koskenvuo M, Kratzer W, Laitinen J, Lamina C, Leander K, Lee NR, Lichtner P, Lind L, Lindstrom J, Lo KS, Lobbens S, Lorbeer R, Lu Y, Mach F, Magnusson PKE, Mahajan A, McArdle WL, McLachlan S, Menni C, Merger S, Mihailov E, Milani L, Moayyeri A, Monda KL, Morken MA, Mulas A, Muller G, Muller-Nurasyid M, Musk AW, Nagaraja R, Nothen MM, Nolte IM, Pilz S, Rayner NW, Renstrom F, Rettig R, Ried JS, Ripke S, Robertson NR, Rose LM, Sanna S, Scharnagl H, Scholtens S, Schumacher FR, Scott WR, Seufferlein T, Shi J, Smith AV, Smolonska J, Stanton AV, Steinthorsdottir V, Stirrups K, Stringham HM, Sundstrom J, Swertz MA, Swift AJ, Syvanen AC, Tan ST, Tayo BO, Thorand B, Thorleifsson G, Tyrer JP, Uh HW, Vandenput L, Verhulst FC, Vermeulen SH, Verweij N, Vonk JM, Waite LL, Warren HR, Waterworth D, Weedon MN, Wilkens LR, Willenborg C, Wilsgaard T, Wojczynski MK, Wong A, Wright AF, Zhang Q, LifeLines Cohort S, Brennan EP, Choi M, Dastani Z, Drong AW, Eriksson P, Franco-Cereceda A, Gadin JR, Gharavi AG, Goddard ME, Handsaker RE, Huang J, Karpe F, Kathiresan S, Keildson S, Kiryluk K, Kubo M, Lee JY, Liang L, Lifton RP, Ma B, McCarroll SA, McKnight AJ, Min JL, Moffatt MF, Montgomery GW, Murabito JM, Nicholson G, Nyholt DR, Okada Y, Perry JRB, Dorajoo R, Reinmaa E, Salem RM, Sandholm N, Scott RA, Stolk L, Takahashi A, Tanaka T, van 't Hooft FM, Vinkhuyzen AAE, Westra HJ, Zheng W, Zondervan KT, Consortium AD, Group A-BW, Consortium CAD, Consortium CK, Glgc, Icbp, Investigators M, Mu TC, Consortium MI, Consortium P, ReproGen C, Consortium G, International Endogene C, Heath AC, Arveiler D, Bakker SJL, Beilby J, Bergman RN, Blangero J, Bovet P, Campbell H, Caulfield MJ, Cesana G, Chakravarti A, Chasman DI, Chines PS, Collins FS, Crawford DC, Cupples LA, Cusi D, Danesh J, de Faire U, den Ruijter HM, Dominiczak AF, Erbel R, Erdmann J, Eriksson JG, Farrall M, Felix SB, Ferrannini E, Ferrieres J, Ford I, Forouhi NG, Forrester T, Franco OH, Gansevoort RT, Gejman PV,

Gieger C, Gottesman O, Gudnason V, Gyllensten U, Hall AS, Harris TB, Hattersley AT, Hicks AA, Hindorff LA, Hingorani AD, Hofman A, Homuth G, Hovingh GK, Humphries SE, Hunt SC, Hypponen E, Illig T, Jacobs KB, Jarvelin MR, Jockel KH, Johansen B, Jousilahti P, Jukema JW, Jula AM, Kaprio J, Kastelein JJP, Keinanen-Kiukaanniemi SM, Kiemeney LA, Knekt P, Kooner JS, Kooperberg C, Kovacs P, Kraja AT, Kumari M, Kuusisto J, Lakka TA, Langenberg C, Marchand LL, Lehtimaki T, Lyssenko V, Mannisto S, Marette A, Matise TC, McKenzie CA, McKnight B, Moll FL, Morris AD, Morris AP, Murray JC, Nelis M, Ohlsson C, Oldehinkel AJ, Ong KK, Madden PAF, Pasterkamp G, Peden JF, Peters A, Postma DS, Pramstaller PP, Price JF, Qi L, Raitakari OT, Rankinen T, Rao DC, Rice TK, Ridker PM, Rioux JD, Ritchie MD, Rudan I, Salomaa V, Samani NJ, Saramies J, Sarzynski MA, Schunkert H, Schwarz PEH, Sever P, Shuldiner AR, Sinisalo J, Stolk RP, Strauch K, Tonjes A, Tregouet DA, Tremblay A, Tremoli E, Virtamo J, Vohl MC, Volker U, Waeber G, Willemsen G, Witteman JC, Zillikens MC, Adair LS, Amouyel P, Asselbergs FW, Assimes TL, Bochud M, Boehm BO, Boerwinkle E, Bornstein SR, Bottinger EP, Bouchard C, Cauchi S, Chambers JC, Chanock SJ, Cooper RS, de Bakker PIW, Dedoussis G, Ferrucci L, Franks PW, Froguel P, Groop LC, Haiman CA, Hamsten A, Hui J, Hunter DJ, Hveem K, Kaplan RC, Kivimaki M, Kuh D, Laakso M, Liu Y, Martin NG, Marz W, Melbye M, Metspalu A, Moebus S, Munroe PB, Njolstad I, Oostra BA, Palmer CNA, Pedersen NL, Perola M, Perusse L, Peters U, Power C, Quertermous T, Rauramaa R, Rivadeneira F, Saaristo TE, Saleheen D, Sattar N, Schadt EE, Schlessinger D, Slagboom PE, Snieder H, Spector TD, Thorsteinsdottir U, Stumvoll M, Tuomilehto J, Uitterlinden AG, Uusitupa M, van der Harst P, Walker M, Wallaschofski H, Wareham NJ, Watkins H, Weir DR, Wichmann HE, Wilson JF, Zanen P, Borecki IB, Deloukas P, Fox CS, Heid IM, O'Connell JR, Strachan DP, Stefansson K, van Duijn CM, Abecasis GR, Franke L, Frayling TM, McCarthy MI, Visscher PM, Scherag A, Willer CJ, Boehnke M, Mohlke KL, Lindgren CM, Beckmann JS, Barroso I, North KE, Ingelsson E, Hirschhorn JN, Loos RJF, Speliotes EK. Genetic studies of body mass index yield new insights for obesity biology. Nature. 2015; 518: 197-206

Lohse MJ. Molecular mechanisms of membrane receptor desensitization. Biochim Biophys Acta. 1993; 1179: 171-188

Lynes MD, Tseng YH. The Thermogenic Circuit: Regulators of Thermogenic Competency and Differentiation. Genes Dis. 2015; 2: 164-172

Malbon CC. A-kinase anchoring proteins: trafficking in G-protein-coupled receptors and the proteins that regulate receptor biology. Curr Opin Drug Discov Devel. 2007; 10: 573-579

Mandel M, Higa A. Calcium-dependent bacteriophage DNA infection. J Mol Biol. 1970; 53: 159-162

Matsushita M, Yoneshiro T, Aita S, Kameya T, Sugie H, Saito M. Impact of brown adipose tissue on body fatness and glucose metabolism in healthy humans. Int J Obes (Lond). 2014; 38: 812-817

Mongillo M, McSorley T, Evellin S, Sood A, Lissandron V, Terrin A, Huston E, Hannawacker A, Lohse MJ, Pozzan T, Houslay MD, Zaccolo M. Fluorescence resonance energy transfer-based analysis of cAMP dynamics in live neonatal rat cardiac myocytes reveals distinct functions of compartmentalized phosphodiesterases. Circ Res. 2004; 95: 67-75

Mongillo M, Zaccolo M. A complex phosphodiesterase system controls beta-adrenoceptor signalling in cardiomyocytes. Biochem Soc Trans. 2006; 34: 510-511

Morrison SF, Madden CJ. Central nervous system regulation of brown adipose tissue. Compr Physiol. 2014; 4: 1677-1713

Mukherjee J, Baranwal A, Schade KN. Classification of Therapeutic and Experimental Drugs for Brown Adipose Tissue Activation: Potential Treatment Strategies for Diabetes and Obesity. Curr Diabetes Rev. 2016; 12: 414-428

Musri MM, Gomis R, Parrizas M. A chromatin perspective of adipogenesis. Organogenesis. 2010; 6: 15-23

Nedergaard J, Bengtsson T, Cannon B. Unexpected evidence for active brown adipose tissue in adult humans. Am J Physiol Endocrinol Metab. 2007; 293: E444-452

Nedergaard J, Bengtsson T, Cannon B. Three years with adult human brown adipose tissue. Ann N Y Acad Sci. 2010; 1212: E20-36

Nedergaard J, Cannon B. The browning of white adipose tissue: some burning issues. Cell Metab. 2014; 20: 396-407

Ohno H, Shinoda K, Spiegelman BM, Kajimura S. PPARgamma agonists induce a white-to-brown fat conversion through stabilization of PRDM16 protein. Cell Metab. 2012; 15: 395-404

Ostrom KF, LaVigne JE, Brust TF, Seifert R, Dessauer CW, Watts VJ, Ostrom RS. Physiological roles of mammalian transmembrane adenylyl cyclase isoforms. Physiol Rev. 2022; 102: 815-857

Pitcher JA, Freedman NJ, Lefkowitz RJ. G protein-coupled receptor kinases. Annu Rev Biochem. 1998; 67: 653-692

Pitman JL, Wheeler MC, Lloyd DJ, Walker JR, Glynne RJ, Gekakis N. A gain-of-function mutation in adenylate cyclase 3 protects mice from diet-induced obesity. PLoS One. 2014; 9: e110226

Premont RT, Chen J, Ma HW, Ponnapalli M, Iyengar R. Two members of a widely expressed subfamily of hormone-stimulated adenylyl cyclases. Proc Natl Acad Sci U S A. 1992; 89: 9809-9813

Premont RT, Matsuoka I, Mattei MG, Pouille Y, Defer N, Hanoune J. Identification and characterization of a widely expressed form of adenylyl cyclase. J Biol Chem. 1996; 271: 13900-13907

Prospective Studies C, Whitlock G, Lewington S, Sherliker P, Clarke R, Emberson J, Halsey J, Qizilbash N, Collins R, Peto R. Body-mass index and cause-specific mortality in 900 000 adults: collaborative analyses of 57 prospective studies. Lancet. 2009; 373: 1083-1096

Puigserver P, Wu Z, Park CW, Graves R, Wright M, Spiegelman BM. A cold-inducible coactivator of nuclear receptors linked to adaptive thermogenesis. Cell. 1998; 92: 829-839

Qi C, Sorrentino S, Medalia O, Korkhov VM. The structure of a membrane adenylyl cyclase bound to an activated stimulatory G protein. Science. 2019; 364: 389-394

Rajagopal S, Shenoy SK. GPCR desensitization: Acute and prolonged phases. Cell Signal. 2018; 41: 9-16

Reverte-Salisa L, Sanyal A, Pfeifer A. Role of cAMP and cGMP Signaling in Brown Fat. Handb Exp Pharmacol. 2019; 251: 161-182

Rich TC, Fagan KA, Tse TE, Schaack J, Cooper DM, Karpen JW. A uniform extracellular stimulus triggers distinct cAMP signals in different compartments of a simple cell. Proc Natl Acad Sci U S A. 2001; 98: 13049-13054

Saeed S, Bonnefond A, Tamanini F, Mirza MU, Manzoor J, Janjua QM, Din SM, Gaitan J, Milochau A, Durand E, Vaillant E, Haseeb A, De Graeve F, Rabearivelo I, Sand O, Queniat G, Boutry R, Schott DA, Ayesha H, Ali M, Khan WI, Butt TA, Rinne T, Stumpel C, Abderrahmani A, Lang J, Arslan M, Froguel P. Loss-of-function mutations in ADCY3 cause monogenic severe obesity. Nat Genet. 2018; 50: 175-179

Saito H, Kubota M, Roberts RW, Chi Q, Matsunami H. RTP family members induce functional expression of mammalian odorant receptors. Cell. 2004; 119: 679-691

Santos-Rosa H, Schneider R, Bannister AJ, Sherriff J, Bernstein BE, Emre NC, Schreiber SL, Mellor J, Kouzarides T. Active genes are tri-methylated at K4 of histone H3. Nature. 2002; 419: 407-411

Scherer PE. The many secret lives of adipocytes: implications for diabetes. Diabetologia. 2019; 62: 223-232

Scott JD, Dessauer CW, Tasken K. Creating order from chaos: cellular regulation by kinase anchoring. Annu Rev Pharmacol Toxicol. 2013; 53: 187-210

Sieber JJ, Willig KI, Heintzmann R, Hell SW, Lang T. The SNARE motif is essential for the formation of syntaxin clusters in the plasma membrane. Biophys J. 2006; 90: 2843-2851

Silverman WA, Zamelis A, Sinclair JC, Agate FJ. Warm Nap of the Newborn. Pediatrics. 1964; 33: 984-987

Simonds WF. G protein regulation of adenylate cyclase. Trends Pharmacol Sci. 1999; 20: 66-73

Simons PC, Shi M, Foutz T, Cimino DF, Lewis J, Buranda T, Lim WK, Neubig RR, McIntire WE, Garrison J, Prossnitz E, Sklar LA. Ligand-receptor-G-protein molecular assemblies on beads for mechanistic studies and screening by flow cytometry. Mol Pharmacol. 2003; 64: 1227-1238

Skroblin P, Grossmann S, Schafer G, Rosenthal W, Klussmann E. Mechanisms of protein kinase A anchoring. Int Rev Cell Mol Biol. 2010; 283: 235-330

Son Y, Choi C, Saha A, Park JH, Im H, Cho YK, Seong JK, Burl RB, Rondini EA, Granneman JG, Lee YH. REEP6 knockout leads to defective beta-adrenergic signaling in adipocytes and promotes obesity-related metabolic dysfunction. Metabolism. 2022; 130: 155159

Stergiakouli E, Gaillard R, Tavare JM, Balthasar N, Loos RJ, Taal HR, Evans DM, Rivadeneira F, St Pourcain B, Uitterlinden AG, Kemp JP, Hofman A, Ring SM, Cole TJ, Jaddoe VW, Davey Smith G, Timpson NJ. Genome-wide association study of height-adjusted BMI in childhood identifies functional variant in ADCY3. Obesity (Silver Spring). 2014; 22: 2252-2259

Sun W, Dong H, Balaz M, Slyper M, Drokhlyansky E, Colleluori G, Giordano A, Kovanicova Z, Stefanicka P, Balazova L, Ding L, Husted AS, Rudofsky G, Ukropec J, Cinti S, Schwartz TW, Regev A, Wolfrum C. snRNA-seq reveals a subpopulation of adipocytes that regulates thermogenesis. Nature. 2020; 587: 98-102

Sunahara RK, Dessauer CW, Gilman AG. Complexity and diversity of mammalian adenylyl cyclases. Annu Rev Pharmacol Toxicol. 1996; 36: 461-480

Surdo NC, Berrera M, Koschinski A, Brescia M, Machado MR, Carr C, Wright P, Gorelik J, Morotti S, Grandi E, Bers DM, Pantano S, Zaccolo M. FRET biosensor uncovers cAMP nano-domains at beta-adrenergic targets that dictate precise tuning of cardiac contractility. Nat Commun. 2017; 8: 15031

Terrin A, Di Benedetto G, Pertegato V, Cheung YF, Baillie G, Lynch MJ, Elvassore N, Prinz A, Herberg FW, Houslay MD, Zaccolo M. PGE(1) stimulation of HEK293 cells generates multiple contiguous domains with different [cAMP]: role of compartmentalized phosphodiesterases. J Cell Biol. 2006; 175: 441-451

Tesmer JJ, Sunahara RK, Gilman AG, Sprang SR. Crystal structure of the catalytic domains of adenylyl cyclase in a complex with Gsalpha.GTPgammaS. Science. 1997; 278: 1907-1916

Tesmer JJ, Sunahara RK, Johnson RA, Gosselin G, Gilman AG, Sprang SR. Two-metal-Ion catalysis in adenylyl cyclase. Science. 1999; 285: 756-760

Tian Y, Peng B, Fu X. New ADCY3 Variants Dance in Obesity Etiology. Trends Endocrinol Metab. 2018; 29: 361-363

Tong T, Shen Y, Lee HW, Yu R, Park T. Adenylyl cyclase 3 haploinsufficiency confers susceptibility to diet-induced obesity and insulin resistance in mice. Sci Rep. 2016; 6: 34179

Toumba M, Fanis P, Vlachakis D, Neocleous V, Phylactou LA, Skordis N, Mantzoros CS, Pantelidou M. Molecular modelling of novel ADCY3 variant predicts a molecular target for tackling obesity. Int J Mol Med. 2022; 49

Tune JD, Goodwill AG, Sassoon DJ, Mather KJ. Cardiovascular consequences of metabolic syndrome. Transl Res. 2017; 183: 57-70

Vallin B, Legueux-Cajgfinger Y, Clement N, Glorian M, Duca L, Vincent P, Limon I, Blaise R. Novel short isoforms of adenylyl cyclase as negative regulators of cAMP production. Biochim Biophys Acta Mol Cell Res. 2018; 1865: 1326-1340

van der Lans AA, Hoeks J, Brans B, Vijgen GH, Visser MG, Vosselman MJ, Hansen J, Jorgensen JA, Wu J, Mottaghy FM, Schrauwen P, van Marken Lichtenbelt WD. Cold acclimation recruits human brown fat and increases nonshivering thermogenesis. J Clin Invest. 2013; 123: 3395-3403

van Marken Lichtenbelt WD, Vanhommerig JW, Smulders NM, Drossaerts JM, Kemerink GJ, Bouvy ND, Schrauwen P, Teule GJ. Cold-activated brown adipose tissue in healthy men. N Engl J Med. 2009; 360: 1500-1508

Vegiopoulos A, Rohm M, Herzig S. Adipose tissue: between the extremes. EMBO J. 2017; 36: 1999-2017

Virtanen KA, Lidell ME, Orava J, Heglind M, Westergren R, Niemi T, Taittonen M, Laine J, Savisto NJ, Enerback S, Nuutila P. Functional brown adipose tissue in healthy adults. N Engl J Med. 2009; 360: 1518-1525

Vosselman MJ, van der Lans AA, Brans B, Wierts R, van Baak MA, Schrauwen P, van Marken Lichtenbelt WD. Systemic beta-adrenergic stimulation of thermogenesis is not

accompanied by brown adipose tissue activity in humans. Diabetes. 2012; 61: 3106-3113

Wallach J, Droste M, Kluxen FW, Pfeuffer T, Frank R. Molecular cloning and expression of a novel type V adenylyl cyclase from rabbit myocardium. FEBS Lett. 1994; 338: 257-263

Wang X, Zhu WG. [Advances in histone methyltransferases and histone demethylases]. Ai Zheng. 2008; 27: 1018-1025

Wang Z, Li V, Chan GC, Phan T, Nudelman AS, Xia Z, Storm DR. Adult type 3 adenylyl cyclase-deficient mice are obese. PLoS One. 2009; 4: e6979

White U. Adipose tissue expansion in obesity, health, and disease. Front Cell Dev Biol. 2023; 11: 1188844

Wu Z, Puigserver P, Andersson U, Zhang C, Adelmant G, Mootha V, Troy A, Cinti S, Lowell B, Scarpulla RC, Spiegelman BM. Mechanisms controlling mitochondrial biogenesis and respiration through the thermogenic coactivator PGC-1. Cell. 1999; 98: 115-124

Yoneshiro T, Aita S, Matsushita M, Kayahara T, Kameya T, Kawai Y, Iwanaga T, Saito M. Recruited brown adipose tissue as an antiobesity agent in humans. J Clin Invest. 2013; 123: 3404-3408

Yoshimura M, Cooper DM. Cloning and expression of a Ca(2+)-inhibitable adenylyl cyclase from NCB-20 cells. Proc Natl Acad Sci U S A. 1992; 89: 6716-6720

Zhang G, Liu Y, Ruoho AE, Hurley JH. Structure of the adenylyl cyclase catalytic core. Nature. 1997; 386: 247-253

9. Acknowledgements

First and foremost, I would like to express my deepest appreciation to my supervisor, Prof. Dr. Dagmar Wachten, for her guidance, her invaluable patience, her constant feedback, and for challenging me to grow as a scientist and as a person.

I am also extremely grateful to Dr. Vera Beckert, who, from the very beginning of my scientific career, has taken her time to teach me the technical abilities this endeavor has required. Thank you for being such a supportive mentor.

I would like to extend my sincere thanks to Jens Henning Krause for his support and wide-ranging technical capabilities in the laboratory.

Also, this venture would not have been possible without the SciMed Foundation, which financed my research.

I would be remiss in not mentioning my family, especially my parents, Giovanna and Enzo, and my brothers, Federico and Gianluca. It would have been impossible to finish my studies without their unwavering support. Lastly, I would like to thank my cats, Eliot, Seikhu, and Rafa, for the emotional support.

Publication

Khani S, Topel H, Kardinal R, et al. Cold-induced expression of a truncated adenylyl cyclase 3 acts as rheostat to brown fat function. Nat Metab. Published online April 29, 2024. doi:10.1038/s42255-024-01033-8